The application of CW and FM sonar technology to detect a decrease in air in the swim bladder of Atlantic salmon, measurements and modeling

THESIS FOR THE DEGREE

MASTER OF SCIENCE

IN

MARINE MEASUREMENT SYSTEMS

ACOUSTICS

BY

MAREN FORSTRØNEN RONG

DEPARTMENT OF PHYSICS AND TECHNOLOGY

UNIVERSITY OF BERGEN

JUNE, 2022

Abstract

Salmon lice and poor surface conditions are challenging for salmon aquaculture. A new innovative preventative solution is to submerge the cages below the sea surface to avoid the surface-dwelling infestation of lice larvae. However, the physostomous salmon require daily surface access, or the swim bladder will deflate. The ensues negative buoyancy leads to increased swimming speed, and over a prolonged time (2-3 weeks), the appetite and growth rate may be reduced, resulting in poor welfare. For 28 days, 500 salmon were placed in a cage submerged to 1 m depth, preventing the salmon from reaching the sea surface and refilling the swim bladder. Beneath the cage, three EK80 scientific wide-band echo sounders with 70, 120, and 200 kHz split-beam transducers were deployed to study the acoustic backscatter over time. From the backscattered signals, parameters such as the target strength (TS), volume backscattering strength (S_V), the frequency response of both TS and S_V, and the swimming speed could be calculated. These parameters are studied to determine the first to indicate an insufficient air level based on signal type and frequency. The results show an increase in swimming speed and a decrease in both TS and S_V values. From the measured daily $\overline{TS}$ values from both FM and CW signals, the decrease appeared to begin from day 6 of submergence. As the air in the bladder diminished, the ratio between the values from the three echo sounders increased, which was evident from TS and S_V measurements, and the frequency responses. The swimming speed acquired from the acoustical recordings decreased from day 5, but the speeds were unexpectedly high. These findings may be used to develop automatic alarms that detect low swim bladder inflations or poor welfare and provide new fundamental knowledge about backscattering from salmon.

Acknowledgment

This thesis was conducted in cooperation between the University of Bergen (UiB), Faculty of Mathematics and Natural Science, Department of Physics and Technology, and the Institute of Marine Research (IMR) as part of the CRIMAC project.

First and foremost, I would like to thank my supervisors, Prof. Per Lunde at UiB, and Tonje Nesse Forland, Frode Oppedal, and Geir Pedersen from the IMR. Per, for teaching me all the fundamental knowledge in acoustics over the past years and providing me with insightful comments and guidance during this thesis. My sincere gratitude goes to you, Tonje, for all the great discussions we have had and for your inspiration when I needed it. The experiment in Matre would not be the same without the contribution from Frode and Geir's help with the thesis' simulation and acoustic attributions has been invaluable.

Additionally, I would like to acknowledge Rolf Korneliussen, leader of the Ecosystem Acoustic group at IMR, for his enthusiasm and many hours put into helping with LSSS. Every member of the research station in Matre contributed greatly to collecting the data. My fellow master's student, Kristin, made my five weeks in Matre a memorable experience, resulting in a new friend.

I would like to end by thanking my boyfriend, family, and friends for their immense support and encouragement.

Maren Forstrønen Rong

June 1, 2022

Bergen, Norway

Contents

Chapter 1

Introduction

1.1 Motivation

Atlantic salmon, *Salmo salar*, has been one of Norway's most important export products over the past decades. Norway produces nearly half of the world's Atlantic salmon, with approximately 1.1 million tons exported in 2019 [1]. The global population continues to grow every year, and it is predicted that there will be 8.5 billion people on this planet by 2030 [2]. To meet the UN's Sustainable Goal 2: Zero Hunger, food production needs to keep pace with the population, and an increase in farmed salmon will contribute to reaching the goal. Although modern technology, vaccines, and medicine have vastly improved the industry, it still faces significant obstacles.

A major parasite and problem of Norwegian aquaculture is the salmon louse, *Lepeophtheirus salmonis* [3]. The louse feeds on the salmon's skin, blood, and mucus, resulting in wounds and infections [4]. Apart from salmon louse, algae blooms and poor surface conditions like low oxygen, excessive temperatures, and biofouling stress the salmon's growth and health [5]. Large budgets and resources are devoted to devising an answer for the problems, and one solution can be to submerge the cages below the sea surface [6]. This, however, presents additional challenges due to the salmon's biological structure. They belong to the group of fish known as physostomous, which means that the swim bladder is connected to the pharynx by a channel. They swim to the surface and swallow or snap air to adjust the bladder's volume [7]. Other species are physoclistous, meaning they have no connection between the pharynx and the swim bladder and use gas from the blood to fill and empty it. Conversely, some species have no swim bladders and continuously swim with negative buoyancy [7]. A low air level is detrimental to their health and gradually results in behavioral changes. Due to insufficient air, salmon have difficulty maintaining neutral buoyancy. The salmon swim faster with a vertical tilt, head up and tail down, to compensate for the negative buoyancy, and findings show that a negative buoyancy may reduce appetite, followed by a reduction in growth [7, 8].

Fish have been studied using acoustic instruments throughout the last century, where the first detection of fish using echo sounders dates to 1929 by Kimura [9]. The amount of signal returned to the echo sounders depends on the species. Due to the air within the swim bladder, physostomous

or physoclistous fish backscatters the signal better than fish without one, as the swim bladder is the primary source of the backscattering [10]. Thus, acoustic signals, such as target strength (TS) from individual fish and volume backscattering strength (S_V), are highly relevant for observing the air level of salmon in submerged cages. Both TS and S_V are measures of how much of the transmitted signal is scattered back to the echo sounder [9].

Hence, a drop in the air level of submerged salmon can be detected using echo sounders. In light of the acoustic data, a feasible alarm system could be designed to alert farmers that the salmon need more air. However, research is still in its early stages in this area. Which signal types and frequencies to use and parameters to look for are still unidentified and will be studied in this thesis.

1.2 Prior work

Echo sounders are essential tools in the fishery industry and have been used to study aquatic species since the 1930s. Already in 1949, echo sounders were applied in surveys to observe the behavior and identification of different types of fish [11]. Echo sounders transmitting single frequencies, called continuous waves (CW)[1], are most commonly used [12]. Further development of the technology led to echo sounders transmitting broadband signals, which have been used in experiments on fish since the 1990s [13]. Broadband echo sounders transmit a range of frequencies, usually frequency modulated signals, denoted FM [14]. The scattering of species varies with frequency, and thus FM signals can provide more information about a fish than CW signals [15]. In 2015, Kongsberg Maritime released the EK80 wideband scientific echo sounder, which transmits both FM and CW signals [16]. It was not until 2020 that it was discovered how well FM signals could be used for fish identification [17]. In their study of the classification of targets from TS and S_V using FM and simulated CW pulses, Benoit-Bird et al. saw how FM signals returned better results than CW [17].

The technology within acoustics is still limited in fish farming and not as developed as it is for target classifications and surveys [12, 18]. In fish farming, the technology is increasingly used where in commercial aquaculture, CW echo sounders are applied to optimize feeding and monitor the fish's behavior [19, 20]. The echo sounders are usually not split beam and cannot see the fish's position when swimming through the beam [12]. However, echo sounders have been implemented in more advanced areas in recent years. SalMar has a pilot project for offshore salmon farming called "Ocean Farm 1". They use twelve Simard EK80 echo sounders to monitor the behavior of salmon, biomass, gas bubbles, feed, and more [21]. Sintef Ocean, in cooperation with the Hellenic Centre for Marine Research in Greece, started "PerformFish" in 2020. As "Ocean Farm 1", they are using Simard's echo sounders to measure the biomass of the salmon [22].

The application of acoustics in research has become increasingly appealing regarding the submerged cages, and the study of the welfare of farmed salmon, in which results from four experiments are examined [23–26]. Each of the experiments had one or more cages submerged to 3 m [23], or below 10

[1] FM and CW signals will be further explained in Section 2.1

m depth [24–26], and they all applied a PC-based echo integration system to measure the echo intensity. Echo integration is used when calculating the backscattered signals from a volume of multiple depths (ref. Subsection 2.3.4) [9]. The results of the echo integration from the 22 days of submergence at 3 m depth from [23] can be seen in Fig. 1.1.

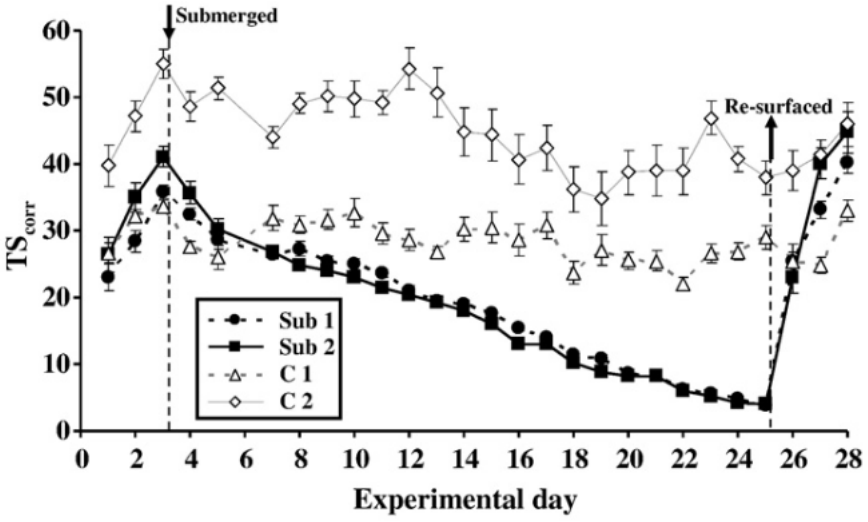

Figure 1.1: Total target strength corrected for biomass (TS_{corr}) given as means per day ± standard error (SE) for two submerged (Sub 1 and sub 2) and two control cages (C1 and C2) over the 28-day experimental period. TS_{corr} is a relative quantity and has no unit. (Text and figure taken from [23], pp. 259). The stippled vertical lines on days 3 and 25 represent the days for submerging and resurfacing the cage.

The 28-day experimental period and TS_{corr} for C1 and C2, and Sub1 and Sub2 are seen in Fig. 1.1. The total target strength is denoted TS_{corr}. However, the notation, in this case, is deceptive, as TS_{corr} is the total echo strength for the measured volume divided by biomass to adjust for the growth in size, and TS is normally a measure of intensity from a single target [23]. For both Sub1 and Sub2, the TS_{corr} was decreasing rapidly during the first days before it started to decrease linearly from day 5 [23]. After 22 days of submergence (on day 25), TS_{corr} were 5-7 times lower compared to day 3. Throughout the experiment, the swimming speed was measured, where the fish in Sub1 and Sub2 swam 1.6 times faster than the fish in C1, and C2 [23]. Further, the results from [24] are presented in Fig. 1.2, where the cages where submerged below 10 m depth.

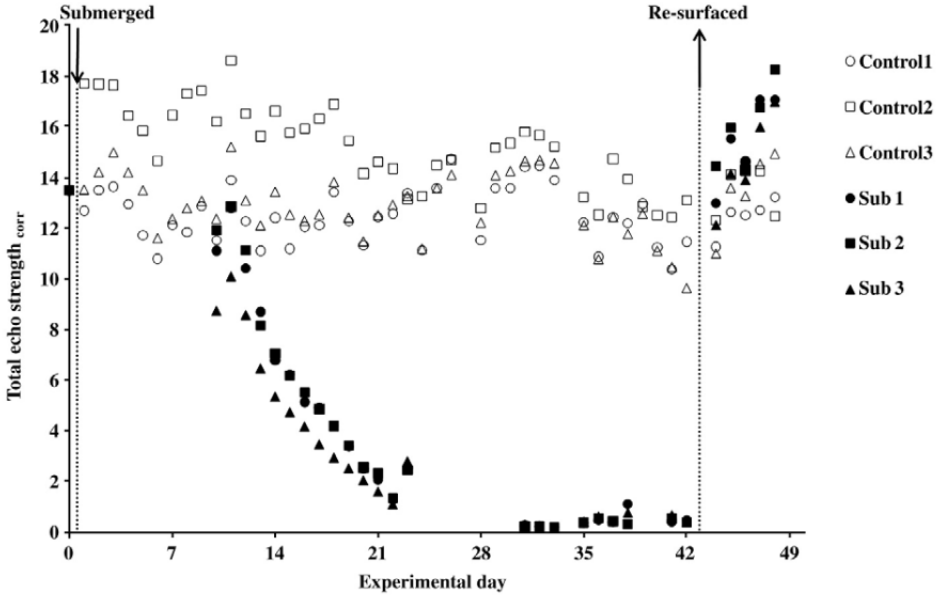

Figure 1.2: Total echo strength$_{corr}$ (corrected for biomass) given as means per day for three submerged (Sub1, Sub2, and Sub3) and control cages (Control1, Control2, and Control3) over 50 days. Day 0 was the measurement prior to submergence, and day 43 was the day where the submerged cages were resurfaced (text and figure taken from [24], pp. 328)

Fig. 1.2 shows the mean total echo strength corrected for biomass as a function of days for six cages: Sub1, Sub2, Sub3, Control1, Control2, and Control3. The vertical stippled lines represent the day of submergence and the day of resurfacing. There are some missing values between days 2 and 10, but a linear decrease is seen from day 11 until almost no echo intensity some day between days 23 and 31. The fish in the submerged cages swam 1.3 – 1.4 times faster than in the control cages. Furthermore, in [25], three cages were submerged to 10 m depth which were submerged for eight weeks and resurfaced once a week, and the results can be seen in Fig. 1.3.

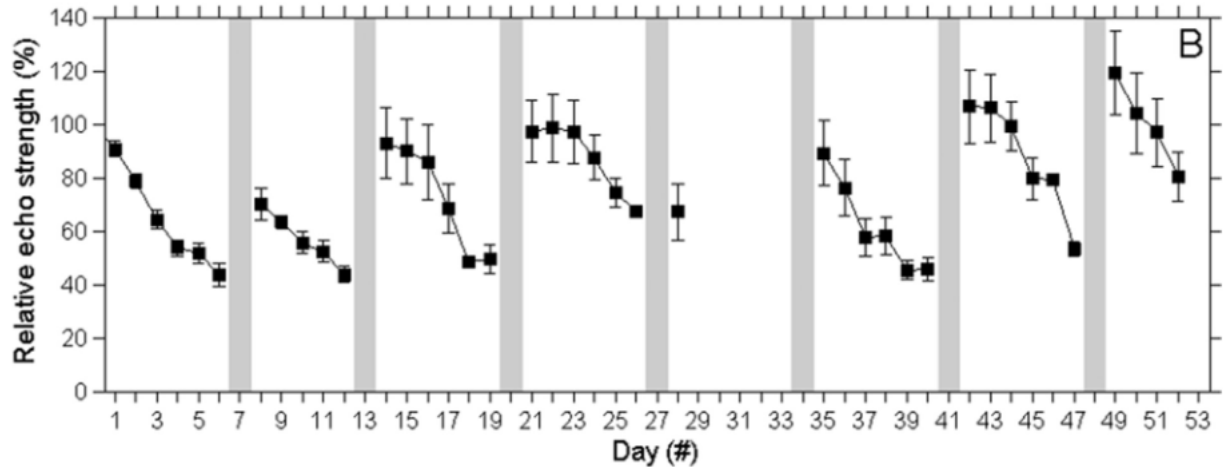

Figure 1.3: Percentage echo strength ± SE compared to total echo strength of the submerged fish in the hours after the first submergence. Some data points are missing due to a malfunction of the echo sounder system. Vertical grey bars indicate days of lifting of the nets and surface access (Text and figure taken from [25])

The change in relative echo strength [%], which is the echo strength relative to the total echo strength measured of the salmon right after the cages were submerged on day 1 is shown in Fig. 1.3. The gray bars are the days when the cages were lifted, and the salmon had access to the surface. During the experiment, the relative echo strength exceeded 100 %, which means the measured echo strength was higher than what was measured on day 1 [25]. As in [23], the echo strength decreased quite rapidly and linearly after the salmon was submerged. The swimming speed of the submerged fish was 1.4 – 3.4 times faster than the control fish [25]. Lastly, the results from [26] is presented in Fig. 1.4

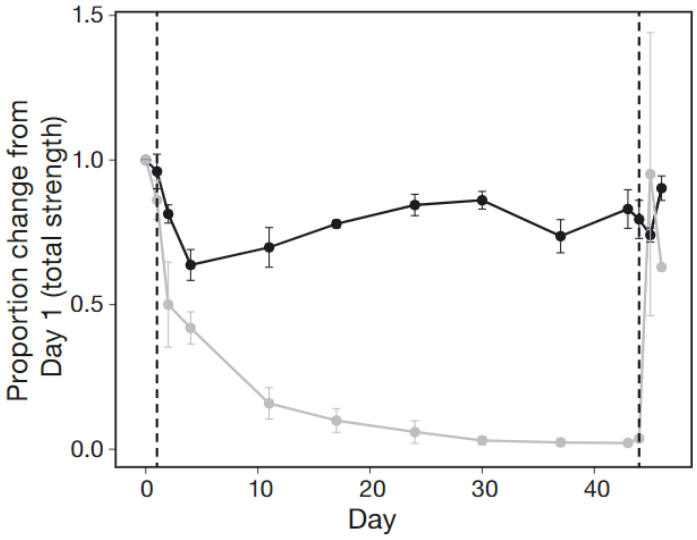

Figure 1.4: Proportion change in echo strength for the control (black) and submerged (grey) salmon cages. Data are means ± SE recorded 13 times throughout the experimental period. Vertical dashed lines represent submergence and resurfacing of submerged cages; n = 3, except for the last time point for submerged cages when n = 1 due to hardware error. (Text and figure taken from [26], pp. 505)

Fig. 1.4 shows the average total target strength per day for the 42 days experimental period for three submerged cages, and three control cages [26]. The total strength decreased more rapidly during the first week and was almost 0 at the end of the experiment. In addition to the acoustical measurements, they measured the swimming speed in the cages, where the speed of the fish in the submerged cages was 1.64 times faster than in the control cages [26].

Based on the results from [23–26], the overall echo intensity is expected to decrease and the swimming speed to increase. However, due to the divergent results, how fast the decrease in echo intensity will occur is difficult to predict. Common for the four experiments is the use of echo intensity from an echo sounder transmitting CW signals, which has not been calibrated [18]. In addition, the results are presented differently in each of the publications, expressing relative values. The use of calibrated, scientific echo sounders transmitting CW and FM signals and studying swimming speed and TS of individual farmed salmon in a submerged cage has not been done and is in the preliminary stages of research [18, 27].

Furthermore, Knudsen et al. [28] studied the correlation between TS and length of Atlantic salmon using Simard's EK60 echo sounders, transceiving frequencies at 120 and 200 kHz. The experiment

resulted in a linear relationship between the two parameters, where the target strength increased with the increasing fish length. For a 38 cm long salmon with normal conditions: access to the surface and neutral buoyancy, the anticipated TS values are -30 dB re. 1 m^2 from 120 and 200 kHz. The calculations are based on the Eqs. (2.27) and (2.28), defined in Subsection 2.3.3. Further, the expected TS from a lower frequency, 50 kHz, calculated using Eq. (2.26), is - 34 dB re. 1 m^2. As the air level decreases, a fish with an empty swim bladder is estimated to result in a TS value at - 55 dB re. 1 m^2, from Eq. (2.29) based on measurements from a 38 kHz echo sounder [29].

Various analytical and numerical models have been developed to increase the understanding of acoustic scattering from aquatic species, where models of the TS can be used to support the results from measurements. The Kirchhoff's-Ray mode (KRM) [30] is a hybrid between an analytical and numerical model of phystomous fish. In 2000, Horne et al. [31] estimated the TS from a two-chambered swim bladdered fish, *Acanthobrama terraesanctae*, by using KRM and compared the results with experimental measurements. The measurements were done using 120 kHz, and 420 kHz frequencies, where the measured results were less than the results from the KRM model [31]. Later, in 2008, Henderson et al. [32] studied how the orientation of the fish will affect the TS, and KRM simulations were an essential tool in the study. Using the acoustic wave's incident angle, they applied KRM to calculate the anticipated TS values. Further, Reeder et al. [15] measured the TS from a fish called alewife, using FM signals with a frequency range from 40 - 95 kHz. In addition, the TS was simulated for three frequencies within 20° of the main lobe, using the KRM model [15]. From the simulation, the TS values were very close to or just below the measured values [15].

1.3 Objectives

The main objective of this thesis is to use acoustic measurements to detect a decrease in the air level of the salmon swim bladder. The scientific echo sounders applied in the experiment transceive two pulse types, FM and CW, over three frequency bands, ranging from 55 to 260 kHz. The acquired data will be used to calculate the TS, S_V, the frequency response of TS and S_V, and the swimming speed. These parameters are studied to determine which is the first to indicate an insufficient air level based on signal type and frequency. In the prior work on salmon in submerged cages, echo sounder has not been the main focus of the study. The presented echo intensities have been based on relative values, thus, a prerequisite is that the scientific echo sounders are able to measure the TS from individual fish. If so, the goal is to quantify the decreasing TS of individual salmon as the air level in the bladder is diminishing. It will be examined whether FM signals can reveal more information than CW signals due to their frequency range.

Additionally, the intended post-processing software, LSSS, has been developed for CW signals and survey data. Thus, through this thesis, the post-processing tool will be explored to see if it is sufficient for FM signals, calculating the swimming speed, and processing data acquired from farmed salmon. Kirchhoff's-Ray Mode simulation will be used to model the swim bladder and to simulate the frequency response of TS and a decrease in TS as the volume of the swim bladder decreases.

1.4 Outline of thesis

Chapter 2 presents the theory of the thesis. It includes the basic theory of FM and CW signals, backscattering, target strength, and volume backscattering strength. In addition, it addresses the theory behind the tracking in LSSS. Further, Chapter 3 describes the experimental setup and the methods used to implement the experiment. Both the acoustic measurement methods and the complementary measurement methods will be described. Next, Chapter 4 presents Kirchhoff's Ray Mode (KRM) method used to simulate the TS for both CW and FM signals. The results obtained from the measurements and modeling are addressed in Chapter 5, while Chapter 6 includes an overall discussion of the methods used and the results from Chapter 5. Chapter 7 presents a conclusion and some further work. Lastly, the appendixes are included after the references, containing additional information and the scripts used when obtaining the data exported from LSSS.

Chapter 2

Theory

This chapter will address the theory behind the thesis. The theory of the two pulse types, FM and CW, the parameters of interest, TS, S_V, the frequency response of both TS and S_V, and swimming speed will be explained. Additionally, it includes a description of the post-processing software applied, LSSS.

2.1 FM and CW signals

Signals from an echo sounder, e.g., the EK80 echo sounder from Simrad [33], can be transmitted using either narrowband, referred to as CW (continuous wave) or broadband called FM (frequency modulated), signals. While CW is a sinusoidal signal consisting of one frequency, FM signals are transmitted over a broader range of frequencies [34]. FM signals are often sent as a chirp signal, which is a signal where there is a continuous, linear change in the frequency. The chirp is often sweeping from low to high frequencies [35].

The axial spatial resolution, ΔR, decides the quality and the details of the received signals. If the scatters from the targets are closer than ΔR, it will be difficult to distinguish between multiple targets as the received signals may overlap. Therefore, it is important to have a good spatial resolution and signal-to-noise ratio (SNR) when detecting single targets and measuring TS [14], Eq. (2.1),

$$\Delta R_{CW} = \frac{c\tau_{CW}}{2}, \tag{2.1}$$

from [14] shows how to determine the spatial resolution of CW signals, where c is the speed of sound in seawater and τ_{CW} is the duration of the emitted digital signal sent to the transceiver. The bandwidth, B, of the input FM signal can be used to express the output pulse duration, τ [14],

$$\tau = \frac{1}{f_2 - f_1} = \frac{1}{B}, \tag{2.2}$$

where f_1 and f_2 are the start and end frequency in the frequency band, respectively, which are further

used to derive the equation for the axial spatial resolution of FM signals,

$$\Delta R_{FM} = \frac{c}{2B}, \tag{2.3}$$

as shown in [14]. Both Eq. (2.1) and (2.3) are given in m. Higher frequencies provide a higher spatial resolution. This makes it easier to distinguish between targets within proximity, but the higher the frequency, the more energy is lost due to absorption [9]. Using FM signals instead of CW signals can improve the spatial resolution and SNR of the received data. The spatial resolution of FM signals, Eq. (2.3), is higher than for CW from Eq. (2.1), and it is, therefore, more accessible to detect single targets, e.g., in a dense fish shoal and aquaculture. However, since FM signals have a wider bandwidth, the data often include more noise than the data acquired from CW pulses. Due to the wide range of frequencies, FM data require more storage, and the speed of processing and analyzing may slow down [34].

For each frequency in the bandwidth, FM signals return TS and S_V values expressed as functions of frequency, TS(f) and $S_V(f)$, called the frequency response. As a result of their differences in behavior and structure, every species will have a different frequency response, making it possible to use acoustics to distinguish between them [9]. The frequency response from TS can provide information about the size of the species, where two minimums in the frequency band can be used to calculate the distance, d, between two objects [36],

$$d = \frac{c}{2\Delta f}, \tag{2.4}$$

where the two objects are, e.g., the top and bottom of the fish's body, or the swim bladder, Δf is the frequency band between the two minimums.

2.1.1 Processing of FM data using pulse compression

The EK80 Wide Band Transceiver [37], WBT, converts digital voltage signals, $\mathbf{y_{tx}}(n)$, to analog acoustical pressure signals, $\mathbf{y_{tx,a}}(t)$, where bold letters implies complex quantities. The analog signal is sent through the water column and scattered back to the transceiver, where the reflected pressure signals are filtered, amplified, and converted back to digital voltage signals [37]. Signal processing and filtering are necessary when targets are close to one another, as in a fish shoal or near a boundary. Processing of FM signals improves the SNR and the spatial resolution, making it easier to detect single targets [34]. The received signals from the WBT are run through a matched filter, called pulse compression, to improve the signals [38]. Fig. 2.1 illustrates a four-sectioned split-beam transducer, where each section, u_s, receives the signal.

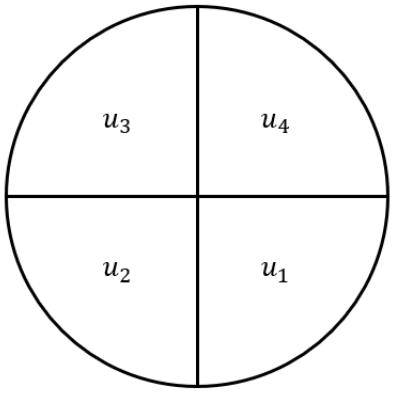

Figure 2.1: A four-sectioned split-beam transducer, where u_s represents the individual sections (modified from [38], pp. 7).

A four-sectioned split-beam transducer, as in Fig. 2.1, is used to estimate the angles and positions of the targets, where u_s is the s-th section and $s = 1,2,3,4$. The signal is filtered through a complex band pass filter before pulse compression to remove noise [38]. Additionally, it is decimated for a reduction in data, where the decimation takes place in multiple stages, v, where $v = 1,...,N_v$ and N_v is the number of filtering stages [38]. The output signal for each stage is denoted $\mathbf{y_{rx}}(n,u_s,v)$, where the last stage, $\mathbf{y_{rx}}(n,u_s,N_v)$, is the data saved as .raw files for further processing, e.g. in LSSS (ref. Section 2.4) [38]. In LSSS, the transmitted signal, $\mathbf{y_{tx}}(n)$, can be used to generate a normalized ideal transmitted signal [38],

$$\tilde{\mathbf{y}}_{\mathbf{tx}}(n) = \frac{\mathbf{y_{tx}}(n)}{\max(\mathbf{y_{tx}}(n))}. \tag{2.5}$$

Eq. (2.5) is filtered and decimated with the same methods as for $\mathbf{y_{rx}}(n,u_s,v)$. After going through N_v filter stages, the final output signal, $\tilde{\mathbf{y}}_{\mathbf{tx}}(n,N_v)$, for simplicity called $\mathbf{y_{mf}}(n)$, is applied in the pulse compression of FM signals [38],

$$\mathbf{y_{pc}}(n,u_s) = \frac{\mathbf{y_{rx}}(n,u_s) * \mathbf{y_{mf}}^*(-n)}{||\mathbf{y_{mf}}||_2^2}, \tag{2.6}$$

where $\mathbf{y_{mf}}^*(-n)$ is the complex conjugate, time-reversed version of the matched filter signal and is convoluted with the received signal [38]. $||\mathbf{y_{mf}}||$ is the l^2-norm of the matched filter [38]. The signals from Eq.(2.6) are obtained for each of the four quadrants, u_s, in the split-beam transducer. Further, the mean signal from all quadrants can be found and expressed as in [38],

$$\mathbf{y_{pc}}(n) = \frac{1}{4}\sum_{u=1}^{4} \mathbf{y_{pc}}(n,u_s). \tag{2.7}$$

Eq. (2.7) is used when calculating the total received power from all of the quadrants [38],

$$\mathbf{p_{rx,e}} = 4\left(\frac{|\mathbf{y_{pc}}(n)|}{2\sqrt{2}}\right)^2\left(\frac{|\mathbf{z_{rx,e}}+\mathbf{z_{td,e}}|}{\mathbf{z_{rx,e}}}\right)^2\frac{1}{|\mathbf{z_{td,e}}|}, \tag{2.8}$$

which is dependent on a receiver load, $\mathbf{z_{rx,e}}$, in series with the impedance of the transducer, $\mathbf{z}_{td,e}$ [38]. Eq. (2.8) is used when calculating the TS and S_V and will be further explained in Section 2.3.

2.2 Absorption

Absorption is when a part of the acoustic energy is converted to heat when a signal is sent through the water [39]. The process is dependent on the signal's frequency but also on the temperature and salinity of the seawater [9]. Absorption is expressed by α, which for seawater is given in dB/km [9]. When waves with higher frequencies interact with particles in seawater, the particles move faster, which leads to a more significant friction loss than with waves with lower frequencies. Additionally, the absorption is dependent on the thermal and chemical relaxation [39]. A standard algorithm used for calculating the absorption is the Francois & Garrison method [40], which is applied by Simrads EK80 echo sounders [41]. The absorption can be expressed using Np/km instead of dB/km using the ratio [39],

$$\text{Np/km} = 8.7\,\text{dB/km}. \tag{2.9}$$

2.3 Backscattering

2.3.1 Backscattering cross-section from a single target

Waves are the result of the transformation of electrical energy into acoustic energy. When the waves propagate through water, the acoustic energy is scattered in different directions if it interacts with a target, e.g., fish [42]. The scattering is dependent on the polar angle, θ, and the azimuth angle, φ, where $\theta \in [0,\pi]$ and $\varphi \in [0,2\pi]$. Fishery acoustics uses active echo sounders, meaning the echo sounder is used for transmitting signals. The transmitted signals are assumed to be plane pressure waves, the echo sounder is assumed to be in the far-field of the targets, and the speed of sound in the seawater is assumed constant [42]. The acoustic field close to the transducer is complicated, hence the targets are desired to be in the far-field of the transducer [39]. The far-field of a transducer is found by calculating the Rayleigh length [39],

$$r > \frac{\pi a_t^2}{\lambda}, \tag{2.10}$$

where a_t is the radius of the transducer and λ is the wavelength of the transmitted signal [39]. When the polar angle, θ, equals π, the signal is scattered back to the echo sounder, and this is known as backscattering [42]. The backscattering cross-section is defined as the extent to which a body scatters

sound back to the transducer and is given by Eq. (2.11) as shown in [42],

$$\sigma_{bs} \equiv \frac{I_{bs}}{I_p} r^2 = S_{bs}(\theta, \phi, \omega) A, \tag{2.11}$$

where I_{bs} is the intensity of the backscattered wave and I_p is the intensity of the plane incident wave at the target's position [42]. As the plane wave is scattered spherically, a geometric loss is included by introducing r^2, where r is the distance from the target to the echo sounder. The backscattering cross-section can be expressed using a scattering function, $S_{bs}(\theta, \varphi, \omega)$, and a cross-section area, A. The dimension of σ_{bs} is m^2 [42]. By using the relationship between the intensity and the pressure of the waves, along with current response and open-circuit free-field receiving voltage sensitivity, described in [43], the transmit-receive electrical voltage transfer function can be expressed as [43],

$$\left| \frac{\mathbf{V_R}}{\mathbf{V_T}} \right| = F_{VV} G(\theta, \varphi) \frac{\lambda}{4\pi} \frac{e^{-2\alpha r}}{r^2} \sqrt{\sigma_{bs}}, \tag{2.12}$$

where in Eq. (2.12), V_R and V_T are the received and transmitted electrical voltage, respectively, and $G(\theta, \varphi)$ is the transducer gain, defined in [43], and is the two-way electroacoustic "efficiency," dependent on the direction, (θ, φ). The two-way amplitude loss, $\frac{e^{-2\alpha r}}{r^2}$, is the loss due to absorption, α (ref. Section 2.2), here in Np/m, and spherical spreading, $\frac{1}{r^2}$. Lastly, F_{VV}, is the electrical impedance factor, defined in [43]. Further, the transfer function in Eq. (2.12) can be integrated over time to find the time-integral-voltage-squared (tivs) for the transmitted voltage signal [44],

$$[tivs]_T \equiv \int_0^{\tau_p} |V_T(t)|^2 dt, \tag{2.13}$$

and the received voltage signal [44],

$$[tivs]_R^{st} \equiv \int_{t_{st1}}^{t_{st2}} |V_R^{st}(t)|^2 dt. \tag{2.14}$$

The transmitted signal, Eq. (2.13), is integrated over the time duration of the signal, τ_p, and starts at t = 0. For the received voltage signal in Eq. (2.14), the superscript "st" specifies a received signal from a single target, e.g individual fish. The received signal has a time duration of,

$$\tau_{st} \equiv t_{st2} - t_{st1}, \tag{2.15}$$

where t_{st1} is the start and t_{st2} is the end time of the signal [44]. However, applying the peak value is often chosen for measuring individual targets instead of Eq. (2.14) [44]. The echo integral for the received signal is written as in [44],

$$[tivs]_{R,max}^{st} \equiv |V_R^{st}|_{max}^2 \tau_p. \tag{2.16}$$

Eq. (2.16) is a simplified estimate of Eq. (2.14), where $|V_R^{st}|_{max}$ is the maximum value of the backscattered signal. Going from Eq. (2.12), using Eqs. (2.13) and (2.16), to the backscattering cross-section is shown in [44], and results in,

$$\sigma_{bs} = \frac{16\pi^2 r^4 e^{4\alpha r}[tivs]^{st}_{R,max}}{G^2_{eff}(\theta,\varphi)\lambda^2 F^2_{VV}[tivs]_T}, \tag{2.17}$$

also known as the electroacoustic power budget equation for single targets. In Eq. (2.17), $G^2_{eff}(\theta,\varphi)$ an "effective" value of the gain to correct the error from applying Eq. (2.16) [44]. The derivation of Eqs. (2.12) - (2.17) is based on the theory from [43, 44] and the assumptions applied there. The electrical input values can be measured by an EK80 echo sounder and Eq. (2.17) is used to express the TS from FM and CW signals, explained in Subsection 2.3.3

2.3.2 Scattering from gas bubbles

Salmon use the swim bladder to maintain a natural buoyancy. From Archimedes's principle, neutral buoyancy is achieved when the body mass of salmon is equal to the volume of water displaced; salmon is neutral when the density of their body (tissue + air in the bladder) is equal to the density of the surrounding seawater [45].

The air in the swim bladder has a lower characteristic acoustic impedance than the surrounding water and tissue, $(\rho c)_{air} << (\rho c)_{surroundings}$. The high contrast in the characteristic acoustic impedance between air and surroundings is the main contribution to the backscattered intensity, where larger contrast leads to more scattering [9]. Foote showed in 1980 that the swim bladder accounted for more than 90 % of the TS from fish [10]. Due to behavioral similarities between swim bladders and gas bubbles, it can be assumed the bladder scatters the pressure wave the same way as a gas bubble [9]. The common swim bladder is usually cylindrical and surrounded by the fish's body, but in this approximation, the bladder is assumed to be a free, spherical gas bubble in water [9]. A bubble is at equilibrium when it is at rest, but once an external pressure wave influences it, it expands and contracts. When the frequency of the added force, e.g., from a pressure wave, matches the natural frequency of the bubble, the bubble resonates [9]. There will be a more significant scattering of intensities at the resonance frequency than at other frequencies [9]. The resonance frequency for a swim bladder can be calculated using Eq. (2.18) [9],

$$f_r = \frac{1}{2\pi a}\sqrt{\frac{3\gamma P_0}{\rho}}, \tag{2.18}$$

where a is the equilibrium radius of the swim bladder, P_0 is the ambient pressure, ρ is the density of seawater, and γ is the ratio of the specific heats of the air in the bubble, where γ = 1.4 for air [9]. The calculated resonance frequency of a swim bladder with a radius a = 0.006m (ref. Section 4.2), measured , at 1 m depth in seawater is 575 Hz. The same bladder at 14 m depth has the resonance frequency of 850 Hz. Normally, Eq. (2.18) is used for free gas bubbles only surrounded by water, but it

can be applied as an approximation for the swim bladder's resonance frequency [9]. The theoretical scattering cross-section of a gas bubble as derived in [42] is given by Eq. (2.19),

$$\sigma_s = \frac{4\pi a^2}{\left[(\frac{\omega_R}{\omega} - 1\right]^2 + \delta^2}. \tag{2.19}$$

The equation includes the resonant angular frequency, ω_R, the angular frequency, ω, and the damping, δ which is comprised of three different fragments [42],

$$\delta = \delta_v + \delta_r + \delta_t, \tag{2.20}$$

where δ_r is due to reradiation, δ_v is due to the shear viscosity in water, and δ_t is due to the thermal conductivity in gas [42].

2.3.3 Target strength

The values of σ_{bs} can often be very small or very large and increase/decrease exponentially. Therefore, expressing the values using decibel (dB) is appropriate. Target strength, TS, is defined as the logarithmic values of σ_{bs} and is defined as [9],

$$TS = 10log_{10}\left(\frac{\sigma_{bs}}{A_1}\right) \qquad [\text{dB re. } 1m^2], \tag{2.21}$$

were A_1 is a reference area, $A_1 = r_1^2 = 1m^2$ [9]. The processing software, LSSS, applies σ_{bs} from Eq. (2.17) and $\mathbf{p_{rx,e}}$ from Eq. (2.8) when obtaining the TS(f). The mathematical transition from σ_{bs} to TS is not that simple, but from [38], TS(f) is given by,

$$TS(f) = 10log_{10}(P_{rx,e,t}(f)) + 40log_{10}(r) + 2\alpha(f)r - 10log_{10}\left(\frac{\mathbf{p}_{tx,e}\lambda^2 g^2(\theta,\varphi,f)}{16\pi^2}\right). \tag{2.22}$$

Here, $\mathbf{P_{rx,e,t}}$ is the Fourier transform of Eq. (2.8), $\mathbf{p_{tx,e}}$ is the transmitted electrical power, and g is the transducers gain [38]. In addition, the equation addresses the absorption from Section 2.2, here given in Np/m. Eq. (2.22) can be used for both FM and CW signals, where TS(f) for the CW signals are independent of f, and $\mathbf{P}_{rx,e,t}$ is the received power before pulse compression. There will be TS values for each frequency in the frequency band from FM signals, and to obtain a single TS value from the FM data, the average of TS(f) is calculated. Since TS is logarithmic, the values are converted from logarithmic to original units,

$$\sigma_{bs} = 10^{\frac{TS}{10}}. \tag{2.23}$$

Following [46], the average of each $\sigma_{bs,k}$ in the frequency band is found,

$$\overline{\sigma}_{bs} = \frac{1}{n}\sum_{k=1}^{n}\sigma_{bs,k}, \tag{2.24}$$

where n is the number of $\sigma_{bs,k}$ observations. Using Eq. (2.21), the mean TS can be calculated as,

$$\overline{TS} = 10log_{10}(\overline{\sigma}_{bs}). \tag{2.25}$$

Further, TS is strongly dependent on the angle of the target relative to the direction of the incident pressure wave, shown by [47], as seen in Fig. 2.2.

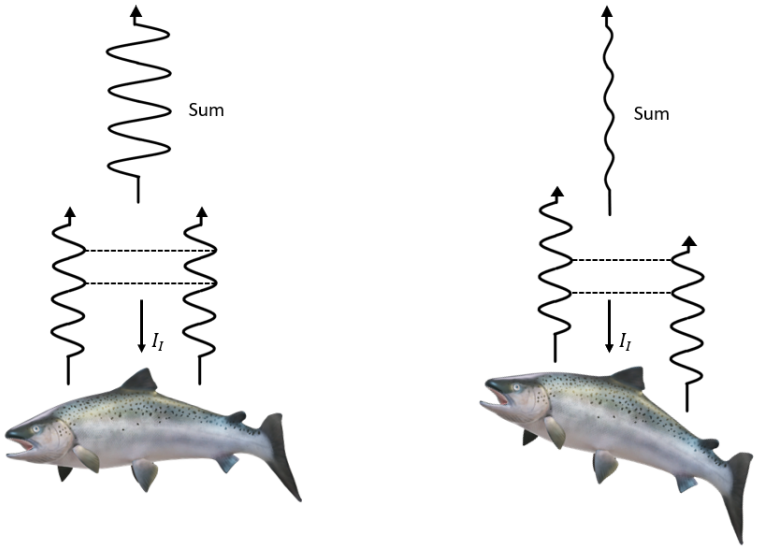

Figure 2.2: Horizontal swim bladder increases the returned signal. Tilted fish creates destructive interference and a returned signal smaller than the original signal (Modified from [9], pp. 57).

Fig. 2.2 illustrates how the swim bladder of a fish swimming with a tilt affects the scattered signal. When the fish is horizontal (left), each of the backscattered waves is in phase and creates a signal with a strong amplitude [9]. In contrast, if the fish is tilted (right), the backscattered signals will be out of phase, generating destructive interference and a returned signal with a small amplitude [9]. Furthermore, a horizontal fish has a greater cross-section area, A, (ref. Eq. (2.11)), which returns a stronger backscattered signal than a tilted fish [9]. Thus, the TS is highly dependent on the length and shape of the swim bladder. Experiments have been done to derive equations for theoretical TS as a function of the fish's length, L in cm. [47] expresses TS as a function of the length of salmon based on data from a 50 kHz echo sounder,

$$TS = 24.2log_{10}(L) - 72.0. \tag{2.26}$$

Knudsen et. al [28] used a 120 kHz and a 200 kHz transducer and found the correlation between the length of salmon and the TS. The experiment resulted in the two equations,

$$TS = 25log_{10}(L) - 69, \tag{2.27}$$

and,

$$TS = 24.7log_{10}(L) - 69.3, \tag{2.28}$$

where Eq.(2.27) is for 120 kHz and Eq. (2.28) is for 200 kHz. The constants in Eqs. (2.26) - (2.28) are found empirically. For fish without a swim bladder, the length-dependent TS,

$$TS = 20log_{10}(L) - 86.5, \tag{2.29}$$

is found by [29] using a 38 kHz echo sounder. The equation can be applied, e.g., when calculating the TS of a physostomous or physoclistous fish with an empty swim bladder.

2.3.4 Volume scattering coefficient, backscattering from multiple-targets

TS is a measure of the backscattered signal of individual targets [9]. However, sometimes the fish is too close to measure the TS, e.g., in a fish shoal or when studying the biomass. Hence, the volume backscattering coefficient,

$$s_v = \frac{\sum \sigma_{bs}}{V}, \tag{2.30}$$

is used instead, which is given in m^{-1} [9]. To calculate the volume backscattering coefficient, it must be assumed that the scattered intensities from each target in the volume can be summarized. In addition, only the direct scatter is considered, and both the multiple scattering effects and the scattering between targets are ignored [48]. Eq. (2.30) summarizes all the backscattered signals from the targets measured from a volume, V. An observation volume, V_{obs}, is illustrated in Fig. 2.3, which is assumed to be in the far-field of the transducer [43]. Additionally, the echos in the volume are assumed to have random phases, and the effect of volume scattering of power extinction is assumed to be neglectable [43].

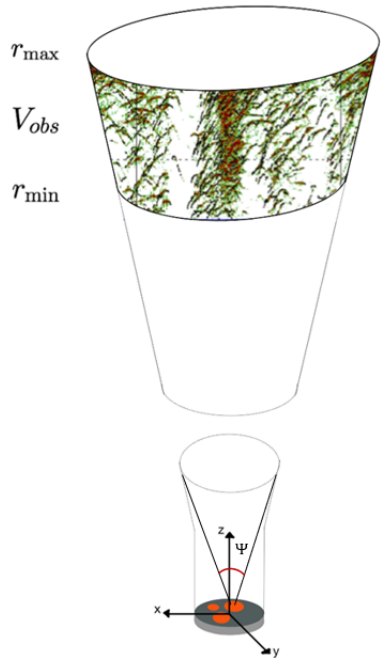

Figure 2.3: A transducer transmits signals in the positive z-direction, showing the observation volume, V_{obs}, ranging from r_{min} to r_{max} (Modified from [43], pp. 20).

Fig. 2.3 illustrates three transducers transmitting signals facing upwards, measuring the observation volume, V_{obs}, which ranges between r_{min} and r_{max}. The thickness of V_{obs}, ΔR_V, is, [43]

$$\Delta R_V = r_{max} - r_{min}. \tag{2.31}$$

However, the spatial extension of the transmitted ping insonifying the observation volume is assumed to be much smaller than V_{obs}, $c\tau_p << \Delta R_V$. The insonified volume by the ping is defined as the "ping volume", V_p, with a thickness of $dr_p \equiv r_{p_2} - r_{p_1}$ [43]. Further, as explained in [43] s_v can be defined as the sum of $\Delta\sigma_{bs}$ per unit volume, ΔV,

$$s_v = \lim_{\Delta V \to 0} \frac{\Delta\sigma_{bs}}{\Delta V} \equiv \frac{d\sigma_{bs}}{dV}, \tag{2.32}$$

which is used to derive the electroacoustic power budget equation for volume backscattering measured by the EK80 echo sounders. The size of dV is found [43],

$$dV = \frac{c\tau_p r^2 d\Omega}{2}, \tag{2.33}$$

were $d\Omega \equiv sin\theta d\theta d\varphi$ is the 3D solid angle, given in steradians [sr], and is used to derive the equivalent two-way beam solid angle, ψ, from Fig. 2.3. "Formulation D" from [44] is used by the processing software to obtain s_v, which is given by,

$$s_v = \frac{32\pi^2 r^2 e^{4\alpha r}[tivs]_R^v}{G_{0,eff}^2 \psi \lambda^2 c\tau_g s_{a,corr}^2 F_{VV}^2 [tivs]_T}, \tag{2.34}$$

where $G_{0,eff}^2$ is a calibration factor defined in [44], $s_{a,corr}^2$ is the relationship between the actual average electrical power and the "maximum average electrical power" of the same echo [44]. τ_g represents the gate opening and closure time of the "gated volume" from the received signal [44]. Eq. (2.34) is applied when obtaining the volume backscattering strength, S_V (explained in Subsection 2.3.5). Further, from [44],

$$[tivs]_R^v \equiv \int_{t_{g1}}^{t_{g2}} |V_R^v(t)|^2 dt, \tag{2.35}$$

is the time-integral-voltage-squared for the received signal, integrated over the "gate opening time", $\tau_g = t_{g2} - t_{g1}$. Lastly, the two-way beam solid angle of the transducer, as seen in Fig. 2.3 [43],

$$\psi = \int_{4\pi} |\mathbf{B}_i(\theta,\phi)|^4 d\Omega, \tag{2.36}$$

includes the beam pattern of the incident pressure wave, $\mathbf{B}_i(\theta,\varphi)$. The producer usually provides this value and the value of the circular beam width, BW, in the transducer's manual. From the circular beam width, the diameter, b, of the beam at a certain distance, d, can be calculated using trigonometry,

$$b = 2d \cdot tan\left(\frac{BW}{2}\right), \tag{2.37}$$

where d is the distance from the transducer surface to b, given in m. The observation volume is calculated using,

$$V_{obs} = \frac{\pi}{3} \cdot \Delta R_V \cdot \left(\left(\frac{b_1}{2}\right)^2 + \left(\frac{b_2}{2}\right)^2 + \frac{b_1}{2} \cdot \frac{b_2}{2}\right), \tag{2.38}$$

where b_1 is the diameter at r_{min}, b_2 is the diameter at r_{max}, illustrated in Fig. 3.5. V_{obs} consists of a continuous succession of thin ping volumes, V_p. Since s_v from Eq. (2.34) is a measure of the volume backscattering coefficient from V_p, s_v has to be integrated from r_{min} to r_{max} to obtain the area backscattering coefficient of V_{obs} [44],

$$s_a \equiv \int_{r_{min}}^{r_{max}} s_v(r) dr. \tag{2.39}$$

s_a is a dimensionless coefficient, and due to this, the nautical area scattering coefficient (NASC),

$$s_A = 4\pi 1852^2 s_a, \tag{2.40}$$

is often applied instead of s_a [44], by processing tools such as LSSS.

2.3.5 Volume backscattering strength

As for the backscattering cross-section, the volume scattering coefficients are often very small or very large, and the logarithmic values are preferred [9]. s_v expressed in dB re. 1 m^{-1} is given by [38],

$$S_V = 10log_{10}\left(\frac{\sigma_{bs}}{V}\right) \tag{2.41}$$

which is defined as the volume backscattering strength. The S_V applied by the processing software uses the power-budget equation as shown in [38],

$$S_V(f) = 10log_{10}(\mathbf{P_{rx,e,v}}(f)) + 20log_{10}(r) + 2\alpha(f)r - 10log_{10}\left(\frac{\mathbf{p_{tx,e}}\lambda^2 ct_w\psi(f)g_0^2(f)}{32\pi^2}\right), \tag{2.42}$$

and is based on s_v from Eq. (2.34). The mathematical transition from Eq. (2.34) to Eq. (2.42), is done by [38], but will not be accounted for in this thesis. $\mathbf{P_{rx,e,v}}$ is the received electrical power from the volume [38]. The two-way equivalent beam solid angle, ψ, is a function of the frequency and is an empirical estimate of ψ and the nominal frequency, f_n, shown in [38]. Additionally, Eq. (2.42) depends on the duration of the time window, t_w, and r is, in this regard, the distance to the center of the volume, $r = ct_w$, and $g_0^2(f)$ is the transducer gain on-axis [38]. As S_V is in logarithmic values, Eqs. (2.23) - (2.25), are applied in order to calculate the average value S_V.

2.4 LSSS algorithms

Large Scale Survey System [49], LSSS, was developed by the Institute of Marine Research and CMR/NORCE and is used for interpreting survey data from echo sounders. This is a post-processing tool that consists of several processing modules. Which modules to use is determined by the desired output information, e.g., splitting recordings from channels with different acoustic frequencies into separate files or tracking individual fish to retrieve TS, the frequency response of TS, or the fish's position [50].

Tracking is applied to distinguish between individual fish from acoustic measurements acquired from echo sounders, where a single track belongs to an individual fish swimming through the acoustic beam, see Fig. 2.4. One track is a successive detection of pings, where one ping equals a detected reflection from a single fish. It is impossible to identify the same fish if it swims through the beam more than once during the measurement period, hence, one fish can be tracked multiple times. The tracking in LSSS is done in multiple steps, where the first step is to select samples that are likely to be representative of a single individual for each ping. Samples are selected according to one of several algorithms, which will be further explained. Then, a prediction of the following sample is conducted within the same track for each selected sample. For the next measured ping, the samples are chosen

according to the same algorithm as for the previous ping. If the sample matches the criteria specified for the predicted sample, it will be associated to the track [50]. Through this process, successive pings are investigated to determine whether they may belong to the same track based on a set of criteria. A further investigation of the potential tracks follows: among the criteria are a minimum length and a maximum number of pings missing a sample that would be accepted, according to the algorithm [50].

The selection of samples occurs according to one of the three algorithms in LSSS: aggregation, SED (single-echo detection), and peak, where aggregation is from Handegards publication [51]. Candidate samples are detected in each ping based on the TS. The TS-value must exceed a defined TS threshold, provided their gain compensation (based on the beam shape) is less than a given maximum [50].

For the peak algorithm, several samples that are candidates to belong to different individuals are selected for each ping. The algorithm employs the same criterion for a sample as aggregation, as well as it requires that samples belonging to one track must not be too close to other targets (based on split-beam data) [50]. Peak is a modification of the SED algorithm implemented for the Simrad EK500, EK60, and EK80 split-beam echo sounders. However, the samples are very dense due to the high spatial resolution of the EK80 echo sounders, and an individual fish may have two maxima of equal strength. In contrast to SED, which considers those tops as two separate targets and rejects both, peak considers the two close local maxima as the same target [50]. The tracking algorithms return one track per fish, which can be seen in Fig. 2.4.

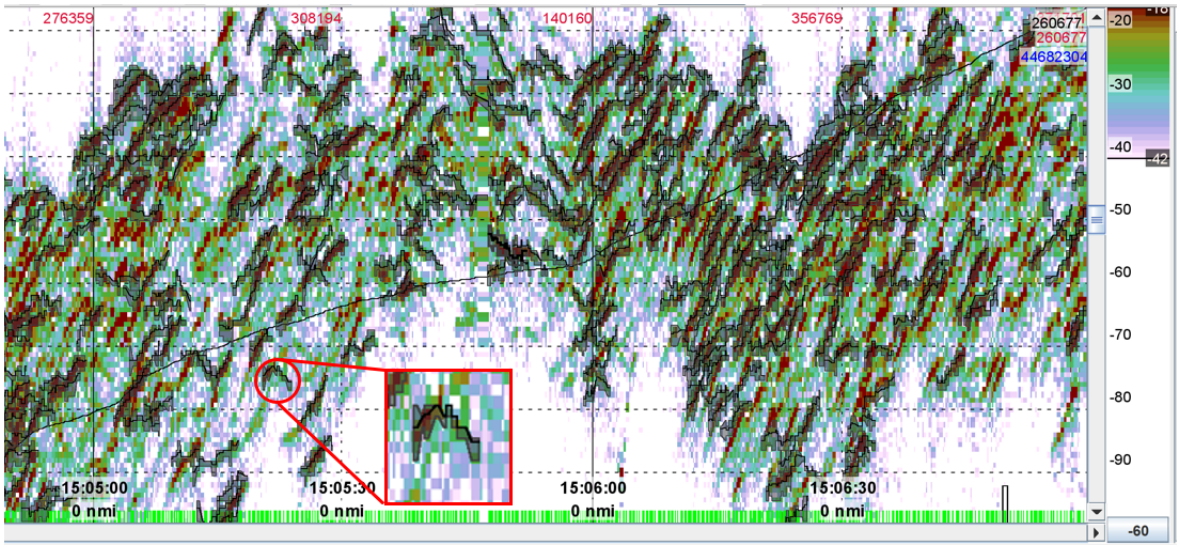

Figure 2.4: FM data from a 70 kHz echo sounder of a fish shoal after being tracked using the aggregation algorithm. The thick black lines represent one track, seen in the red square. The right side shows the dB threshold.

Fig. 2.4 shows a fish shoal as seen in LSSS, which was acquired from a 70 kHz FM echo sounder. Individual fish, before tracking, are represented by the dark red color, which indicates a high dB re 1 m^2 level (the dB threshold is seen on the right side of the figure). When the data has been tracked, the output files include tracks for individual fish, seen as dark black lines surrounding the fish in the red square. The tracks include, amongst others, a timestamp, and x, y, and z positions for each ping in the

track. Before finding the total time of the track, the time difference between ping n+1 and n is found,

$$t_q = t_{n+1} - t_n, \tag{2.43}$$

where n is the number of pings in the track, and t_q is the time difference between the pings. The total time is then found,

$$t_{tot} = \sum_{q=1}^{n} t_q, \tag{2.44}$$

which summarizes the time differences, t_q, between each ping, n. The distance, d_q, between each ping is found by using the x, y, and z positions for ping n+1 and n,

$$d_q = \sqrt{(x_{n+1} - x_n)^2 + (y_{n+1} - y_n)^2 + (z_{n+1} - z_n)^2}, \tag{2.45}$$

and the total distance swam by the fish is then calculated by,

$$d_{tot} = \sum_{q=1}^{n} d_q. \tag{2.46}$$

From Eqs. (2.44) and (2.46) the total swimming speed of a fish can be calculated,

$$v_m = \frac{d_{tot}}{t_{tot}}, \tag{2.47}$$

given in m/s or in body length per second, bl/s,

$$v_b = \frac{v_m}{BL}, \tag{2.48}$$

where BL is the body length of the fish given in m. The experimental standard deviation, s_{v_m}, of the swimming speeds within a selected file, can be found [46],

$$s_{v_m} = \sqrt{\frac{\sum_{j=1}^{k} (v_{m,j} - \overline{v_m})^2}{k-1}}, \tag{2.49}$$

where $v_{m,j}$ is the j-th value, $\overline{v_m}$ is the average of the swimming speed within the file, and k is the number of tracks.

2.5 Linear regression

Linear regression can be applied to calculate a linear fit to scattered values. This can be of interest, e.g., to see how the overall trend is changing over a period and is illustrated in Fig. 2.5 [52].

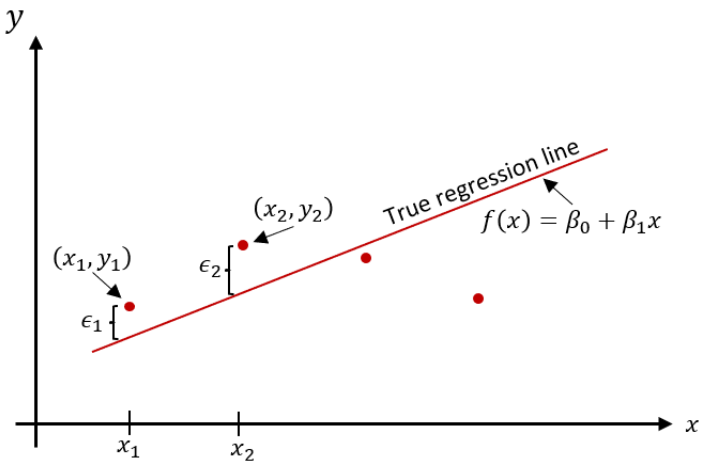

Figure 2.5: The regression line $f(x) = \beta_0 + \beta_1$ calculated to fit the scattered values (x_i, y_i). The vertical deviations from the true regression, ϵ, is drawn for each position (Modified from [52], pp. 618)

The points in Fig. 2.5 are randomly scattered around the true regression line. In order to obtain the line that fits the scattered value the best, the principle of least square is applied [52]. The principle proposes a measure of the best possible fit between the scattered values and the linear line and consists of the relationship between x, an independent variable, and y, a dependent variable, [52],

$$Y = f(x) + \epsilon = \beta_0 + \beta_1 x + \epsilon, \tag{2.50}$$

were f(x) is the true regression line, β_0 is the intercept coefficient and is described as the value of y when x = 0, and β_1 is the slope coefficient, which is the increase in y when x increases. ϵ, is a random deviation from the linear line, called true error, seen in Fig. 2.5 [52]. How well the true regression line fits the scattered values are described by the coefficient of determination [52],

$$R^2 = 1 - \frac{SSE}{SST}, \tag{2.51}$$

where SSE is the error sum of squares and SST is the total sum of squares, as explained in [52]. Eq. (2.51) is used to describe how much of the total variation is explained by the linear relationship. A R^2 value close to 1, implies the linear regression model (Eq. (2.50)) has done a great job in justifying the y variation [52]. The true regression line can be used to calculate the total increase or decrease through a period by implementing,

$$\text{increase/decrease} = \frac{f_N - f_1}{f_1} \times 100\%, \tag{2.52}$$

which uses the first and last, N, values of the regression line and returns the decrease/increase in percentage.

Chapter 3

Experimental setup and method

This chapter addresses the setup in the experimental aspect of the thesis. It includes a description of the sampling techniques used for acquiring echo data, camera data, and how the data was post-processed.

3.1 Location and experimental setup

The experiment was conducted in Matre, western Norway, at the Cage Environmental Laboratory at the Institute of Marine Research's field station Smørdalen (see Fig. 3.1). Smørdalen and the cages that were used are located in the inner part of Masfjorden. The Norwegian Food Safety Authority approved the experiment with the FOTS-id 26559.

Figure 3.1: Location of the experiment, 1.5 hour drive from Bergen. The Cage Environmental laboratory is shown in the red ellipse at the top left corner (*Google maps, 2021)*

Fig. 3.2 shows the cages in Smørdalen from above. The cage used, cage 16, had the dimensions 12x12 m^2 wide and long and 14 m deep, and is circled with red in the picture.

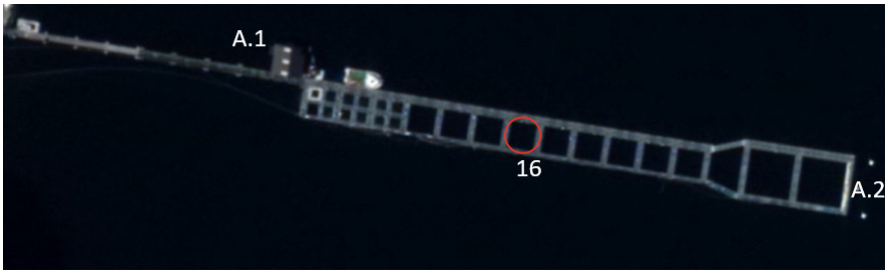

Figure 3.2: The Cage Environmental Laboratory seen from above. A.1: house where the computer was placed. 16: cage 16. A.2: placement of ABF bouy (*Google maps, 2021)*

Three transducers with frequencies 70 kHz, 120 kHz, and 200 kHz were used to measure the TS, S_V, and salmon's position. The transducers were mounted in a gimbal, a tool used to stabilize the transducers. The gimbal levels the transducers horizontally even when there are disturbances in the water column or if the ropes have different lengths. Fig. 3.3 shows the transducer setup and the gimbal. Each echo sounder consisted of an EK80 scientific wide-band transceiver (WBT) from Kongsberg Maritime [37] connected to a transducer.

Figure 3.3: Transducer setup and gimbal, illustrating how the transducers were facing upwards when placed underneath the cage

On the 12th of March 2021, defined as day -7 in Table 3.1, the transducers were set as active and started transceiving signals. A pan-tilt camera mounted on a profiling winch [53] was placed in the cage to study the fish visually and their behavior during the experiment (see C in Figs 3.4 and 3.5). The camera was controlled from a computer placed in Fig. 3.2 A.1, and could be moved vertically and 360 degrees around its own axis. Further, a blue led light 400W [54] was placed at 8 m depth to study the behavior every other night (B in Figs. 3.4 and 3.5). The light will not be further discussed in this

thesis as it was used for a different experiment [55]

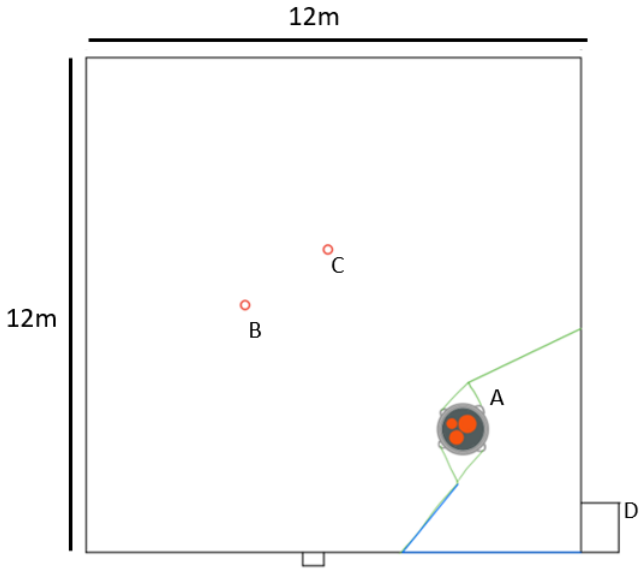

Figure 3.4: The 12x12 m^3 cage setup seen from above. A: transducers. B: light. C: camera. D: box with EK80 WBT

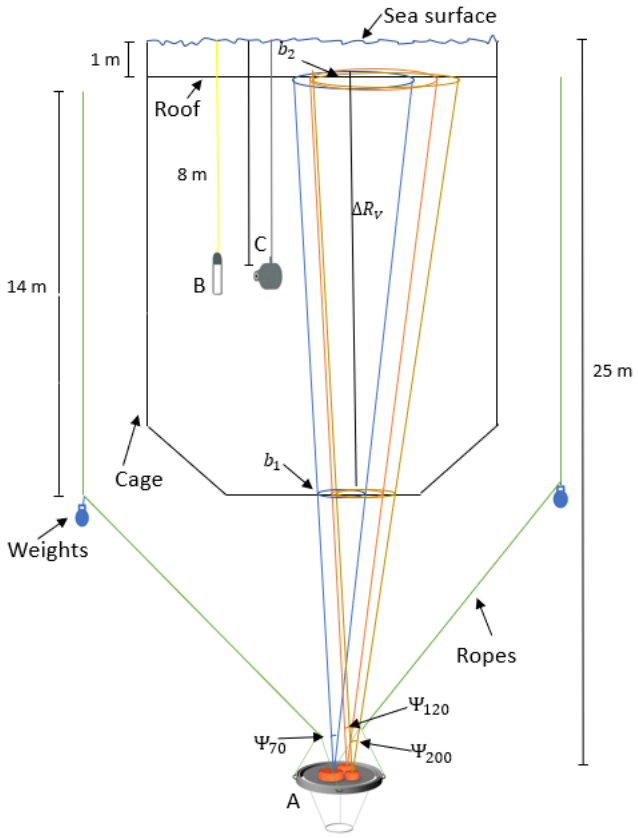

Figure 3.5: The cage setup seen from the side. A: gimbal and transducers at 25 m below the sea surface, B: light and C: camera 8 m depth. The roof was attached 1 m below the sea surface. b_1 was the beam width at 14 m depth, b_2 was the beam width at 1 m depth (ref. Eq. 2.37), ΔR_V was the length of the beam, from b_1 to b_2. Note this is an schematic drawing and is not proportionally correct.

Fig. 3.4 and 3.5 show how the camera and light were positioned in the cage relative to the transducers. The light and camera were placed in the middle of the cage, B and C, respectively. The EK80 WBTs were placed in a box in D, covered by a tarpaulin to prevent seawater and rain from reaching the electronics. Further, the transducers were placed at the corners of the cage as salmon normally swim in circles rather than in the center. Hence, the individual salmon will swim through the beams multiple times in an hour, resulting in a new track for the fish each time it swims through the beam. Fig. 3.5 shows how the gimbal was attached to a rope on either side and moored to the cage. The 200 kHz echo sounder were placed 2 cm from both the 70 and 120 kHz echo sounders, while the 70 and 120 kHz echo sounders were placed 1.8 cm from each other. The transducers were hung facing upwards, at 25 m beneath the sea surface and 10 m below the cage bottom. Two weights were attached to the ropes to prevent them from leaning against the cage. Note that the illustrations in Figs. 3.4 and 3.5 are not proportionally correct.

The equivalent two-way beam solid angle, ψ, in Fig. 3.5 is 0.009 sr for each of the transducers, and the circular beam width, BW, is 7° [33, 56, 57]. From Eq. (2.37) the theoretical beam width, b_2 in Fig. 3.2, at 1 m from the surface was approximately 3.0 m, and at 15 m, b_1, the width was 1.2 m, and was the same for all three transducers. The total sampling volume inside the cage, calculated using Eg. (2.38), from 1 m to 15 m was 43 m^3. The 70 kHz, 120 kHz, and 200 kHz transducers had diameters of 250 mm [33], 180 mm [56], and 120 mm [57], respectively. From Eq. (2.10) the far-field of the 70 kHz echo sounder is between between 2-3 m for the 55 - 90 kHz frequency band, for the 120 kHz frequency band, the far-field is from 1.5 - 2.7 m from the transducer, and for the 160 - 260 frequency band from the 200 kHz echo sounder, the far-field is 1.2 - 2 m.

The Gantt Chart in Table 3.1 shows the timeline of the experiment. On day 0 at 17.30 local time, a white roof, made from the same material as the net, was sewn onto the net cage at approximately 1 m depth to prevent the fish from reaching the sea surface. The roof was attached during the 28 days of submerging the cage. On day 24, a Mid-Norwegian ring [58] was placed diagonally from the transducers underneath the cage. The ring produced air bubbles of sizes varying from 1 – 14 mm to give the salmon a possibility to refill their swim bladder. Since the bubbles disrupted the echo sounder signals, the bubbling was turned on and off every 30 minutes, three times on day 24 and five times on days 25 and 26. In addition, day 26 had continuous bubbling from the hours 16-21 local time. The days with bubbles will be included in the results but will not be further discussed due to the short bubbling periods. The roof was removed on day 28 at approximately 13.40 local time, and the salmon had free access to the surface for five days before the experiment ended on the 20th of April.

Table 3.1: Gantt Chart showing the experimental period from day -7 (starting the echo sounders) until day 32 (ending of the experiment). The roof was attached on day 0 and removed day 28, and days 24-26 had occasionally bubbling.

Task/Time	-7	-6	-5	-4	-3	-2	-1	0	1	2	3	4	5	6	7	8	9	10	11	12	13	14	15	16	17	18	19	20	21	22	23	24	25	26	27	28	29	30	31	32
Camera Sample	x	x	x	x	x	x	x	x	x	x	x	x	x	x	x	x	x	x	x	x	x	x	x	x	x	x	x	x	x	x	x	x	x	x	x	x	x	x	x	x
Echo Sample	x	x	x	x	x	x	x	x	x	x	x	x	x	x	x	x	x	x	x	x	x	x	x	x	x	x	x	x	x	x	x	x	x	x	x	x	x	x	x	x
Fish Sample								x							x			x				x					x					x				x				x
Treatment																																								

As seen in Table 3.1, the yellow period represents the 7 days before the access to the sea surface was removed. The green period, from day 0, is the days were the roof was attached to the net cage. Lastly, the red is when the salmon could refill the swim bladder after the roof was detached. Data from before and after the green period allows the study of a naturally filled swim bladder. Further, the chart shows that both camera and echo samples were taken daily and which days the fish samplings were conducted (ref. Section 3.3). The echo samples were continuously sampled for 24 hours a day, while the camera samples were alternately measured three and five times every other day. Further explanation of the sampling technique is done in Section 3.3.

3.2 Experimental fish

On day -9, the 10th of March 2021, 524 Atlantic salmon were randomly chosen from supply cage 15 and placed in cage 16. In order to capture the desired number of salmon, a $5x5x5m^3$ sweep net was utilized. The number of fish needed to be as few as possible to study individuals, but it was necessary to achieve a typical behavior among fish farmed salmon. Thus, 500 individuals were deemed adequate to meet both requirements. After eight samplings, explained in Section 3.3, and one death, there were 376 left on day 32. The surface froze the day before the planned submergence, and it is believed that the salmon died due to hitting ice on the sea surface. Between 11-26 fish were sampled twice a week to study the swim bladder's amount of air, and the results can be seen in Appendix A. Additionally, to monitor the health of the salmon, a welfare measurement was done according to [59]. The fish were given a score between 0 and 3, where 0 indicates perfect condition up to 3, which means significant damage. They were also assessed for sea lice. A M1100 Bench scale [60] was applied to measure the weight of the fish, and a ruler was used to measure the fork length. *Fork length* is defined as the length from the tip of the salmon's nose to the middle of the caudal fin.

3.3 Sample technique

A small hole was cut in the corner of the roof to reach the salmon. Using pellets, the salmon was enticed to the hole and brought to the surface using a dead fish collector net. Afterward, they were netted into an anesthetic bath. The amount of sedation was approximately 10 g per 20 liters of seawater and the euthanasia alternated between two diverse types of sedation; Finquel and Tricaine.

Following, the mouth was cut open with a scalpel to expose the channel from the salmon's pharynx to its swim bladder. With tweezers, the opening became more discernible (see Fig. 3.6). The air was removed from the bladder by inserting a 1.57 mm (outer diameter) polyethylene tube [61], as shown in Fig. 3.6. In order to measure the amount of air in ml, the tube was connected to a 12 ml plastic syringe [62]. When the syringe was challenging to pull, the bladder was said to be empty.

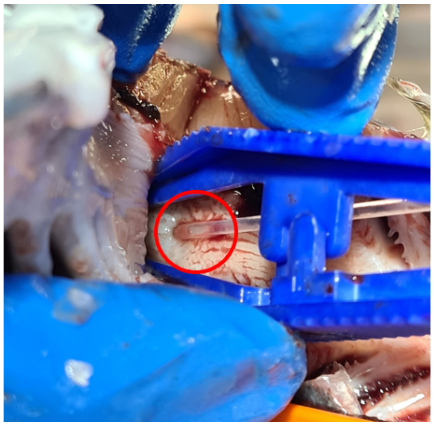

Figure 3.6: A physostomous fish's swim bladder is found in the pharynx, which is seen in the red circle. The polyethylene tube was inserted, and a pair of tweezers were used to better visualize the opening.

After the air was removed, the fish was carefully placed in a tub filled with seawater (see Fig. 3.7). The tube was kept inside the bladder the entire time to make sure no air went back into the bladder.

Figure 3.7: The fish was placed in a tub filled with seawater, and the swim bladder was refilled using the syringe. The bladder was filled until it floated just below the water's surface.

The swim bladder was filled with air until the fish was floating right below the water's surface. This state was defined as the fish's neutral buoyancy. Based on neutral buoyancy and the amount of measured air, the relative quantity of air in the bladder can be calculated. This was done due to the difficulty in identifying a naturally full swim bladder. Using a similar technique, a bladder can be filled with more than 30 ml of air without breaking, which is unrealistic. The same person did the procedure each time to achieve more accurate results. Appendix A includes the length, weight, air quantity, and relative air.

Furthermore, the swimming speed obtained from the echo sounders is a fundamental parameter in this thesis. As a complementary measure to the acoustic results, the swimming speed was assessed using the same method as in previous publications [5, 7, 23, 25]. The camera was placed in front of a reference point, often a rope, and the fish were recorded for five minutes. In order to measure the swimming speed, a stopwatch was used to time the distance traveled by the fish once it passed the reference point. The distance is defined as the fish's fork length, and the procedure was repeated 15 times for each recording. From this method, the speed was found in seconds per body length (s/bl) and converted to m/s and bl/s by using Eq. (2.48).

3.4 Environmental variables

As seen in Fig. 3.1, the Cage Environmental Laboratory is located in the inner part of Masfjorden. The site is in a typical fjord location, with a constant brackish water layer varying in depth in response to precipitation, snowmelt, and the hydroelectric power plant. Water currents in this area are mainly eastward or westward, are tidal driven, and move at speeds between 1 and 10 cm/s. To quantify the water column's conductivity, temperature, depth, and oxygen level, a CTD [63] was connected to an Automatic Profiling Buoy (APB5) (see A.2 in Fig. 3.2). The CTD instrument did two profilings at 01 and 13 every day, from 0 – 25 m. Fig. 3.8, 3.9, and 3.10 show the change in oxygen, temperature, and salinity measured by the CTD. Additionally, a CTD profile was taken to calibrate the EK80 echo sounders before the experiment, where the values are presented in Section 3.5.

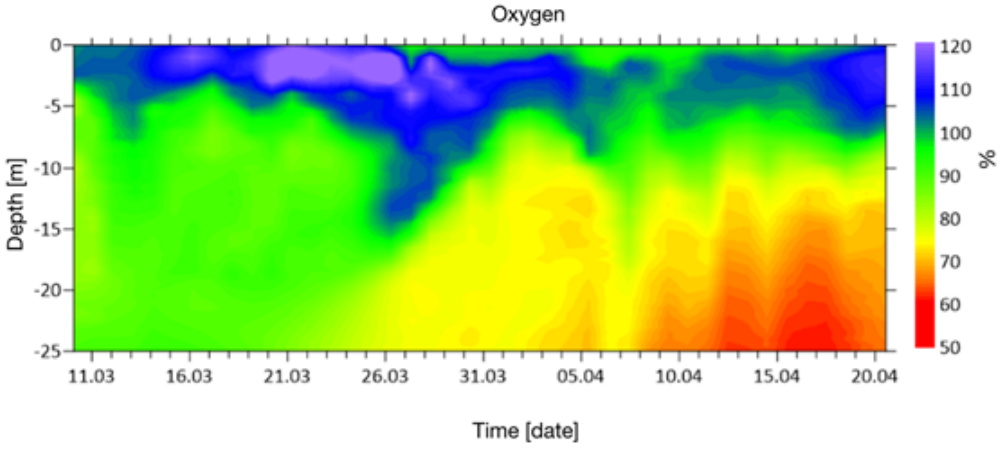

Figure 3.8: Change in O_2 level, [% of air saturation], as a function of depth in m during the experimental period.

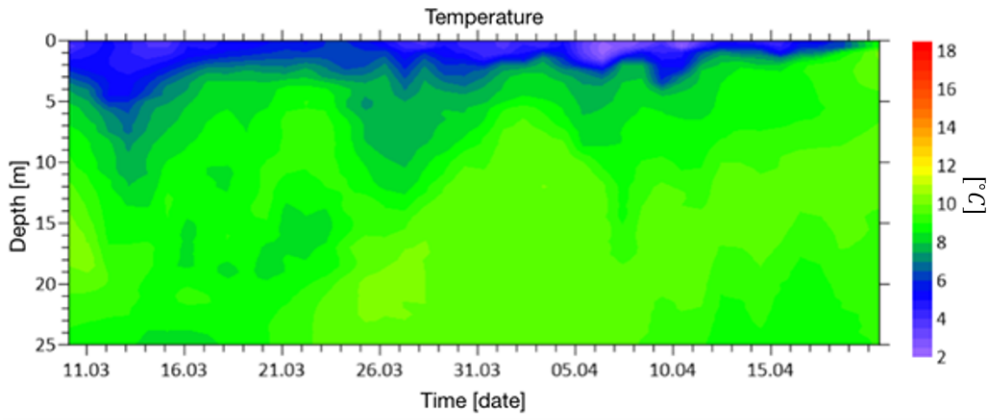

Figure 3.9: Change in temperature, [$°C$], as a function of depth in m during the experimental period.

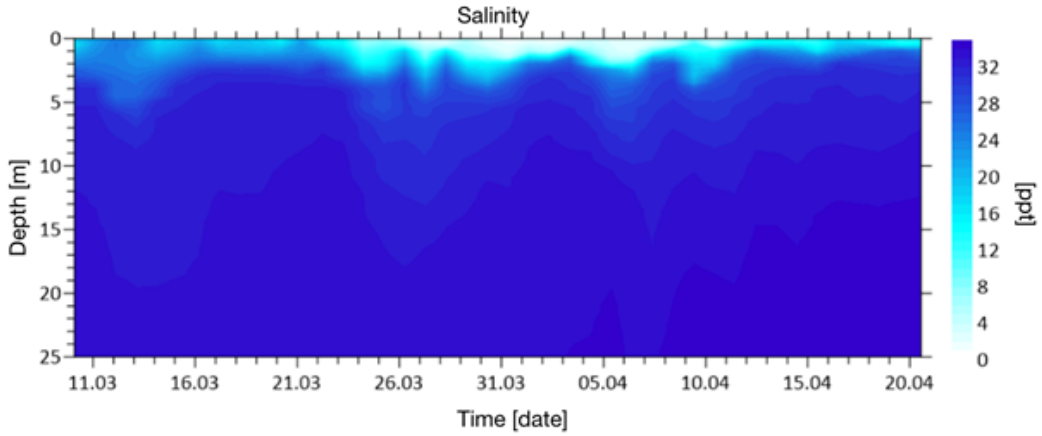

Figure 3.10: Change in salinity, [ppm], as a function of depth during the experimental period.

As the experiment progressed, the dissolved O_2 concentration varied in the upper 15 m of the water column (Fig. 3.8). The dissolved O_2 in seawater occurs mainly due to the photosynthesis of algae, where algae absorb the carbon dioxide, CO_2, from the ocean, and O_2 is released [64]. The % of saturation reached 120 % during the experiment, where the 20 % extra is due to the photosynthesis [18].

3.5 Data collection from echo sounders

The composite split beam transducers was of the type Simrad ES70-7CD, ES120-7CD, and ES200-7CD [37]. The split beam transducer is divided into four quadrants, as seen in Fig. 2.1. Each of the four quadrants detects the received signal, and the phase difference between the recorded signals provides information about the position of the target, which is used to estimate the target's direction and swimming speed [51].

Before the experiment, all three transducers were calibrated using a WC (tungsten carbide) 38.1 mm sphere. On day -9, the calibration was performed next to the cages (Fig. 3.2) at 25 m depth, and Table 3.2 shows the calibration settings for the three transducers. The CTD profile used to calibrate had a

temperature of $T_0 = 8.1°C$, speed of sound $c_0 = 1489 m/s$, and a salinity $s = 33.2 ppt$. After calibration, the transducers were placed 25m below the cage facing upwards, measuring the ventral aspect of the fish.

Table 3.2: The settings used to calibrate the transducers for both CW and FM fast signals. The start and stop frequencies in the parenthesis was used by LSSS

Serial number	Frequency [kHz]	Pulse type	Pulse duration, τ [ms]	Power [W]	Start freq. [kHz]	End freq. [kHz]
112	70	CW	0.256	50	70	70
		FM fast	2.048	50	55 (56.8)	90 (88.2)
113	120	CW	0.256	50	120	120
		FM fast	2.048	50	90 (93.5)	160 (156.5)
147	200	CW	0.256	45	200	200
		FM fast	2.048	45	160 (165)	260 (255)

Table 3.2 shows the settings used when calibrating the two pulse types for the three transducers. From the Table, FM was calibrated by using FM fast, where fast means tapering the signal slightly at the beginning and end of the signal [34]. The table includes the power used on the echo sounders, 50 W for 70 and 120 kHz and 45 W for 200 kHz. The frequencies were chosen to create a continuous signal from 55 kHz to 260 kHz. However, LSSS removed some of the frequencies at both ends of the frequency band, resulting in the frequency bands shown in parenthesis in Table 3.2. The frequency bands used in the measurements were above the resonance frequency for the swim bladder, which is 575 Hz at 1 m depth and 850 at 14 m depth (ref. Eq. (2.18)).

FM and CW signals have different spatial resolutions in z-direction, as explained in Section 2.1. The spatial resolution was found for the FM pulses by using Eq. (2.3), the bandwidth, B (from Table 3.2), and speed of sound in seawater, c. While for the CW pulses, Eq. (2.1) and the pulse duration, τ_{cw}, of the signal was applied, which was found in Table 3.2.

Table 3.3: Theoretical spatial resolution in z-direction for each frequency and signal type, [m]

	70 kHz	120 kHz	200 kHz
CW	0.2	0.2	0.2
FM	0.02	0.01	0.008

Table 3.3 shows the theoretical spatial resolution for the different frequencies and pulse types in z-direction. The pulse length for CW signals were equal for all frequencies, resulting in a similar spatial resolution. For FM signals, the spatial resolution increases with increasing frequency.

The transducers alternated between transmitting one-hour CW signals and one-hour FM signals continuously throughout the experimental period. The EK80 software was installed on a computer placed in A.1 in Fig. 3.2. A "mission plan" in EK80 was created, and the software shifted automatically between the two different pulse types. The first step in creating the mission plan was to assign a channel to each of the six different pulse types (2 per transducer). In addition to the pulse type, the pulse duration, power, and start- and end frequency were set. Further on, a ping group was created where

the three CW and three FM channels were gathered into two groups, CW and FM. The ping rate was defined as 200 ms (18 000 pings/h). Then two ensembles were created, one for each ping group. The ping groups had to be repeated 60 times in the ensembles to reach the desired number of pings per hour. Lastly, the mission was created by repeating three CW ensembles followed by three FM ensembles. Each ensemble was run with an iteration of 100 (60 x 3 x 100 = 18 000 pings/h).

3.6 LSSS

Large Scale Survey System (LSSS) [49] was the software applied for post-processing data in this thesis. LSSS is made for scientific fisheries surveys and abundance estimation and is therefore not optimized for net cage studies. Additionally, the software is still in the preliminary stages of research when it comes to processing FM data and data from salmon cages [12]. Integrated into LSSS is a processing program called KORONA [49], which includes different computation modules and can be used in numerous ways. In this thesis, KORONA was used for splitting recordings from channels with different acoustic frequencies into separate files and tracking individual fish, as explained in Section 2.4. Finally, TS, S_V, and the position of the salmon were extracted.

3.6.1 Splitting data

The experiment was conducted with another student [55], and the experimental setup was equal for both thesis. The other student had two additional cages with a 200 kHz transducer in each, and the mission planner on EK80 ran all five transducers simultaneously. Due to this, the output files include data that are not of interest to this thesis. KORONA Relay was applied to split the different cages and signal types (FM and CW) from each other. By including "channel removal," which channels to keep can be chose. In this case, channels 1, 3, and 5 indicate CW-data, and channels 2, 4, and 6 indicate FM-data, both for cage 16. During the splitting, unnecessary depths (from echo sounder to bottom of the cage) were removed to decimate the amount of data. After processing, KORONA writes CW- and FM files in separate folders. A more detailed description can be read in Appendix B.

3.6.2 Tracking data

After splitting and keeping only the necessary data, a new KORONA relay was created to track TS values and the position of the individual salmon. As tracks were applied to distinguish the individual fish, the S_V values were independent of the tracking. An upper and lower boundary, seen in Fig. 3.11, was drawn, and only the data inside the regions were processed with the tracking algorithm.

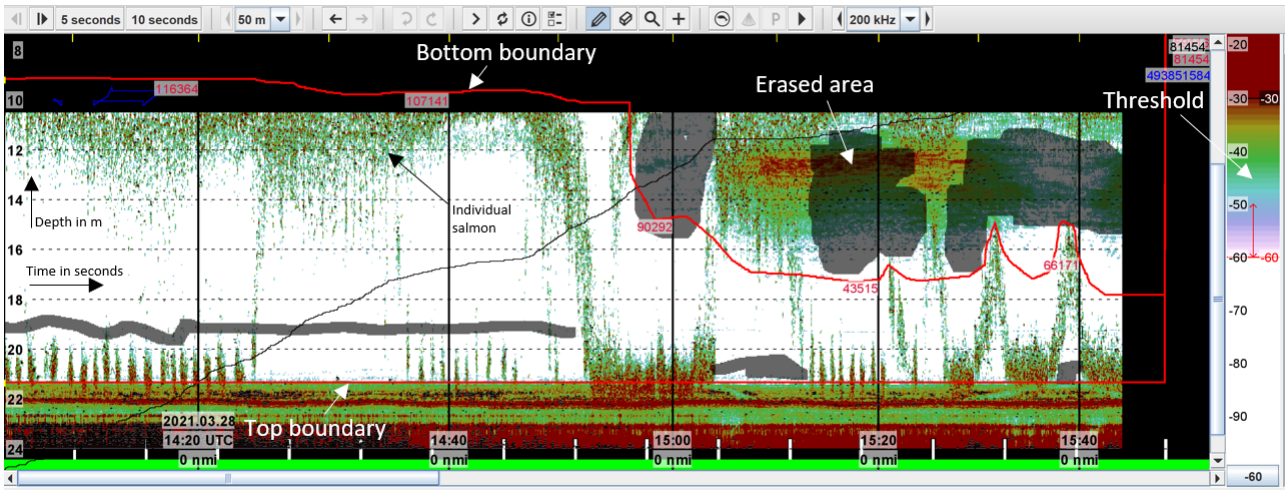

Figure 3.11: Echogram of FM data as visualized by LSSS. The cage is reversed, where the bottom of the echogram and the top is reversed relative to the bottom and top of the cage. The two red lines are the boundary drawn

Fig. 3.11 shows an echogram as seen in LSSS for one hour of FM data from day 9, where the bottom and top are reversed relative to the bottom and top of the cage. The vertical echogram is the depth, z, in m, and the horizontal is the time in seconds. The depth was reduced during the splitting, and data is here seen from 1 m from the surface (24 m in the echogram) to approximately 14 m depth (10 m in the echogram). On the right side is a threshold bar, showing the colors of different dB re. 1 m^2 values and the strength of the measured signal, where red indicates a strong backscattered signal and purple is a weak signal. The threshold is only for visualization and does not affect the values. Salmon is defined as the less dense areas in the echogram, pointed out by an arrow in the center of the figure. The red lines in Fig. 3.11 illustrate the regions for this specific hour of FM data and were set individually for each hour of FM and CW data. Additionally, areas with much noise were erased or excluded, illustrated by the gray areas, to avoid tracking noise, where noise is seen as the denser colored areas. The noise varied with depth and days and is assumed to be tiny organisms like plankton. If the regions were changed or other alterations to the data sets were made, the changes were saved in "work files." Thus, two separate LSSS-surveys were created for the FM and CW data to keep the "work files" from overwriting each other.

Finally, the CW data was tracked by applying the peak tracking algorithm and FM using the aggregation method. Originally, aggregation was the preferred tracking algorithm, as it returned much more tracks than peak (on both FM and CW data), but aggregation turned out not to work well on CW data (ref. Subsection 6.1.6). Thus, CW data was tracked using peak instead. The settings used in KORONA Relay for tracking are presented in Appendix B.

3.6.3 Exporting data

After the post-processing was finished, LSSS allows the export of the parameters of interest for further processing. Due to the large files from using FM signals, it was time-consuming to export all 12 hours

of FM data, and it was decided to export one hour instead. As the fish were fed in in the morning, around 08.00 local time, the hour of data were extracted in the afternoon, before the sun went down. The bubbling were initiated around the time of the desired hour of data, which was inconvenient due to the disturbances from the bubbles on the signal. Hence, areas with much bubbles were excluded.

The tracking using aggregation returned enough data to support the choice of only one hour (ref. Appendix E). The TS(f) values for FM data were exported using the BBTS(f) tracks function, and the output file is a .json-file including TS values for all three frequency bands in the same file. For CW data, the tracks were used for finding both the TS and swimming speed. The desired data was exported to a text file that contains one of the frequencies, 70, 120, or 200 kHz, the associated TS values, and x, y, and z positions for each ping. The same function was exported to obtain the positions from FM data. Further, the swimming speed was calculated using Eqs. (2.43) - (2.47) ((2.48)), and the associated standard deviation was obtained from using Eq. (2.49).

Data from the CW pulses was exported first, and unlike FM data, the entire day (12 hours) was extracted. Two hours of CW data, one before and one after the FM hour, were selected to compare it better with the results from FM data. This process was done in MATLAB (Appendix F). A Python script by Geir Pedersen (IMR) [65] was used to extract S_V values as a function of frequency automatically. The script exported the same hours as for TS and swimming speed from FM data.

Chapter 4

Simulating TS of phystomous fish using the Kirchhoff's Ray Mode model

This chapter addresses the simulation used in the thesis, the Kirchhoff's Ray Mode (KRM) simulation method based on the theory from Clay and Horne [30]. The simulation was applied in the software R using a package called *KRMr: Kirchhoff Ray Mode Model for fisheries acoustics* created by Gastauer et al. [66]. Before doing the simulation, a validation of the method was conducted and can be seen in Appendix D. The simulation is included to support the results from the acoustical measurements.

4.1 KRM simulation based on Clay and Horne

An example of a simulation model is the Kirchhoff's-Ray mode (KRM) [30]. The theory in this section is based on the theory from Clay and Horne, which used Atlantic cod in their modeling of TS from teleost fish [30], and is applied in the KRMr package in the software R [66] (ref. Appendix F.4). *Teleost* fish belongs to the group called actinopterygians, which is a class of ray-finned fish and contains more than 99.5 % of the ray-finned fishes. Examples of teleost fish are Atlantic salmon and rainbow trout, amongst others [67]. The KRM model is applied to simulate and approximate the TS of fish based on the fish's length and the angle of the incident pressure wave [30] relative to the dorsal aspect of the fish. When modeling, the fish and swim bladder is divided into j number of sections relative to the x-axis, as shown in Fig. 4.1 and Table 4.1 [30]. Since the model is based on the bladder and fish body, other important fish elements, such as the target's backbone, are not considered.

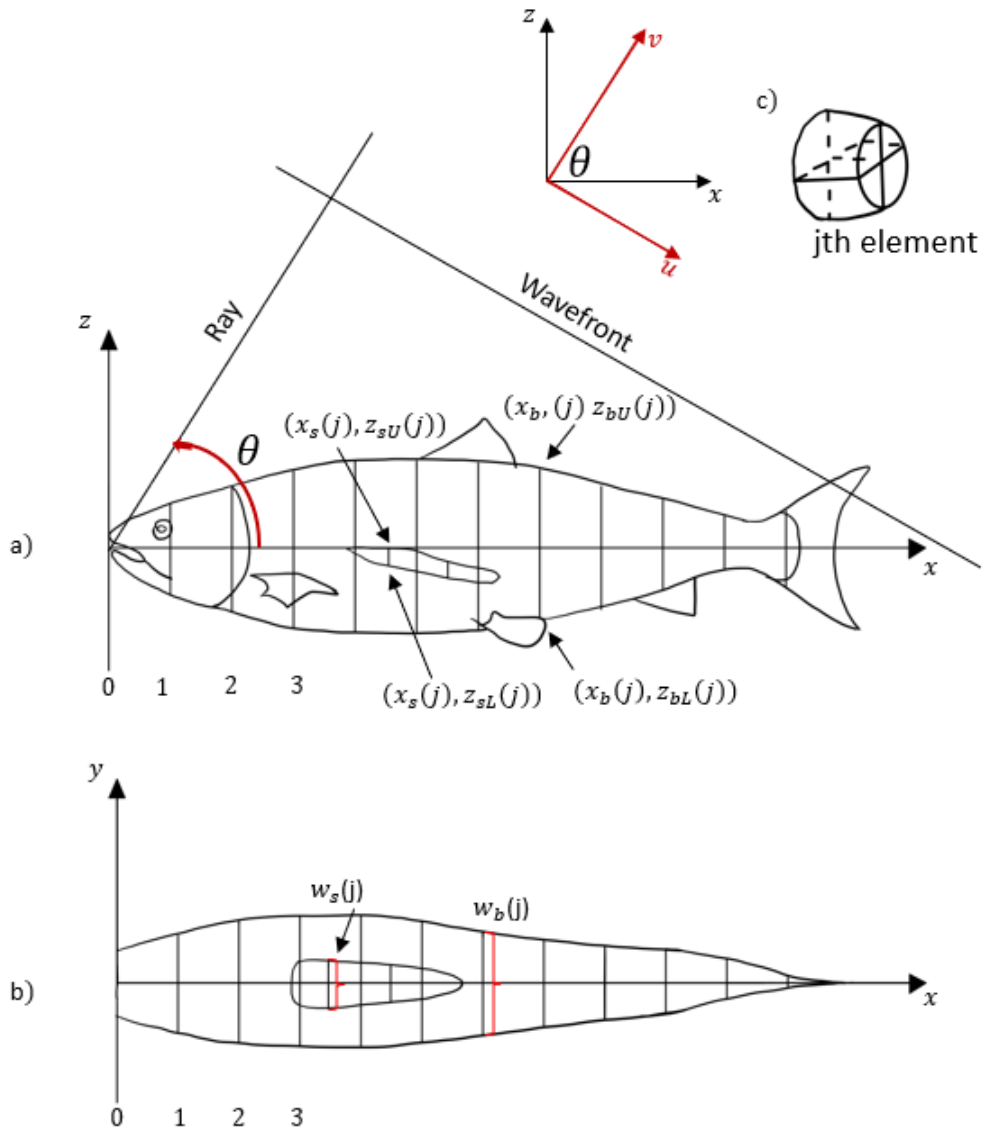

Figure 4.1: Salmon divided into j number of sections along the x-axis. a) shows a salmon from the lateral aspect, x-z plane, and b) the dorsal aspect, x-y plane. c) is the j-th element, between x(j) and x(j+1). The u-v coordinates are defined by the ray and wavefront. The fish's snout is placed in origin (Modified from [30]). Note that the bladder is not the right proportional size to the body.

Fig. 4.1 shows the fish's coordinates in Cartesian coordinates seen from the x-z plane in a) and from the ventral x-y plane in b), where the snout is positioned in origin. The wavefront of the incident wave is illustrated in a), where θ is the angle between the x-axis and the incident ray. θ is limited between 65° and 115° [30]. The x-z plane is rotated into u-v coordinates in the top right corner, where u follows the wavefront and v the incident ray [30]. Further, the fish is divided into j-number of volume sections, between x(j) and x(j+1), illustrated in c). Note that Figs 4.1 a), b), and c) are an illustrative display of the outlines of a salmon and its swim bladder and will not affect the results of the simulation.

Table 4.1: The coordinates for the j-th element of the fish body and the swim bladder used in the model, where the subscript b and s indicates the body and swim bladder, respectively [30].

	Length	Height, upper	Height, lower	Width
Body	$x_b(j)$	$z_{bU}(j)$	$z_{bL}(j)$	$\frac{w_b(j)}{2}$
Swim bladder	$x_s(j)$	$z_{sU}(j)$	$z_{sL}(j)$	$\frac{w_s(j)}{2}$

Table 4.1 presents the fish body's and swim bladder's coordinates. The subscript U denotes the upper z-coordinates, and L denotes the lower [30]. The segmenting of the fish is done to obtain j number of small elements. The elements are summarized to achieve the scattering length, also called scattering amplitude [30], of the body and the bladder, which are given in m. This is done individually for the bladder and the body, and is then used to find the TS. The coordinates in Table 4.1 are transformed to the u-v coordinates for the ray and wavefront [30],

$$u(j) = x(j)sin\theta - z(j)cos\theta, \tag{4.1}$$

$$v(j) = x(j)cos\theta + z(j)sin\theta, \tag{4.2}$$

$$v_j \equiv \frac{v_{s_U}(j) + v_{sU}(j+1)}{2}, \tag{4.3}$$

$$\Delta u_j = [x(j+1) - x(j)]sin\theta, \tag{4.4}$$

$$a_j = \frac{[w(j) + w(j+1)]}{4}, \tag{4.5}$$

where Δu_j is the length of the j-th element given in u-v coordinates, a_j is the radius of the j-th element, and v_j is the middle of the j-th volume element in v direction [30]. The u-v coordinates have equal subscripts as the x-z coordinates from Table 4.1. Due to the similarity between the plane-wave reflection coefficients at the body-bladder, $\mathscr{R}_{bc}$, and water-bladder, $\mathscr{R}_{wc}$, boundaries, the bladder is assumed to be surrounded by seawater [30]. Further, for high frequencies, the Kirchhoff-ray approximation is applied to calculate the scattering length of the fish's body and swim bladder [30]. The sum of the scattering length of the swim bladder (soft) in water, as expressed in [30], is

$$\text{soft}\mathscr{L} \approx -i\frac{\mathscr{R}_{bc}(1-\mathscr{R}_{wb}^2)}{2\sqrt{\pi}} \sum_{j=0}^{N_s-1} A_{sb} \times \sqrt{[(k_b a_j + 1)sin\theta]}e^{-i(2k_b v_j + \psi_p)}\Delta u_j, \tag{4.6}$$

where N_s is the number of (x(j), z(j))-coordinates for the swim bladder, hence $N_s = 7$ in Fig. 4.1. Further, k_b is the body's wave number, $\mathscr{R}_{wb}$ is the plane-wave reflection coefficient at the water-body boundary, A_{sb} is an empirical amplitude factor from the Kirchhoff approximation and ψ_p is the

empirical phase shift for a fluid cylinder in ray-Kirchhoff [30]. A_{sb} and ψ_p are used for correction of small ka_s, where a_s is the radius of the swim bladder [30].

The scattering length of the fluid cylinders (body) is found by the Kirchhoff approximation as in [30], and is given by,

$$\text{fluid}\mathscr{L} \approx -i\frac{\mathscr{R}_{wb}}{2\sqrt{\pi}}\sum_{j=0}^{N_b-1}\sqrt{(ka_j)}\Delta u_j\left[e^{-i2ku_{U,j}} - \mathscr{T}_{wb}\mathscr{T}_{bw}e^{-i2ku_{U_j}+i2k_b(u_{U_j}-u_{L_j})+i\psi_b}\right], \tag{4.7}$$

where N_b is the number of (x(j), z(j))-coordinates of the fish body, where $N_b = 12$ in Fig. 4.1 a) and b) [30]. $\mathscr{T}_{wb}$ is the plane-wave transmission at the water-body boundary, and $\mathscr{T}_{bw}$ is the plane-wave transmission at the body-water boundary [30]. Further, k is the wavenumber of the sea water and ψ_b is the empirical phase shift for a soft cylinder in ray-Kirchhoff [30].

The real and imaginary parts of Eqs. (4.6) and (4.7) are added coherently to obtain the total scattering length/amplitude of the salmon [30],

$$\mathscr{L} = \text{soft}\mathscr{L} + \text{fluid}\mathscr{L}, \tag{4.8}$$

which is used to calculate the bakcscatering cross section [30],

$$\sigma_{bs} = |\mathscr{L}|^2, \tag{4.9}$$

and the TS [30],

$$TS = 20log_{10}\left[\frac{|\mathscr{L}|}{L_0}\right]. \tag{4.10}$$

In Eq. (4.10), L_0 is a reference length at 1 m [30].

4.2 Implementing the KRM model in the R software

Gastauer et al. [66] have created a package in the R software (ref. Appendix F.4) based on Eqs. (4.6) - (4.10) and the theory explained in [30] to model the TS of phystomous and physoclistous fish. The model require the input parameters presented in Tables 4.1 and 4.2. The parameters can be chosen as desired but were kept constant during this simulation, except for the frequency and swim bladder size, which were changed to simulate a decrease in TS with decreasing swim bladder volume.

Table 4.2: Input parameters for the KRMr package in the R software. *Frequency can be chosen, either as a single frequency or over a wider range of frequencies [66]

Input parameters in KRMr		Value
Frequency	f [Hz]	*
Sound speed in sea water	c.w, [m/s]	1489
Density of sea water	rho.w, [kg/m^3]	1026.8
Angle of incidence	theta, [°]	90
Sound speed in fish body	c.fb, [m/s]	1480.3
Sound speed in swim bladder	c.sb, [m/s]	345.0
Density of fish body	rho.sb, [kg/m^3]	1028.9
Density of gas in swim bladder	rho.fb, [kg/m^3]	1.24
Length of fish	L, [m]	0.38

The sound speed in seawater, c.w., was measured during the experiment using a CTD instrument, as explained in Section 3.5. Further, the sound speed and density of the swim bladder and fish body were found in [68]. The frequency can be chosen to simulate a CW pulse and a single TS value or an FM pulse and the frequency response of the swim bladder. Both pulse types were simulated in the thesis to compare the results from the measured values from the experiment, and the frequencies are equal to the ones in Table 3.2. In addition to the frequencies, the incident angle, θ, can be changed to simulate a fish swimming with a tilt. From Subsection 2.3.3, it was explained how the TS is strongly dependent on the angle of the incident acoustic wave. However, based on the measured camera data, approximately no tilt was observed, and θ was kept constant at 90° during the simulation. When the incident angle is 90°, the wavefront is normal to the dorsal aspect of the fish, seen from Fig. 4.1. This is the opposite of the experiment, where the measurements were done from the ventral aspect of the fish. However, the KRM model is limited to angles between 65° to 115° [30], and the simulation was therefore conducted with incident waves normal to the dorsal aspect of the salmon. From previous publications [28, 69], measuring the TS from the ventral aspect of the fish resulted in stronger backscattered signals than from the dorsal aspect, due to the morphometry of the swim bladder [28]. Thus, the simulation of TS with an incident wave normal to the dorsal aspect of the fish will affect the following simulations, and the results will not be fully comparable to the measured TS values.

As the model uses the sum of j number of small volume elements, the KRMr package in the R software requires the coordinates of each element to proceed with the modeling. The coordinates can be changed to simulate different swim bladder sizes, which implies changes in air level. An x-ray image used in [6], shown in Fig. 4.2, was used by Pedersen [65] to obtain the size of the fish body and the swim bladder.

Figure 4.2: The x-ray image of salmon used in [6], where a) is the dorsal aspect of the salmon and b) is the lateral aspect. The swim bladder is only seen in b) as the dark gray elongated shadow.

Fig. 4.2 shows a) the dorsal and b) the lateral aspects of a salmon used in an experiment by [6]. Only the lateral aspect of the swim bladder is seen in the figure, which made it challenging to obtain the coordinates of the dorsal aspect of the bladder. Due to this, the dorsal coordinates were assumed. As the objective of the simulation was to support the measured TS values, the assumption was not deemed a weakness, but nevertheless was not ideal. The coordinates from the x-ray image were based on an assumed full swim bladder.

Further, a MATLAB script by [65] interpolated the coordinates to achieve a resolution good enough for the KRM model. MATLAB returned two separate .csv files, including the coordinates of the swim bladder and the fish body, which were read and plotted by the R software. The volume was decreased as a percentage of the full, 100%, bladder through the MATLAB script. The radius when the bladder is full (in the middle of the bladder) was set to $a = 0.01m$. The upper coordinates of the swim bladder, z_{sU}, were kept constant for each adjustment [65]. The MATLAB script had to be run each time the bladder volume was adjusted. This was done five times to simulate the decreasing TS due to a decrease in air level. As there are no reasonable measures of how fast the volume decreases during the experiment, the volume was decreased to 75 %, 50 %, 20 %, 10 %, and 0 % of the assumed full (100 %) volume. For each volume, the TS was simulated using single frequencies (70, 120, and 200 kHz), as in a CW signal, and using a broad range of frequencies (56.8 - 88.2, 93.5 - 156.5, 165 - 255 kHz) as in an FM signal.

Fig. 4.3 shows the swim bladder at a) 100 % and after decreasing to b) 75 %, c) 20 %, and d) 0 % of the full bladder. The swim bladder is the main contribution for the TS [10]. However, for fish without a bladder, the backbone contributes to the TS [12]. As the backbone is not included in the KRM model, the simulation of an empty bladder will be less accurate. The results of the simulation of TS and

frequency response are presented in Chapter 5

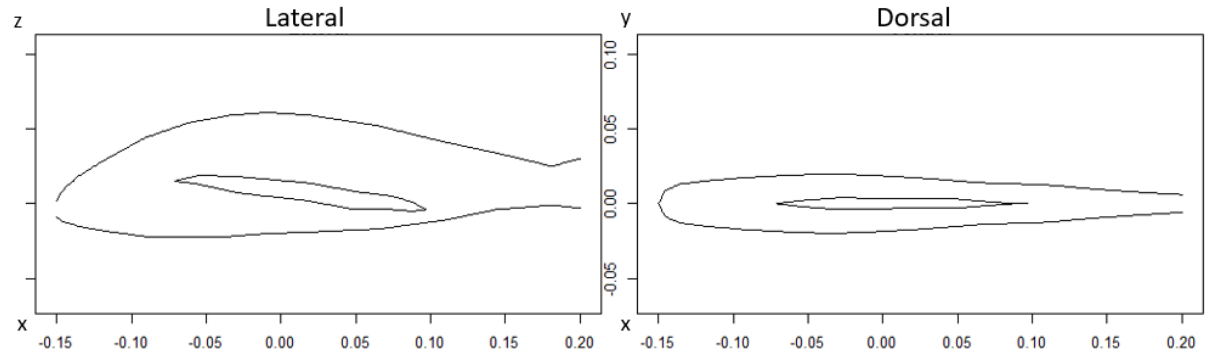

(a) 100 %

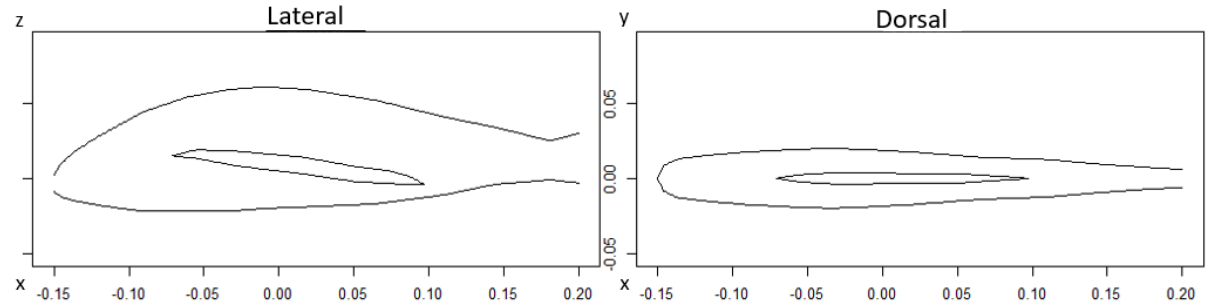

(b) 75 %

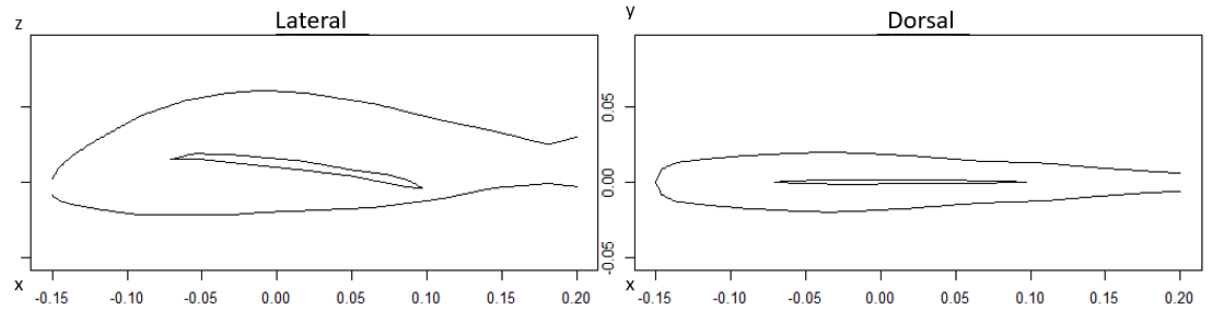

(c) 20 %

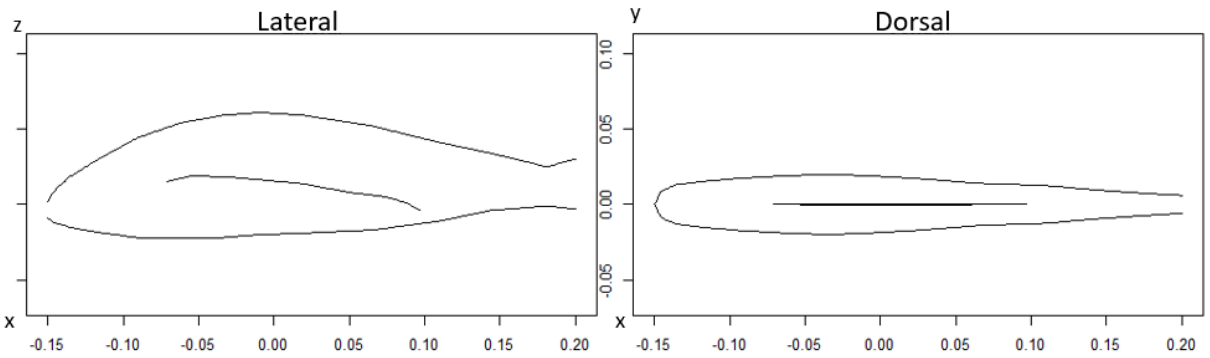

(d) 0 %

Figure 4.3: Fish and swim bladder modeled in the R software. The left figures illustrate the salmon from the lateral, in the x-z plane, where the axis is the length and height of the fish in m. The right figures are the salmon seen from the dorsal, in the x-y plane, where the axis is the salmon's length and width. a) is the assumed full swim bladder, b) is 75 % of the full bladder, c) is 20 % of the full bladder, and d) is 0 % of the full bladder.

Fig. 4.3 shows both the lateral (left figures) and the dorsal (right figures) aspect of the salmon and its swim bladder as the volume of the bladder diminishes from 100 % in a) to 0 % in d). The left figures show the fish's length and height in the x-z plane, and the right figures show the length and width in the x-y plane.

Chapter 5

Results from measurements and simulation

This chapter presents the findings from the measurements and simulations. TS, S_V, swimming speed, and frequency response from TS(f) and S_V(f) will be addressed based on frequency and pulse type. The complementary measurements, camera, and air quantity will be considered. A discussion of the findings and results will be included in Chapter 6.

5.1 Target strength

5.1.1 Measured TS from FM signals

The TS from FM data is obtained using the LSSS-function BBTS(f) tracks (see Appendix B.3). When exported from LSSS, the .json file includes the tracks detected after being processed by using aggregation as explained in Section 2.4, where one track equals one fish. Each track consists of multiple pings, and each ping in the track returns a TS value for every frequency in the bandwidth. TS values were taken from the tracked fish within ± 2° relative to the center axis of the transducer beam, which was done in the MATLAB script in Appendix F.1. In order to compare the FM results with the results from the CW signals, a few frequencies were selected within a 3 kHz bandwidth around the nominal frequencies. Eqs. (2.23) - (2.25) were used three times to obtain the average TS, $\overline{TS}$, per day. First, the average TS per frequency within the 3 kHz bandwidth was found for each ping in the track. Then, to express one TS value per track, $\overline{TS}_{track}$, the average TS was calculated over the frequency band. Lastly, the daily TS value, $\overline{TS}$, was found by averaging the values from every track, $\overline{TS}_{track}$, within the exported file. Each of the calculations was done using the MATLAB script in Appendix F.1. As salmon swim in circles in the cage, they pass through the beam multiple times during the recorded hour, and, thus, the same fish will be tracked several times throughout the experiment.

The experimental period was divided into four sections, as seen in Table 5.1, which were used to calculate the linear regression line from Eq. (2.50) in order to study the overall decrease/increase

during the selected period.

Table 5.1: The experimental period is divided into four sections, where *Before* is the time before the roof was attached, *Mid* is during submergence, *Bubbles* is the days with bubbling, and *After* is the days when the roof was removed.

Period	Before	Mid	Bubbles	After
Days	-4 - 0	0 - 24	24 - 27	28 - 31

Table 5.1 presents the four periods of the experiment; before submergence (day -4 to 0), submerged (day 0 to 24), submerged with bubbles (day 24 to 27), and when the roof was removed (day 28 to 31). The periods were used to calculate a trend line, which was accomplished using Eq. (2.50), and MATLAB. The trend lines were calculated for each nominal frequency within the 3 kHz bandwidth. Additionally, the coefficient of determination, R^2, was calculated by using Eq. (2.51), and is a measure of how well the collected data fit the linear regression line. However, because *Before*, *Bubbles*, and *After* consists of only a few data points, the R^2 values will not be considered as important as for *Mid*. The periods defined in Table 5.1 are used for the rest of the thesis, along with the calculation of the regression line and R^2 values. Fig. 5.1 presents the daily change in $\overline{TS}$ values from the three echo sounders and includes the associated trends.

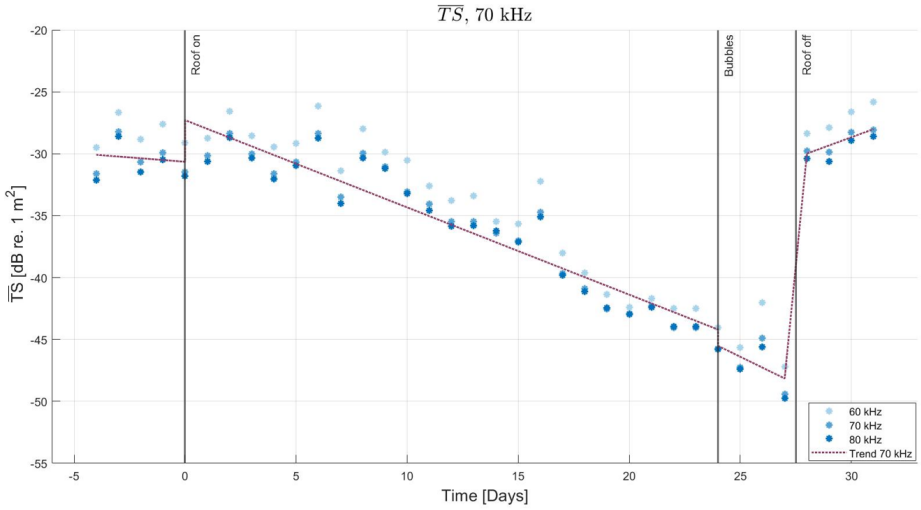

(a) $\overline{TS}$ of FM signals from the 70 kHz echo sounder

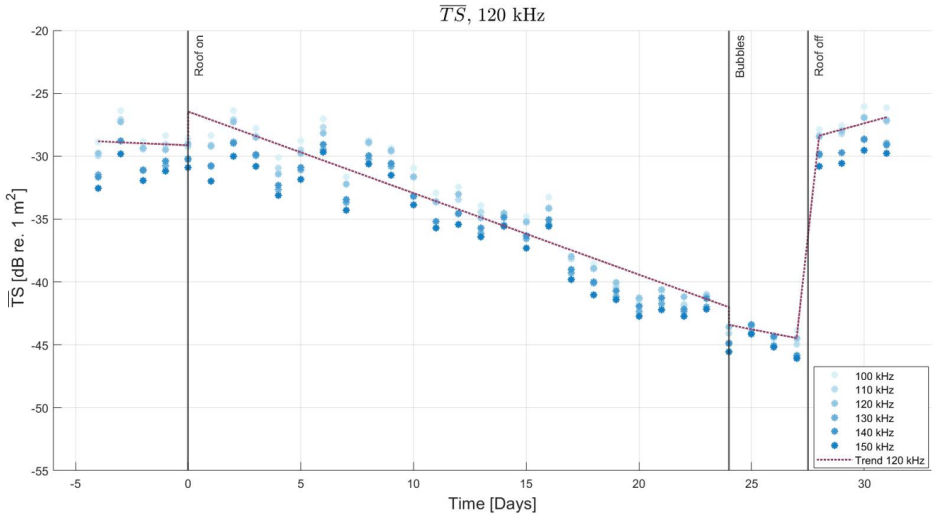

(b) $\overline{TS}$ of FM signals from the 120 kHz echo sounder

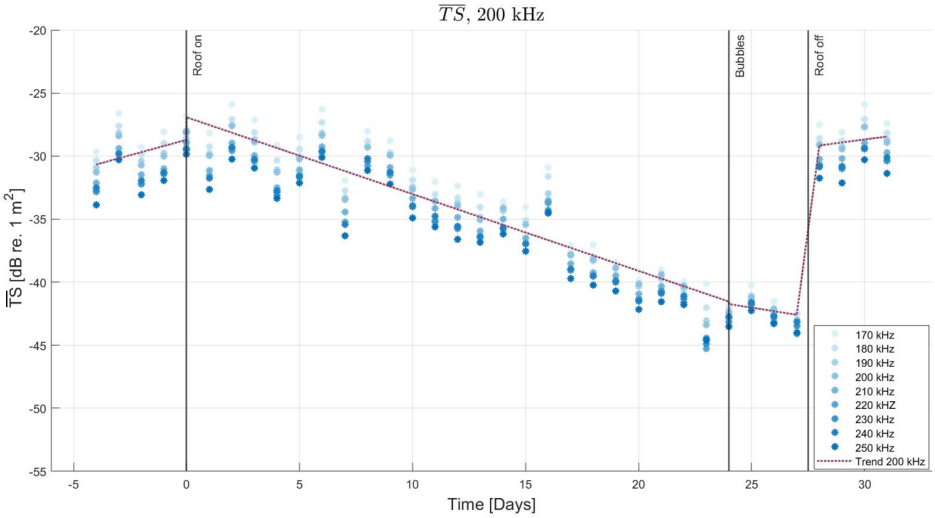

(c) $\overline{TS}$ of FM signals from the 200 kHz echo sounder

Figure 5.1: Change in $\overline{TS}$ from FM data over time for the 70 in a), 120 in b), and 200 kHz echo sounder in c). The TS values were selected with intervals of 10 kHz from f_1 to f_2, all seen in the lower right corner of the figures. The shades of blue increase with increasing frequency, and the purple stippled line represents the trend lines.

Fig. 5.1, shows the three selected frequencies from the 70 kHz echo sounder in a), the six selected frequencies from the 120 kHz in b), and the nine selected frequencies from the 200 kHz echo sounder in c). The figures shows how the $\overline{TS}$ was changing each day during the experimental period. The chosen frequencies start at f_1 and increase with intervals of 10 kHz until f_2, and are presented from light blue to dark blue. Further, the trend line is presented as the purple stippled line and is calculated based on the nominal frequencies for each of the three echo sounders. The vertical lines show the days when the cage was submerged, when the bubbling started, and when the roof was removed. There are variations between the different frequencies within a given day, where the $\overline{TS}$ values decrease as the frequency increases. The daily values vary, but as seen in the purple stippled line, the overall trend in the submerged period is decreasing. For each echo sounder, the $\overline{TS}$ values appear to start decreasing from day 6. After removing the roof, there is a clear leap in the $\overline{TS}$, and the values are back at the same level as before the cage was submerged. To compare the $\overline{TS}$ from the FM signals for each echo sounder, the nominal frequencies are plotted in Fig. 5.2.

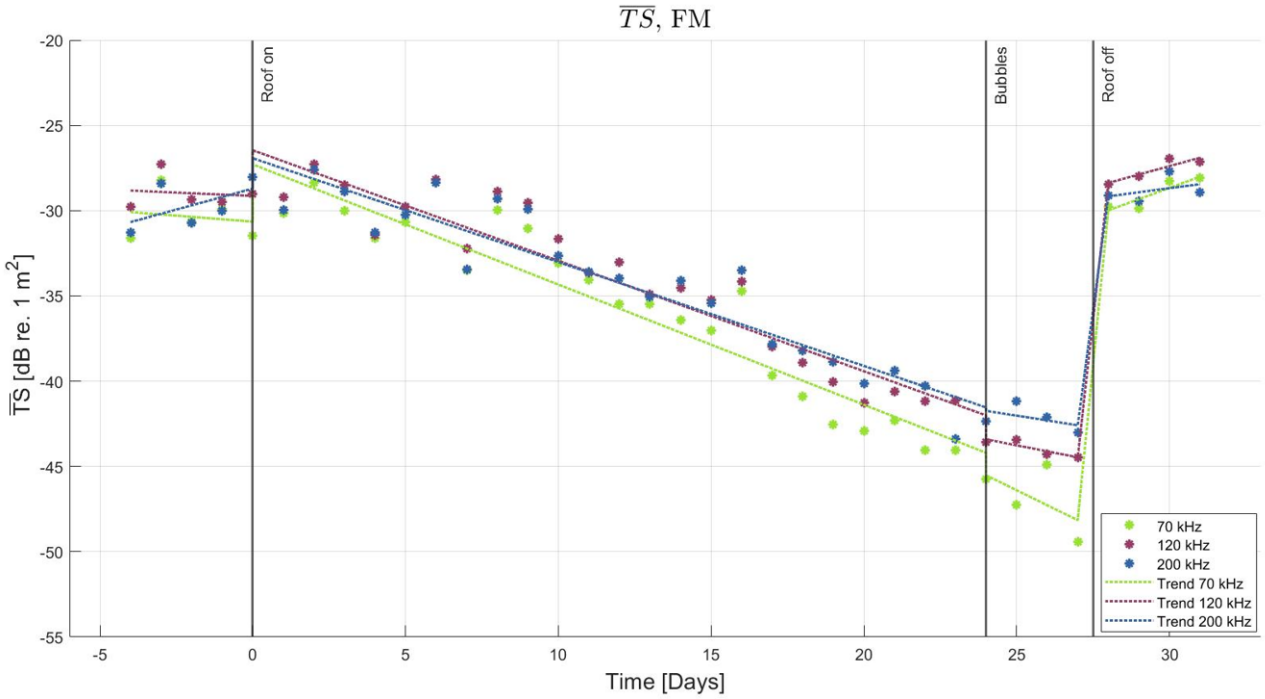

Figure 5.2: The $\overline{TS}$ from FM signals of the nominal frequency for each echo sounder is plotted as a function of time (in days) to compare the results, where the dots are the daily values and the stippled lines are the trends. The green is from the 70 kHz echo sounder, the purple is from the 120 kHz, and the blue is from the 200 kHz.

In Fig. 5.2, the $\overline{TS}$ are the daily values of the nominal frequencies from FM data measured by the three echo sounders. $\overline{TS}$ is plotted as a function of time in days to study the changes throughout the experimental period. The green points represent values acquired from the 70 kHz echo sounder, the purple is from the 120 kHz, and the blue is from the 200 kHz, and the trend line for each frequency is included. Due to an unknown error when collecting the data, day 23 is missing from the 70 kHz FM data, and the value from day 22 has been added to day 23. As in Fig. 5.1, there are variations in

both daily values and between the three frequencies. Initially, the ratio between the frequencies are small, but as the bladder deflates, the ratio between the $\overline{TS}$ values increases. The values measured by the 70 kHz echo sounder are the lowest throughout the experiment, and from day 14, the 200 kHz returns the highest $\overline{TS}$ values. The overall trends for the three frequency bands are decreasing during the submerged period. Once the roof was removed, the values increased and returned to the original level. The gradients of the $\overline{TS}$ trends and R^2 values are shown in Table 5.2.

Table 5.2: The linear regression trends (as shown in Figs. 5.1 and 5.2) of $\overline{TS}$ from FM data for the four periods (as defined in Table 5.1), for each nominal frequency. The trends are presented numerically as in Eq. (2.50), and include the R^2 values for each trend-line.

	70 kHz		120 kHz		200 kHz	
	Trend	R^2	Trend	R^2	Trend	R^2
Before	-0.1x - 31	0.03	-0.1x - 29	0.02	-0.5x - 29	0.3
Mid	-0.7x - 27	0.9	-0.6x - 26	0.9	-0.6x - 27	0.9
Bubbles	-0.9x -24	0.3	-0.4x -35	0.8	-0.3x - 35	0.2
After	0.7x - 48	0.8	0.5x - 42	0.8	0.2x - 36	0.2

Table 5.2 presents the numerical regression lines of the trend-lines from Fig. 5.2 for the three frequency bands, where the different periods are defined in Table 5.1. As the R^2 value for each transducer is close to 1, the calculated linear regression line is a good fit for the $\overline{TS}$ values obtained from the FM data. This is consistent with the plotted values in Figs. 5.1 and 5.2. Additionally, the slopes show how the three frequencies decrease at almost the same rate (-0.7, -0.6, and -0.6), but the values from the 70 kHz echo sounder decrease slightly faster than the values from the 120 and 200 kHz echo sounder.

5.1.2 Measured TS from CW signals

The TS from CW data is extracted after using the tracking function peak (ref. Section 2.4). The returned text files include the tracks for each fish, which consist of multiple pings, and each ping in the track contains one TS value. In order to express a single TS value per track, $\overline{TS}_{track}$, the average TS for each track was calculated by applying Eqs. (2.23) - (2.25). To present the average TS value per day, $\overline{TS}$, the average was calculated over every track within the exported file, using Eqs. (2.23) - (2.25). Each calculation was done in MATLAB, using the script in Appendix F.2, and the results are presented in Fig. 5.3.

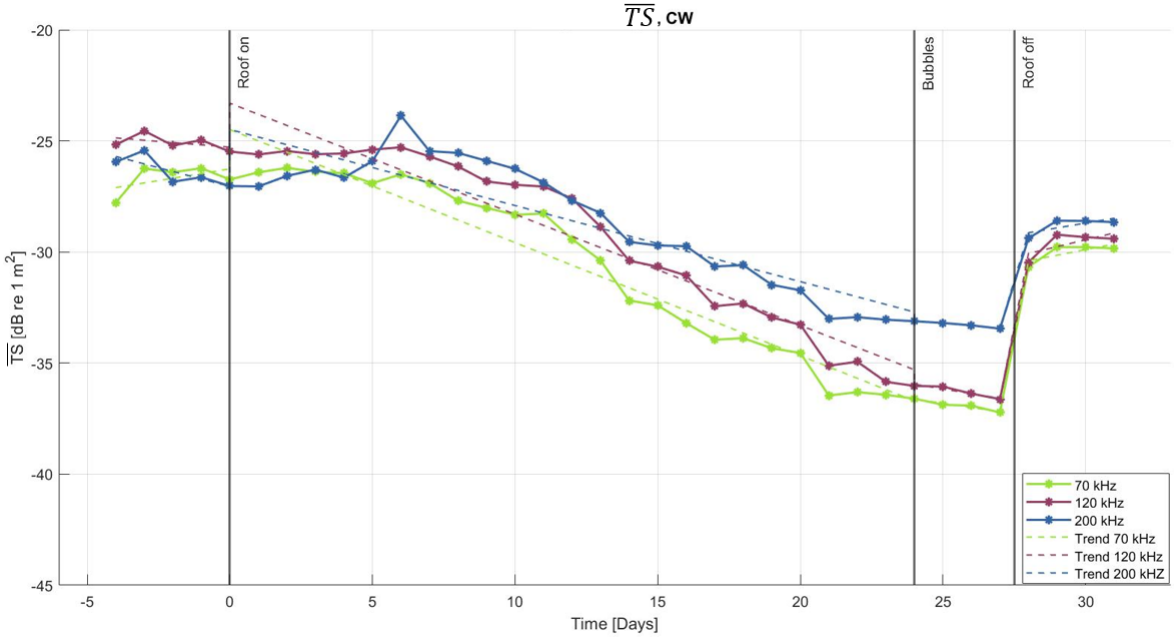

Figure 5.3: $\overline{TS}$ from CW data from all three transducers as a function of time (days) to study the change throughout the experimental period. 70 kHz is the green dots, 120 kHz is the purple, and 200 kHz is the blue. The trends of the $\overline{TS}$ values are presented as stippled lines with the same color as the associated frequency.

Fig. 5.3 shows $\overline{TS}$ values per day from the CW data for all three frequencies, where the green graph is obtained from the 70 kHz echo sounder, the purple is from the 120 kHz, and the blue is from the 200 kHz. The stippled lines represent the overall trend for the four periods defined in Table 5.1. The three frequencies indicate an overall decrease in $\overline{TS}$ values during the submerged period. As seen by the FM data in Fig. 5.2, the ratio between the $\overline{TS}$ values from the three frequencies from the CW data are closer at the beginning of the experiment than when the bladder starts to diminish. Further, there is no significant change in the $\overline{TS}$ values after the bubbling started compared to the three days before. After the roof was removed, the TS values increased considerably from day 27 to day 28. See Table 5.3 for the trends and R^2 values used in the figure.

Table 5.3: Linear regression trends of $\overline{TS}$ from CW data for the four periods, for each nominal frequency, the periods are defined as in Table 5.1. The trends are presented numerically as in Eq. (2.50). In addition, the R^2 values for each trend-line are included.

	70 kHz		120 kHz		200 kHz	
	Trend	R^2	Trend	R^2	Trend	R^2
Before	0.2x - 26	0.3	-0.1x - 25	0.2	-0.3x - 27	0.6
Mid	-0.5x - 25	0.9	-0.5x - 23	0.9	-0.3x - 25	0.8
Bubbles	-0.2x - 32	0.9	-0.2x - 31	0.9	-0.1x - 31	1
After	1.3x - 70	0.6	1.3x - 68	0.5	0.9x - 55	0.5

Table 5.3 shows the TS trends from the CW data calculated for the periods defined in Table 5.1. In Fig. 5.3, it can be observed how the trends for the 70 and 120 kHz echo sounder from the submerged period are decreasing at the same rate, which is confirmed by the numerical values in Table 5.3. The

R^2 values for the two frequencies show how the trend lines are closer to the scattered values than the line from the 200 kHz data.

5.1.3 TS values from a simulated CW signal

Based on the theory from [30] and Eqs. (4.6) - (4.10), TS values from a CW signal was simulated in the R software using the KRM model. The same frequencies were used for the simulation as in the experiment; 70, 120, and 200 kHz, and the results are presented in Fig. 5.4.

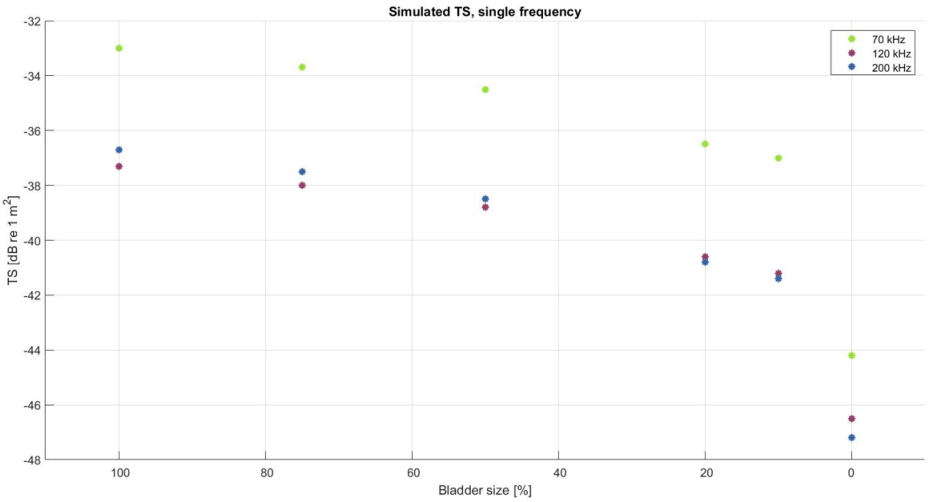

Figure 5.4: TS from a simulated CW signal for frequencies: 70 kHz (green), 120 kHz (purple), and 200 kHz (blue). The x-axis is based on the bladder size from Fig. 4.2, where the volume has been decreased from 100 % to 75%, 50%, 20%, 10%, and 0 %.

Fig. 5.4 shows the results from simulating the TS for six different swim bladder sizes: 100 %, 75 %, 50 %, 20 %, 10 %, and 0 %. The simulation was conducted three times for every swim bladder size in order to reproduce the TS from a CW signal from the 70 kHz (green), 120 kHz (purple), and 200 kHz (blue) echo sounder. The ratio between the 120 and 200 kHz values is approximately equal for each swim bladder size, while the 70 kHz is constantly higher than the other two frequencies. Moreover, the TS values decrease with the decreasing swim bladder volume for all frequencies.

5.1.4 Comparing measured TS from FM and CW signals

This subsection combines the daily $\overline{TS}$ values from FM and CW data for each frequency and compares the results in Fig. 5.5.

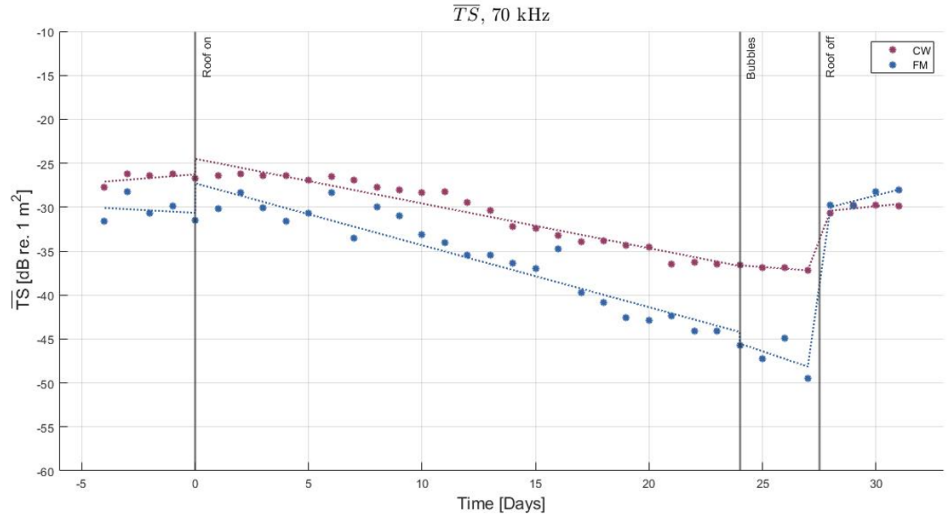

(a) $\overline{TS}$ from both FM and CW signals from the 70 kHz echo sounder

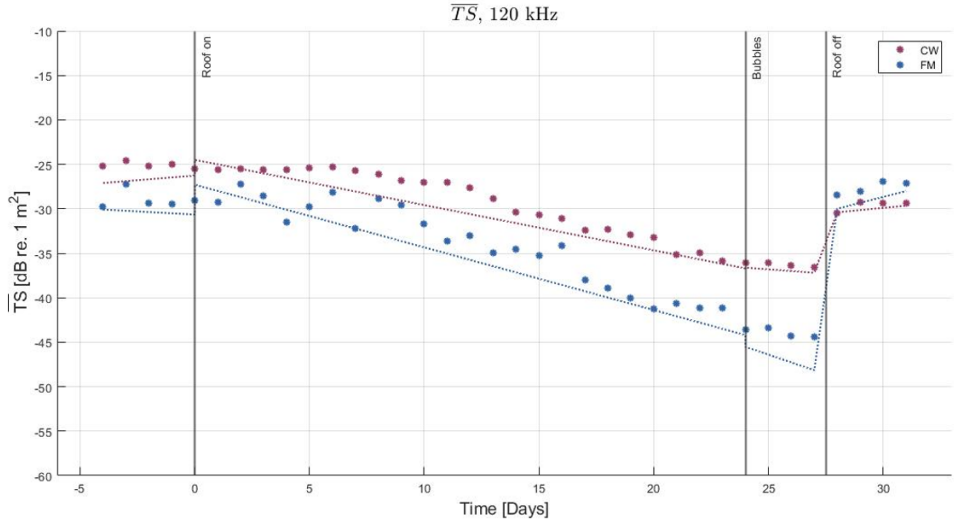

(b) $\overline{TS}$ from both FM and CW signals from the 120 kHz echo sounder

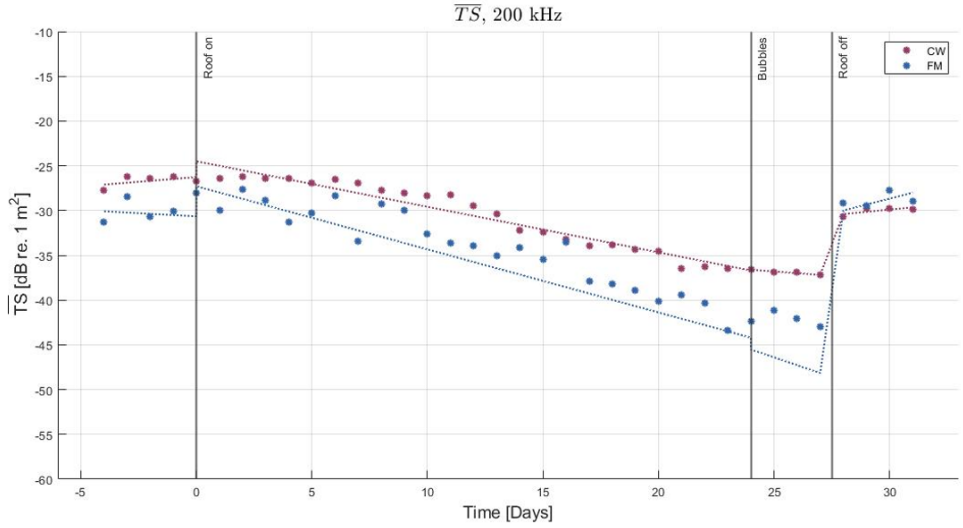

(c) $\overline{TS}$ from both FM and CW signals from the 200 kHz echo sounder

Figure 5.5: $\overline{TS}$ of CW and FM data from the a) 70 kHz transducer, b) 120 kHz transducer, and c) 200 kHz transducer as a function of time (days). The $\overline{TS}$ values are equal to the ones plotted in Subsections 5.1.1 and 5.1.2. The purple dots represents the CW data, and the blue is from the FM data.

Fig. 5.5 a), b), and c) compares the daily changes in $\overline{TS}$ values from CW data (purple) with the results from FM data (blue) for the 70, 120, and 200 kHz echo sounders, respectively. The values of $\overline{TS}$ are consistently lower for the FM data than for CW data throughout the experiment, except for after the roof was removed, where the FM signals are higher than the ones from the CW data. The overall trend decreased for both signal types during the submerged period, and both signal types increased rapidly after the cage was resurfaced. From the R^2 values in Tables 5.2 and 5.3, the linear regression lines are close to 1 for both the FM and CW data during the submerged period, and as seen in Fig. 5.5, both signal types are decreasing almost linearly from day 0 to day 24. Moreover, the daily $\overline{TS}$ values from the CW signals vary less than the values from FM signals, but both signals appear to start decreasing after approximately day 6.

Twice a week, around 15 fish were sampled and checked for air. The amount of air and the neutral buoyancy were measured in order to calculate the relative air in the swim bladder. The sampling method is described in Section 3.3, and the results can be seen in Appendix A. Eq. (2.24) was used when calculating the average relative air for each sampling day. Measuring the air in the bladder was done to support the data collected from the echo sounders and confirm that the air was diminished, and the results from the samples can be seen in Fig. 5.6.

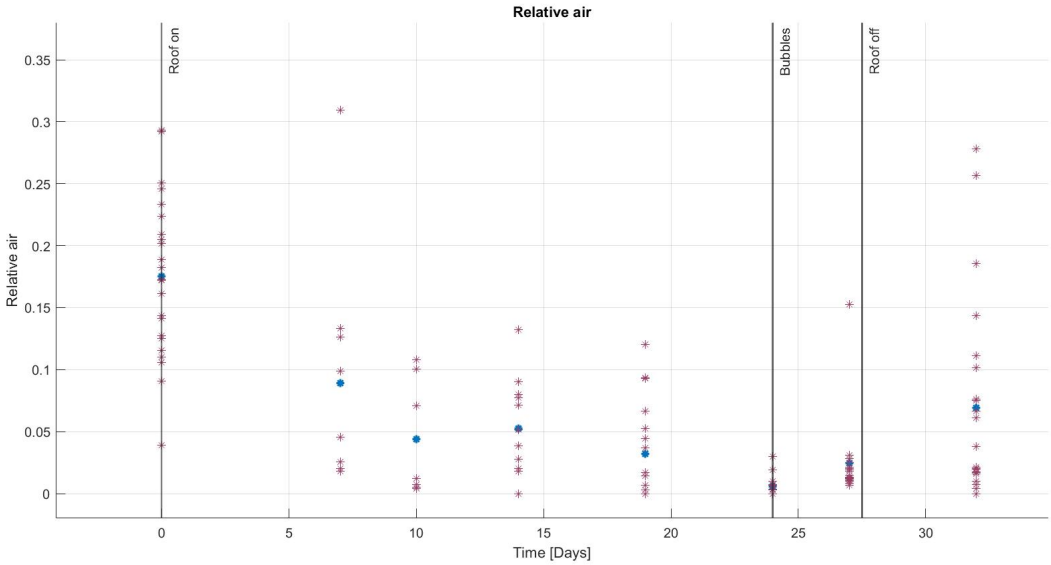

Figure 5.6: Decrease in relative air throughout the experimental period, where the relative air is the ratio between the measured air quantity and the neutral buoyancy. The purple is the individual measurements, and the blue is the average of the individual measurements.

Fig. 5.6 includes the individually sampled values and the average of all measurements as a function of time (days), purple and blue dots, respectively. The period is divided into sections as defined in Table 5.1. As for the $\overline{TS}$ values, the relative air decreases over time until the bubbling starts on day 24. The air increased after the roof was removed, but it did not reach the same level as before the cage was submerged. The samples were scattered more on the first days, whereas the relative air was nearly zero when the bladders were assumed empty. Following the removal of the roof, the values

went back to having more significant gaps amongst the individual values. From Subsection 2.3.2, a deflated swim bladder will scatter the signal less than a bladder filled with air. Comparing the drop in air level from day 0 to day 24 in Fig. 5.6 with Fig. 5.5, it is evident that an empty bladder returns lower values than a full bladder. This can also be seen in the simulated TS values from Fig. 5.4. From the measured $\overline{TS}$ from CW and FM data, it appears the decrease is more prominent from day 6, and from the measured relative air, the biggest change was between day 0 to day 10.

5.1.5 Frequency response of TS(f) from measured FM signals

Subsection 5.1.1 shows the average TS values from FM signals as a function of time, while this section addresses the TS values expressed as a function of frequencies, where the data set is equal in both sections. 5 kHz was excluded to remove the unstable parts of the signal and was done for both sides, where the new bandwidths were between $f_1 + 5$ kHz and $f_2 - 5$ kHz. The average of each frequency of each ping in the track was found by using Eqs. (2.23) - (2.25). To express the average TS(f), $\overline{TS}$(f), for the exported file, every frequency within a track was averaged over the total amount of tracks in the file, using Eqs. (2.23) - (2.25). Four days were selected to study the possible change in the frequency response of measured TS from FM data for swim bladders of different sizes. The frequency response from the four days is shown in Fig. 5.7.

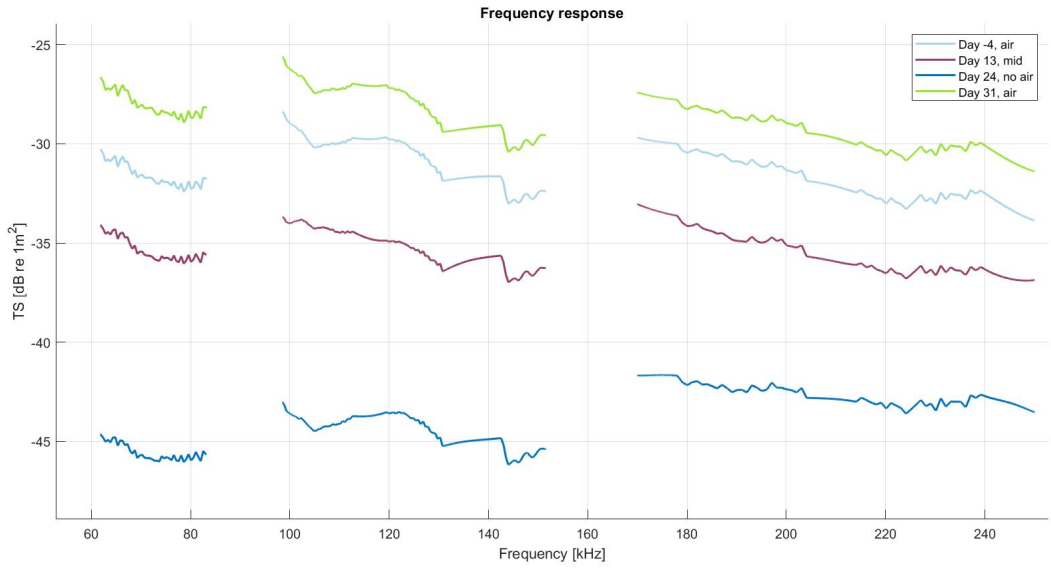

Figure 5.7: Measured $\overline{TS}$ as a function of frequency, $\overline{TS}$(f), from FM data for the three frequency bands, plotted for four selected days: -4 (light blue), 13 (purple), 24 (darker blue), and 31(green).

Fig. 5.7 shows the frequency response from FM signals for four selected days for the three echo sounders. Day -4 (light blue), before the roof was attached, and day 31 (green), after it was removed, were chosen as they were days with assumed full swim bladders. The 13th day (purple) was chosen as it is in the middle of the experiment, and it was valuable to observe if the frequency response changed after two weeks. Lastly, day 24 (dark blue) represents the last day before the salmon got access to air

bubbles, and the bladder was empty, and shows how the TS values are lowest for each frequency band compared to the other days. The frequency responses from the 70 kHz and 200 kHz echo sounders are equal for the four selected days. Further, the frequency response from the 120 kHz frequency band from day 13 slightly differs from the responses from days -4, 24, and 31. In order to study the frequency responses from day -4 and day 24, Fig. 5.8 is included.

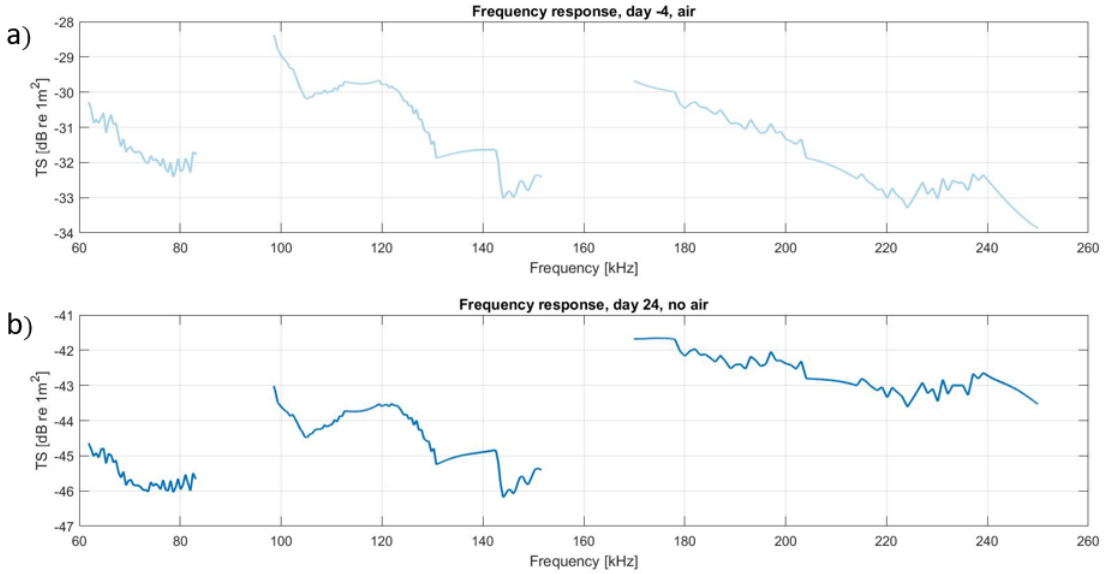

Figure 5.8: Frequency response from measured TS from FM signals, shown for days -4 in a) and 24 in b). It includes the frequency response from each of the three frequency bands. Note: the y-axis are scaled differently in a) and b).

Fig. 5.8 shows the measured frequency response from TS, from the three frequency bands, where a) is the response from day -4 and b) is the response from day 24. The y-axis are different in order to compare the responses better. The discontinuity in between the frequency bands is probably due to an software error in LSSS [12]. From the figure, the frequency response from the two days are approximately equal, with the only difference being the dB re. 1 m^2 levels. For day 24, there is an increase in the ratio between the frequency ranges, which is not observed in day -4. Moreover, the frequency responses from the 120 kHz echo sounder are increasing and decreasing as a cosine wave, where the minimums and Eq. (2.4) can be used to estimate the spatial distance between two reflections. For both days, the spatial distance between the two minimums for the 120 kHz frequency band is 3 cm.

5.1.6 Frequency response from a simulated FM signal

Based on the theory from [30] and Eqs. (4.6) - (4.10), the frequency response of TS(f) from a FM signal was simulated in the R software using the KRM model [30]. The same bandwidth as in the parenthesis in Table 3.2 was used to model the measured frequency response and the results from different bladder sizes are shown in Fig. 5.9.

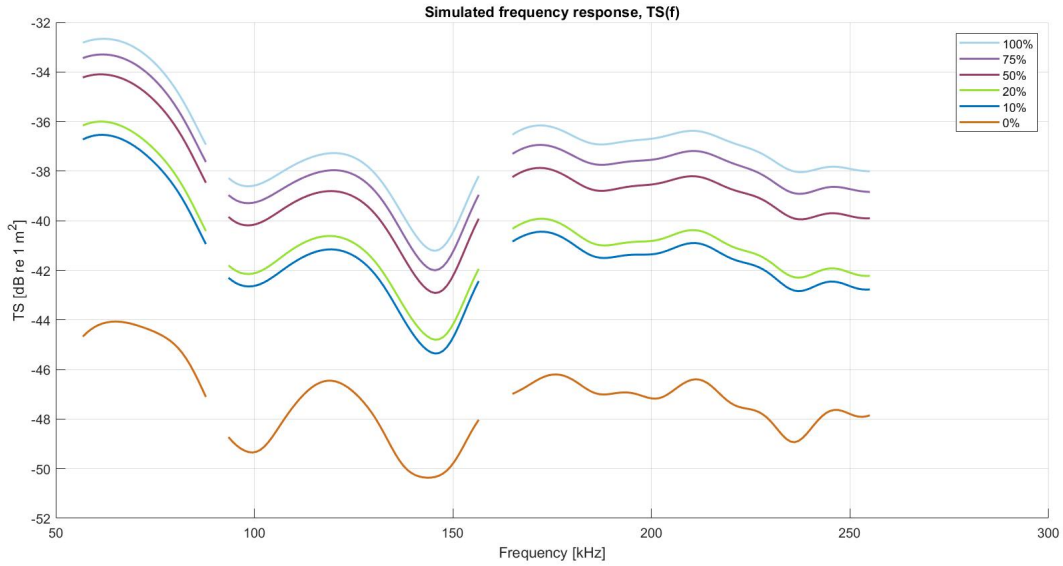

Figure 5.9: KRM simulation of TS for the 70, 120, and 200 kHz frequency bands as a function of frequency. The simulation was run eighteen times to simulate a full bladder at 100 % (light blue), then 75 % of the full bladder (light purple), 50% (purple), 20% (green), 10% (darker blue), and 0 % (orange).

Fig. 5.9 shows the results from simulating the TS(f) from a FM signal for six different swim bladder sizes: 100 % (light blue), 75 % (light purple), 50 % (purple), 20 % (green), 10 % (darker blue), and 0 % (orange). The simulation was conducted three times for every swim bladder size in order to reproduce the TS(f) from an FM signal from the 70 kHz, 120 kHz, and 200 kHz frequency bands from Table 3.2. When studying the figure, the shape of the responses is approximately the same for all sizes. The dB re. 1 m^2 values are decreasing with decreasing bladder volume. Comparing the simulated frequency response in Fig. 5.9 with the measured frequency response in Fig. 5.7, some resemblance can be observed.

5.2 Measured volume backscattering strength

This section will present the results from S_V, where the values were obtained from the EK80 echo sounders and Eqs. (2.30) - (2.34), and Eqs. (2.41) - (2.42). The data was automatically exported from LSSS as a function of frequency by using a Python script created by Pedersen [65]. Unlike the TS values, S_V values extract every value within the selected regions regardless of the tracks. The same regions and time of data as for TS from FM data were used when exporting and analyzing S_V. The returned .json files include one S_V value for each frequency in the bandwidth, where a $\pm$ 1.5 kHz bandwidth of the nominal frequencies was selected for further studies. To observe the day-to-day change in S_V values, Eqs. (2.23) - (2.25) were used to calculate the average S_V, $\overline{S_V}$, per day. The result is shown in Fig. 5.10, including the linear regression lines for each frequency.

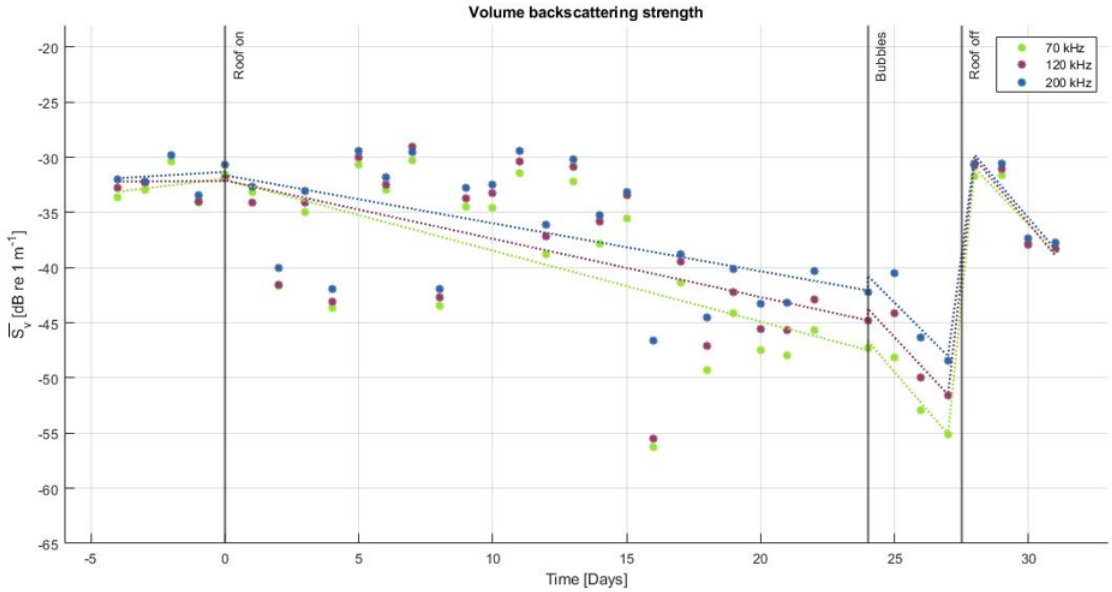

Figure 5.10: $\overline{S_V}$ for each echo sounder, is plotted as a function of time (in days) to compare the results, where the dots are the daily values, and the stippled lines are the trends. The green is data acquired from the 70 kHz echo sounder, the purple is from the 120 kHz echo sounder, and the blue is from the 200 kHz echo sounder.

Fig. 5.10 shows the $\overline{S_V}$ as a function of time for the three frequency bands, where the green points represent the measurements from the 70 kHz echo sounder, the purple is from the 120 kHz, and the blue is from the 200 kHz. The included trends show the overall change for each period, which are defined in Table 5.1. Day 23 is missing in the plot due to an error made when collecting the data. As for the $\overline{TS}$ from the FM and CW data, there are variations in both daily values and between the frequencies. The ratio between the three frequencies increases when the air level decreases. Further, the $\overline{S_V}$ values acquired from the 70 kHz echo sounder are the lowest throughout the experiment, and the values measured by the 200 kHz echo sounder are the highest. This is also seen for the $\overline{TS}$ from both FM and CW data. After removing the roof, the values returned to the same level as before the cage was submerged. The trend lines from the figure are shown numerically in Table 5.4.

Table 5.4: Linear regression trends of $\overline{S_V}$ for the four periods, for each nominal frequency, where the periods are defined in Table 5.1. The trends are presented numerically as in Eq. (2.50). In addition, the R^2 values for each trend-line are included.

	70 kHz		120 kHz		200 kHz	
	Trend	R^2	Trend	R^2	Trend	R^2
Before	0.3x - 32	0.1	0.01 -32	0.0001	0.1x - 31	0.02
Mid	-0.6x -32	0.4	-0.5x -32	0.3	-0.4x -32	0.3
Bubbles	-2.8x +21	0.9	-2.6x + 19	0.8	-2.4x + 18	0.8
After	-2.6x + 41	0.8	-3.0 +52	0.8	-2.8x + 50	0.8

Table 5.4 presents the linear regression lines for $\overline{S_V}$ from Fig. 5.10 numerically. As seen in the figure, the three frequencies decrease at approximately the same rate during the submerged period. Never-

theless, the R^2 values indicate that the linear line does not fit the daily values well, and is due to the significant daily scattering.

5.2.1 Frequency response from measured S_V(f)

The results in Section 5.2 show the daily variation in $\overline{S_V}$, while this subsection focuses on the S_V(f) as a function of frequency. The data sets are equal to those used in the previous section, but 5 kHz was excluded to remove the unstable parts of the signal and was done for both sides of the frequency band. The new bandwidth was between $f_1 + 5$ kHz and $f_2 - 5$ kHz, and the results are shown in Fig. 5.11.

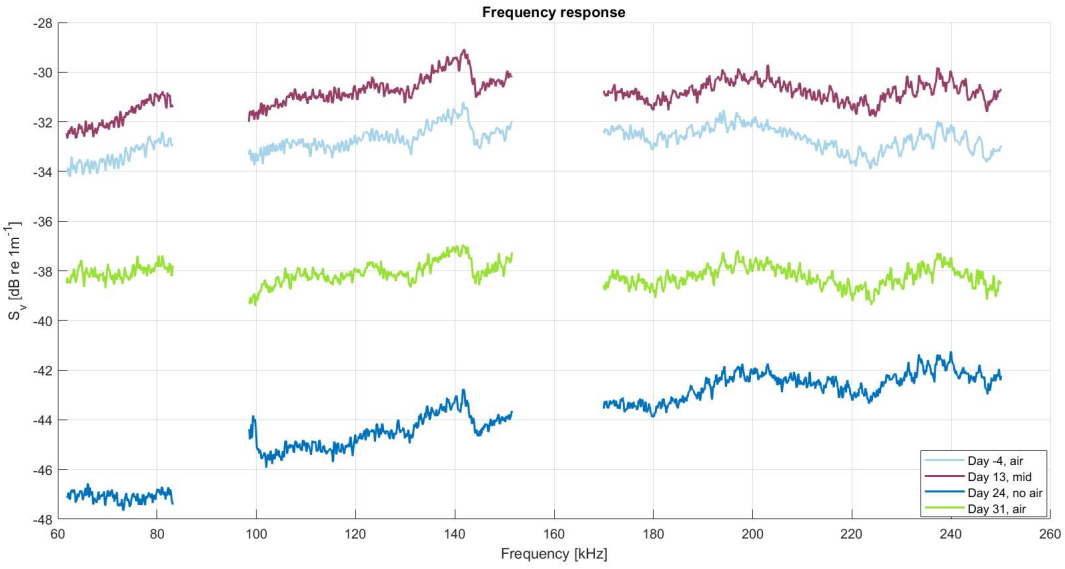

Figure 5.11: Measured S_V from FM data as a function increasing frequency, S_V(f), for the three frequency bands from the four selected days: -4 (light blue), 13 (purple), 24 (dark blue), and 31 (green)

The figure shows the same selected four days as in section 5.1.5 for TS(f). The light blue (day -4) and green (day 31) are days with assumed full swim bladders, while the purple (day 13) and darker blue (day 24) are assumed to be nearly empty and empty, respectively. The frequency response from day 24 returns the lowest values, as expected from an empty swim bladder. Additionally, the frequency response from days -4, 13, and 31 are at approximately the same dB re. 1 m^{-1} level for the three frequency bands, while the response from day 24 is increasing from the 70 kHz band to the 200 kHz band.

5.3 Swimming speed

In this section, the results from the swimming speed will be presented. The text files exported for swimming speed were based on the "Tracks" function in LSSS, as explained in Section 2.4, and includes one track for each fish, where every track consists of several pings. Every ping in a track con-

sists of multiple x,y, and z positions and the timestamp for each position. The total distance swam by the fish was found by using Eqs. (2.45) - (2.46), and the total time used to swim the distance was found from Eqs. (2.43) - (2.44). If one fish's total distance or time were greater than 4 m or 10 s, the fish were considered invalid and was not used for further calculations. According to Section 3.1, the theoretical beam width by the roof was 3 m. Therefore, it is unlikely that a fish would swim through the beam slower than 10 s and longer than 4 m. If the total distance and time exceed these boundaries, it suggests that something is not right, which may be due to the tracking algorithm.

The swimming speed for one fish was calculated using the total distance, total time, and Eq. (2.47). The results from the echo sounders are given in m/s, but by applying Eq. (2.48) the swimming speed is expressed in body length per second, bl/s. In order to study the daily change in swimming speed, Eq. (2.24) was applied to obtain the average swimming speed value for each day, and Eq. (2.49) was applied to calculate the standard deviation of the swimming speed for the whole file. The same method was applied for finding the swimming speed from both FM and CW signals, and the results are shown in Subsections 5.3.1 and 5.3.2.

5.3.1 Swimming speed from FM signals

This subsection addresses the swimming speed results from the FM data, given both in m/s and bl/s. Due to a mistake made in Matre, day 23 from the 70 kHZ echo sounder is missing from the FM data, and the value from day 22 has been added to day 23. The average swimming speed is calculated to study the day-to-day variations, which was done using the script in Appendix F.3. Additionally, the swimming speed trend is included to observe the overall trend for the different periods in the experiment and can be seen together with the calculated R^2 values in Table 5.5. Fig. 5.12 shows the swimming speed from the FM data as a function of time and includes the associated trends.

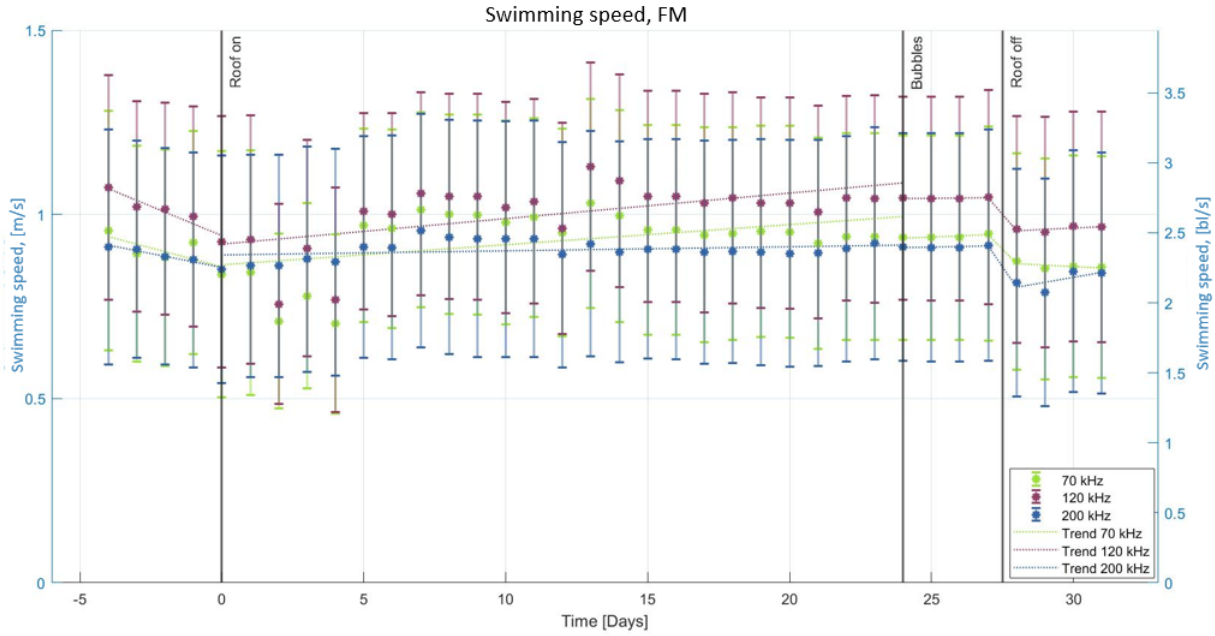

Figure 5.12: Swimming speed given as means per day and standard deviation (± 0.3 m/s) from FM pulses from the three transducers, where the green is for 70 kHz, purple is for 120 kHz, and the blue is for the 200 kHz. The graph includes the swimming speed trends, where green is the trend for the 70 kHz, purple is for the 120 kHz, and blue is for the 200 kHz echo sounder. The left y-axis shows the swimming speed expressed in m/s, while the right side shows the speed expressed by bl/s.

Fig. 5.12 shows the results after calculating the mean swimming speed per day and standard deviation for all three transducers from FM data. The green represents the 70 kHz transducer, the purple is for the 120 kHz, and the blue is the 200 kHz. Additionally, the figure includes the swimming speed trends for the four sections of the experiment, defined in Table 5.1. From the figure, the swimming speed measured by the 120 kHz is consistently higher than the speed measured by the two other echo sounders, where the speed acquired by the 200 kHz echo sounder has the lowest value. The maximum swimming speed during the experiment was measured on day 13 (120 kHz transducer), where the speed was 1.1 m/s. The minimum speed was found on day 4 and was measured at 0.7 m/s by the 70 kHz transducer. The trends show an overall increase in swimming speed during the submerged period. The standard deviation shows that the different frequencies are within each other's uncertainties. Nevertheless, the standard deviation is high (± 0.3 m/s) and indicates significant uncertainties within the calculated swimming speed from the three frequencies.

Furthermore, from day 0 to day 24, there is a 15 % increase in swimming speed measured by the 70 kHz transducer, 18 % increase by the 120 kHz, and 3 % increase by the 200 kHz. The percentage was calculated based on the first and last value of the trend line, using Eq. (2.52). After the roof was removed, there was a significant leap in the values for all frequencies. Table 5.5 shows the trends for the three frequency bands and the R^2 coefficients.

Table 5.5: The swimming speed trends for the FM data are shown numerically for each frequencies in m/s, calculated for the four periods defined in Table 5.1

	70 kHz		120 kHz		200 kHz	
	Trend	R^2	Trend	R^2	Trend	R^2
Before	-0.02x + 1.0	0.5	-0.03x + 2.5	0.9	-0.02x + 2.3	1
Mid	0.01x + 0.9	0.2	0.01x + 0.9	0.3	0.001x + 0.9	0.1
Bubbles	0.003x + 0.9	0.6	0.001x + 1.0	0.9	0.002x + 0.9	0.5
After	-0.004x + 1.0	0.3	0.004x + 0.9	0.6	0.01x + 0.4	0.4

The values in Table 5.5 shows the swimming speed trends for FM data from Fig. 5.12 numerically, including the R^2 values for each period. The 200 kHz is approximately constant, which is also seen in Fig. 5.12. The R^2 values reveal that the regression lines are not a good fit for the measured values, and as the y-axes are zoomed out, this is not easily observed in the figure. By omitting the standard deviation, the scattered values would be more evident.

5.3.2 Swimming speed from CW signals

In this subsection, the results from the CW pulses will be presented. The swimming speed was found using the method explained for the swimming speed obtained from the FM signals and the MATLAB script in Appendix F.2, and the results are expressed in Fig. 5.13. The associated swimming speed trends and R^2 from the CW data are included in Table 5.6.

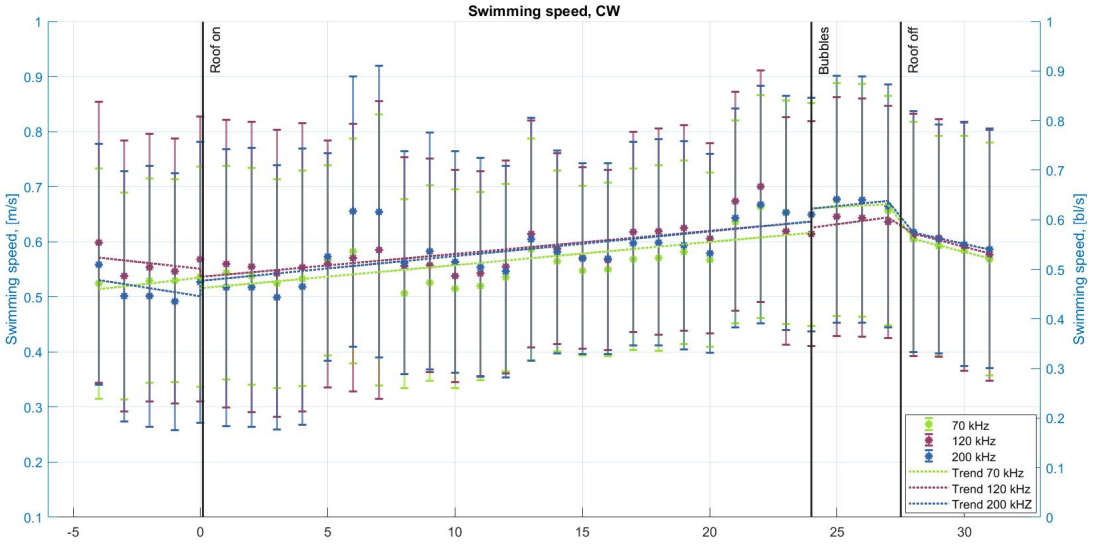

Figure 5.13: Swimming speed given as means per day and standard deviation (± 0.2 m/s) from CW pulses from the three echo sounders, where the green is for 70 kHz, purple is for 120 kHz, and the blue is for the 200 kHz. The graph includes the swimming speed trends, where green is the trend for the 70 kHz, purple is for the 120 kHz, and blue is for the 200 kHz. The left y-axis shows the swimming speed expressed in m/s, while the right side shows the speed expressed by bl/s. NB: axes differ from Figs. 5.12 and 5.14 to show the increase more clearly.

Fig. 5.13 shows the results, including the standard deviation, after calculating the mean swimming speed per day for all three transducers. The green represents the 70 kHz transducer, the purple is for the 120 kHz, and the blue is the 200 kHz. Additionally, the figure includes the swimming speed trends for the four periods in the experiment defined in Table 5.1. The 70 kHz transducer recorded the lowest values for most of the submerged period, and 120 kHz recorded the highest. Moreover, the overall swimming speed increased while the roof was attached, which can be observed for each of the frequencies. The swimming speeds are mainly between 0.5 and 0.7 m/s, and the speed from each frequency is within each other's uncertainty range. However, like the speed from the FM data, the high standard deviations (± 0.2 m/s) indicate significant uncertainties within the calculated swimming speeds, which applies to each of the frequencies. During the 24 days of submergence, the values from the 70 kHz data increased by 20 %, while 120 and 200 kHz increased by 19 % and 20 %. The trends can be seen numerically in Table 5.6, along with the R^2 values.

Table 5.6: The swimming speed trends for the CW data are shown numerically for all frequencies, in m/s, calculated for the four periods defined in Table 5.1

	70 kHz		120 kHz		200 kHz	
	Trend	R^2	Trend	R^2	Trend	R^2
Before	0.005x + 0.5	0.4	-0.005x + 0.6	0.1	-0.007x + 0.5	0.8
Mid	0.004x + 0.5	0.5	0.004x + 0.5	0.6	0.005x + 0.5	1
Bubbles	0.002x + 0.6	0.04	0.006x + 0.5	0.3	0.005x + 0.6	0.1
After	-0.020x + 1.2	1	-0.014x + 1.006	1	-0.02x + 1.16	0.2

Table 5.6 includes the swimming speed trends and R^2 coefficients from CW data. The three frequencies increase at approximately the same rate during the submerged period based on the trends, and from the R^2 value, the trend line for the 200 kHz fits better than for the 70 and 120 kHz.

5.3.3 Comparing the swimming speed from FM and CW signals

In this subsection, the differences between the results from FM and CW speed will be compared. Fig. 5.14 presents the results measured by the echo sounders, and includes the complementary measurement of the swimming speed from the camera data. The figures show the speed in both m/s and bl/s, and the standard deviation calculated using Eq. (2.49).

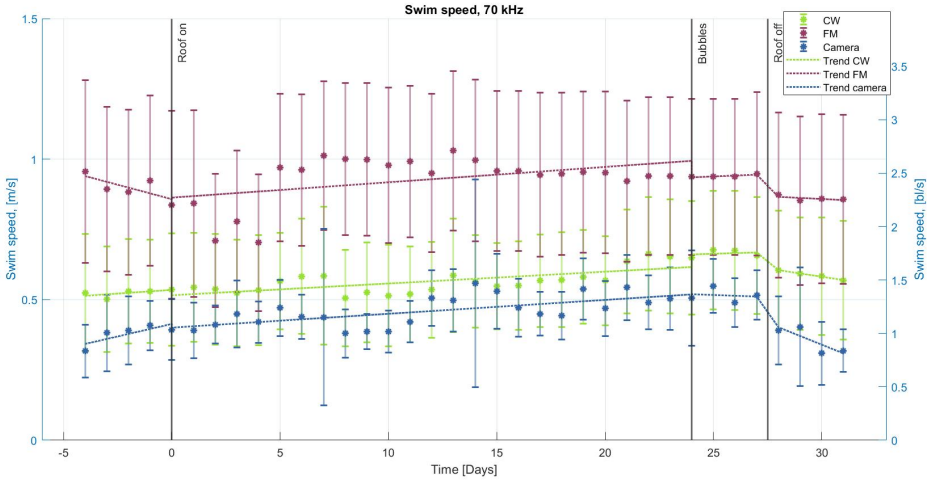

(a) Swimming speed acquired by the 70 kHz echo sounder for both CW and FM data, and measured speed from camera data

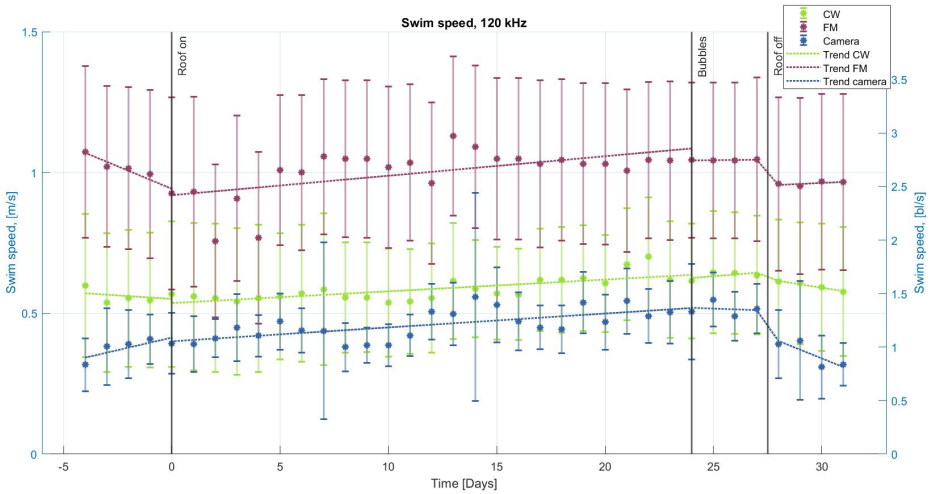

(b) Swimming speed acquired by the 120 kHz echo sounder for both CW and FM data, and measured speed from camera data

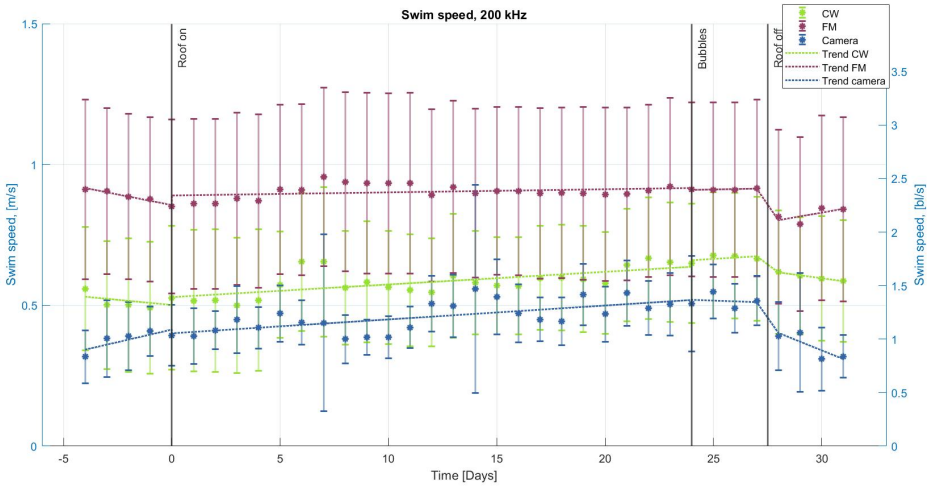

(c) Swimming speed acquired by the 200 kHz echo sounder for both CW and FM data, and measured speed from camera data

Figure 5.14: Swimming speed from CW and FM data from a) the 70 kHz echo sounder, b) 120 kHz, and c) 200 kHz, and the camera measurements. The green represents the CW signals, purple is the FM signals, and blue is the camera data. The graph includes the swimming speed trends and standard deviations, where the same color is used for the different data types. The left y-axis shows the swimming speed expressed in m/s, while the right side shows the speed expressed by bl/s.

Fig. 5.14 shows the swimming speed from the CW, FM, and camera data for the a) 70 kHz, b) 120 kHz, and c) 200 kHz transducer. The green represents the CW values, purple is the FM values, and blue is the camera data. The associated trends and standard deviations are included, where the same colors are applied as for the swimming speed values. The swimming speeds are a function of time (days) and are presented in m/s on the left y-axis and bl/s on the right y-axis.

There are significant differences between the two signal types regarding speed for all three frequencies, with FM data almost twice as fast as the CW data. In addition, the camera data is closer to the values from the CW signals. As shown in the figure, the standard deviation for CW data overlaps the standard deviation from FM and camera data each day, while the standard deviation of the FM and camera data rarely overlaps. Table 5.7 shows the increase from day 0 to day 24 calculated by using Eq. (2.52), based on the trends for the camera data and the values in Tables 5.5 and 5.6.

Table 5.7: The increase in percentage from day 0 to day 24 for the swimming speed from the two pulse types, FM and CW, and camera measurements. The percentage is calculated from the first value of the trend to the last value.

Signal type	70 kHz	120 kHz	200 kHz
FM	15 %	18 %	3 %
CW	20 %	19 %	20 %
Camera	30 %		

Table 5.7 presents the increase from the submerged period, day 0 to day 24, in percentage. The table shows that the increase in the speed from the CW data is approximately the same, while the increase in speed from the FM signals varies. This is especially between the 200 kHz transducer and the 70 and 120 kHz.

Chapter 6

Discussion of methods and the results from measurements and simulations

This chapter is divided into two sections, where the first section will discuss the methods and difficulties of the measurements and data processing. The second section will address the results from both the simulations and the measurements from Chapters 4 and 5.

6.1 Discussion of methods

6.1.1 Number of fish

There are many factors to consider in the experiment, but among the most critical is the number of fish chosen, where roughly 500 salmon were specified as the appropriate number. A requirement for choosing this specific number of fish was to achieve normal behavior. Moreover, as TS is an essential parameter in this study, it was desirable to measure individual salmon, which justified the decision of having a minimum amount. As S_V is a measure of backscattered signals in a volume, the number of fish was not as decisive as for TS. Observations of unusual behavior were evident the first days after attaching the roof, and the salmon was swimming individually in the cage as opposed to in a school. Eventually, they seemed to calm down and started acting as anticipated. As a result of monitoring individual fish on the echo sounder and observing expected behavior, 500 fish was deemed an appropriate quantity.

6.1.2 Environment

The experiment was conducted from mid-March to mid-April, a season with changing weather and temperatures. The sea surface froze during the night prior to the scheduled day of submersion, preventing salmon from replenishing the bladder. Despite the ice being crushed the same morning, the start date had to be postponed ensuring the swim bladder had a natural amount of air. Despite wait-

ing a day, it was not guaranteed that all salmon would be refilled before the attached roof. On the other hand, as it appears in Section 5.1, the values for $\overline{TS}$ are not declining until the 6th day based on data from the CW and FM signals, at the earliest. Furthermore, they began refilling immediately after removing the roof on day 28. Considering these two instances, it is conceivable that one day with ice will not affect the results.

Rain and snowmelt were not considered when analyzing the data and are two factors that may impact seawater salinity, which is vital when finding the sound speed in seawater. After studying Fig. 3.10, it can be assumed that the change in salinity is trivial, and rain and snowmelt were neglected. Additionally, the current fluctuated significantly during the experiment. The transducers were placed in the corner of the cage and could only measure fish swimming either co-currently or against the current, depending on the current's direction. However, this was not taken into consideration when analyzing the swimming speeds. The cage's edges shifted into the beam due to the current, which resulted in noise on the returned signal. In order to avoid including noise in the results, the data was extracted during hours with less current.

6.1.3 Sampling technique

The salmon were initially fed around 2 kg of pellets every day, but it soon became apparent that it was nearly impossible to catch the fish in the relatively large pen. As described in Section 3.3, it was desirable to extract approximately 15 fish two times a week to examine the amount of air in the swim bladder. Due to salmon being fed daily, they did not swim to the surface as readily as expected. A further limitation was the small catcher attached to a pole, making it impossible to reach depths greater than 3 m. As a consequence of overly feeding, the number of days the fish were fed was reduced. They became hungrier and more willing to approach the surface on sampling days. Furthermore, the catcher was replaced with a dead fish collector with a bigger diameter attached to a rope, allowing it to reach deeper depths. The adjustments made it easier to catch the desired 15 fish. Despite the lack of food every day, it is assumed that the growth rate was not impacted.

The sampling method may have affected the amount of air in the bladder. Some salmon were observed emitting bubbles while being caught in the catcher. It was hard to say if this was indeed the salmon's response to being stressed, how much air they released, and if it applied to every salmon. Following, the salmon were taken out of the water and placed into a tub filled with seawater and anesthesia, and once again, air bubbles were observed. Whether the air observed came from the swim bladder or if the fish snapped air while being transferred to the tub was unclear.

The next step was to perform a welfare measurement [59], as described in Section 3.3, which involved lifting the fish from the tub and placing them on a table. Since the tests took a while, the salmon were left on the table for some time before the relative air was measured. The waiting and lifting may have affected the air level, and it is unknown whether or not salmon open the channel between their swim bladder and pharynx as they die. These factors have not been conclusively linked to the amount of air present in the swim bladder and are considered sources of error. If they are affected, it is reasonable

to assume all salmon have experienced it, and it can be ignored when calculating the relative air.

Numerous errors can occur when measuring the relative air level in the salmon's swim bladder. The swim bladder is fragile and can easily break if the end of the tube is pressed against it. Even though 15 fish were removed from the cage, some days had fewer measurements due to ruptured swim bladders. In order to obtain neutral buoyancy, the swim bladder was injected with air, as explained in Section 3.3. However, from day 19, when the bladder was nearly empty, some fish released the injected air before the neutral buoyancy could be found. Initially, the hypothesis was that the fish had grown, and the entrance to the bladder grew proportionally. Consequently, the tube would be too small to fill the hole, and air would be able to escape through the bladder entrance. Nevertheless, the escape of the air stopped after the roof was removed and the bladder was replenished, and the hypothesis proved not to be valid. Further, there was a theory that the bladder ruptured, but further study of the bladder ruled this theory out. The days with leaks can be seen in Appendix A. The observed neutral buoyancies for these fish depend on the amount of air right before the injected air escaped. With all sampled fish nearly empty, the source of error from the escaping air will be deemed trivial as the calculated relative air was approximately 0 (ref. Table A.2).

6.1.4 Setup and positioning of the transducers

The cage was approximately 14 meters deep, and the transducers were positioned 10 meters beneath the bottom of the cage, at 25 meters. The results depend on where the transducers were positioned. Ideally, if the objective is to study the vertical distribution of the fish, the transducers should be placed further away as the beam gets wider with the increasing distance. It can be argued that the transducers should be placed closer to the fish for the purposes of the present study, as the individual fish and TS are more important than the vertical distribution. The LSSS echogram shows singular salmon at all three frequencies and indicates that the transducers were well-positioned at 25 m below the surface. Fig. 3.5 shows an illustration of the coverage of the fish shoal in the cage. Furthermore, the three transducers were mounted on a gimbal, relatively close to each other, where each beam measured the same fish. This was tested by ruling out a single fish on one of the echo sounders and then checking if the same fish appeared on the other two. Thus, it was observed that all three beams overlapped very well.

Previous experiments [6] show that fish submerged below 10 m have sufficiently less salmon louse compared to regular cages. As this experiment was not focused on salmon louse, the roof was only attached at 1 m depth. This made it possible to collect fish throughout the submerged period. However, it can be argued whether the results are as representative as those from a cage submerged below 10 meters.

6.1.5 LSSS: Tracking algorithms for FM data

Compared to previous publications and predictions [23–25], the swimming speed from FM signals found in this thesis, as seen in Fig. 5.12, is unexpectedly high. Prior to submersion, the fish swam approximately 0.9 to 1.1 m/s (2.4 to 2.8 bl/s), measured by the FM signals, while in [25] and [23], the fish swam 0.2 m/s (0.55 bl/s). Hence, it was desirable to determine if this result can be attributed to applying the aggregation algorithm in LSSS when extracting the swimming speed for FM data. In this case, it is imperative to underscore that LSSS is primarily being used for CW data; there is per, today, no well-defined techniques for using tracking algorithms on FM data. A test was performed to determine whether the algorithm was responsible for the high swimming speed. A six-minute area was selected on day 3, as shown in Fig. 6.1.

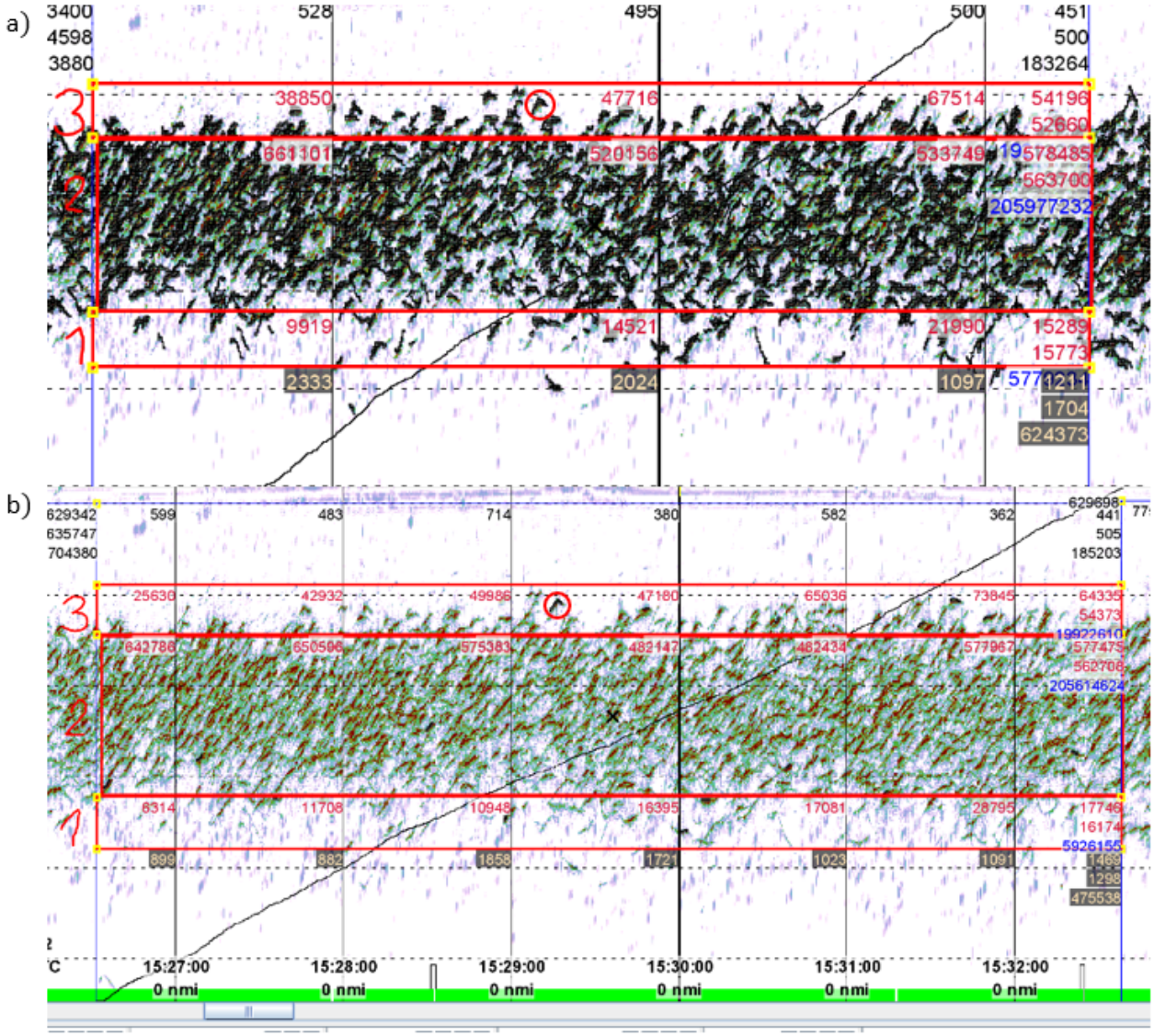

Figure 6.1: Screenshot of an echogram of the salmon from FM data as seen in LSSS. a) shows data from FM signals tracked using the aggregation algorithm, while b) is the same data set as in a) but has been tracked using peak. The red boxes represent 6 minutes of tracks and are equal in a) and b). The boxes are divided into three layers, labeled *1*, *2*, and *3* on the left side of the red box.

Fig. 6.1 shows two screenshots from the echogram as seen in LSSS, where both a) and b) are based on the same FM data set. However, a) shows the tracks from the 120 kHz echo sounder measuring FM data after applying the aggregation algorithm, while b) shows tracks from FM data after using the peak algorithm. The tracks are seen as the black lines surrounding the fish, illustrated in the red circles (or see Fig. 2.4 for a close up). 6 minutes of the data set was selected, seen as the red box in a) and b), which is equal for the two figures. The colors in the figures are the dB re 1 m^2 threshold defined in the echogram, where red indicates a strong backscattered signal, and pink/purple indicates a weaker signal (see Fig. 3.11 for the colored thresholds). The box is divided into layers 1, 2, and 3, indicated on the left side of the boxes, to calculate the swimming speed based on different fish densities. There are evidently more tracks from aggregation seen in a) than peak in b). The data were exported from all three layers (1+2+3), layers 1+2, and each layer individually. The swimming speed were calculated as defined in Section 5.3 and the standard deviation is found by using Eq. (2.49), and the results are shown in Table 6.1.

Table 6.1: Swimming speed from the 120 kHz transducer, using both aggregation and peak. Results shown both in m/s and bl/s, including the standard deviation

	Aggregation, [m/s]	Peak [m/s]	Aggregation [bl/s]	Peak [bl/s]
Layer 1 + 2 + 3	1.0 ± 0.3	0.4 ± 0.1	2.7 ± 0.8	1.0 ± 0.2
Layer 1	0.9 ± 0.3	0.4± 0.03	2.4 ± 0.9	1.0 ± 0.1
Layer 2	1.1 ± 0.3	0.4± 0.1	2.8 ± 0.8	1.0 ± 0.2
Layer 3	0.7 ± 0.2	0.4± 0.1	2.0 ± 0.6	1.0 ± 0.2
Layer 1 + 2	1.1 ± 0.3	0.4 ± 0.1	2.8 ± 0.8	1.0 ± 0.2

As shown in Table 6.1, there is a significant difference in swimming speed between the two algorithms. Layers 1 and 3, with fewer tracks and less density than layer 2, slightly decrease in speed for aggregation and peak. Based on articles [23–26], the swimming speed is more consistent with the results from using peak. In addition, it matches what has been observed and measured with the camera, seen in Fig. 5.14. The number of fish tracked by peak is considerably lower than that of aggregation, where 17 fish are tracked while 924 are tracked by aggregation. However, since 45 - 75 observations a day from the camera data are considered enough, one hour of tracks from peak is sufficient to validate the results.

The aggregation method was chosen because of the increased number of tracks in the primary fish school compared to peak. Moreover, this test was carried out after reviewing the results and analyzing all the data. In contrast, peak may have been the preferred algorithm if the test had been done before exporting the data. Due to the limited time, the tracking was not repeated, and results were based on aggregation. The same test was conducted for the 200 kHz transducer and can be seen in Appendix C. The number of tracks for the 200 kHz data was approximately the same for both peak and aggregation. However, even with the same amount of tracks, the difference between the speeds was the same as in Table 6.1.

LSSS is developed and primarily used for surveys using CW pulses. From this test, it can be assumed

that aggregation has not been established enough to be used on FM data. Even though peak is just as developed as aggregation, it is still more selective of fish, and the algorithm appears to be better at choosing individual fish. As seen in Fig. 6.2, some of the tracks follow individual fish quite well, but in the middle of the shoal, where the fish is denser than the periphery, there is no guarantee that one track follows only one fish.

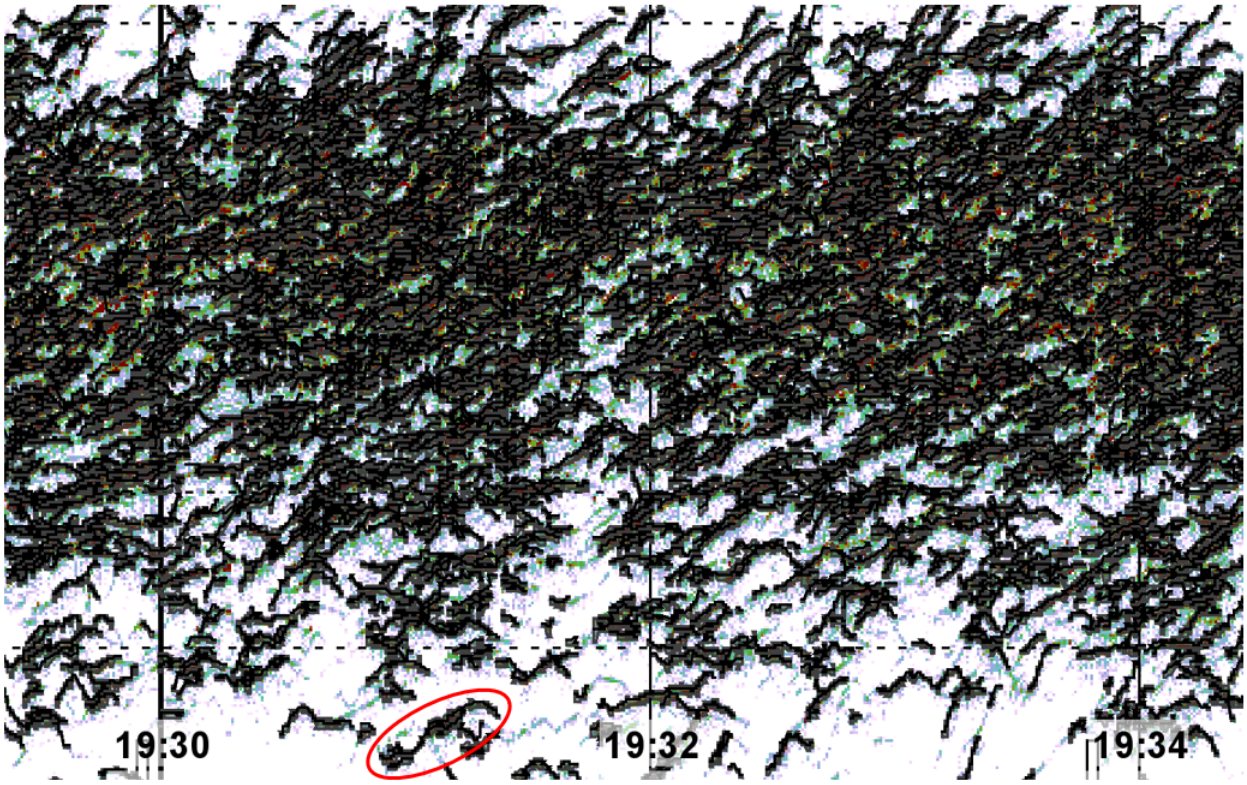

Figure 6.2: Tracks from the FM signals acquired from the 70 kHz echo sounder when using aggregation as the tracking method. The algorithm mostly returns good tracks in the less dense parts of the shoal. Some tracks seem to overlap, as in the red oval, and in the middle of the school.

Fig. 6.2 shows tracks after using aggregation on data from the 70 kHz echo sounder transmitting FM pulses. The data set is approximately 4 minutes long and is taken from day -4. The figure shows that the less dense area at the bottom returns mostly good tracks following individual fish. However, in the red ellipse, a track can be seen jumping from one fish to the next. Due to the amount of fish and tracks in the middle of the fish school, it is not certain how accurate the tracking is. Despite the high swimming speed values, the overall trend and comparison with the CW data are vital to the thesis and will be discussed further in Subsection 6.2.3.

6.1.6 LSSS: Tracking algorithms for CW data

Ideally, the same tracking algorithm for both FM and CW data should be used for better comparison. However, the tracks were not as expected when applying aggregation for CW pulses and can be seen in Fig. 6.3 a)

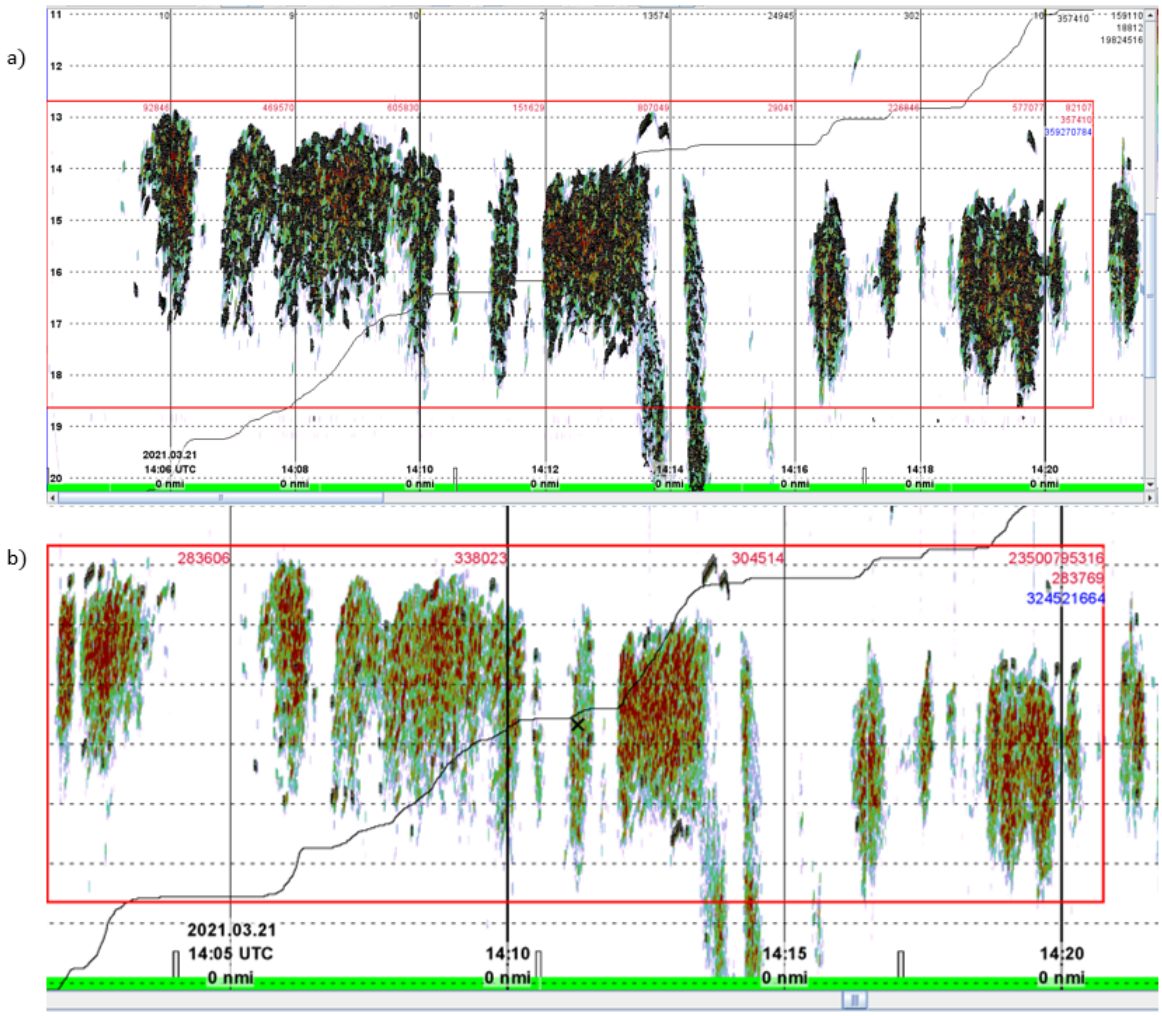

Figure 6.3: Screenshot of the tracks on CW data as shown in the echogram in LSSS. a) shows the tracks on CW data after being tracked using the aggregation algorithm, while b) shows the same data set as in a) after using peak. Tracks are indicated by the black lines surrounding the fish (see Fig. 6.4). The red boxes represent approximately 20 minutes of tracks and are equal in a) and b).

Fig. 6.3 illustrates the CW tracks as seen in the echogram in LSSS, and both a) and b) includes the same fish and data set. a) is after aggregation was applied as the tracking method, while b) is after using peak. In a), there are tracks on almost every fish, seen as the black lines surrounding the fish (see Fig. 6.4). Compared to the tracks using aggregation on FM data in Figs. 6.1 a) and 6.2, the tracks are much thicker as the spatial resolution of CW signals are lower than for the FM signals, see Table 3.3. However, when zooming in on the tracks from aggregation, they are all split into multiple tracks per fish, as shown in Fig. 6.4. Compared to the number of tracks from aggregation in Fig. 6.3 a), there are only a few when using peak in b), and most of them are in the periphery of the fish shoal. A similar test as in Subsection 6.1.5 was conducted for CW data, but only for one layer, and the results are presented in Table 6.2 together with the standard deviations.

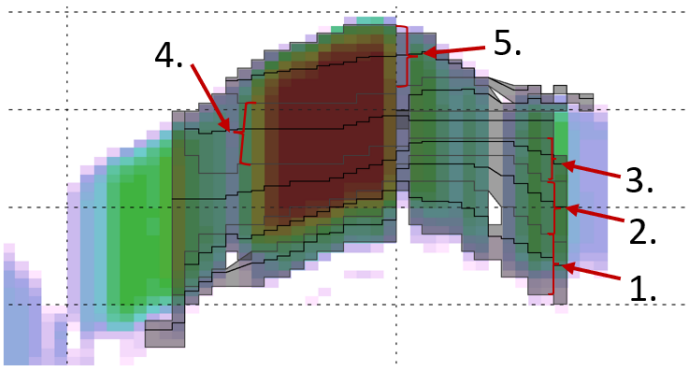

Figure 6.4: Zoomed in on an individual fish, showing 5 tracks after using the aggregation algorithm. Each arrow points at the thickest black lines, which indicates the middle of each track.

Fig. 6.4 shows how the aggregation tracks look on one individual fish. The track is divided into multiple tracks, where the thick, black lines (indicated by arrows) represent the middle of each track. Here, the single fish has five tracks. When each fish have multiple tracks, it will result in more fish than anticipated, and it may affect the results. Although peak returned fewer tracks, as shown in Fig. 6.3 b), the concern of multiple tracks per fish made peak the preferred choice.

Table 6.2: Swimming speed results and standard deviations from testing peak and aggregation on CW data, presented in both m/s and bl/s.

	Peak	Aggregation	Peak	Aggregation
Frequency	[m/s]	[m/s]	[bl/s]	[bl/s]
70 kHz	0.6 ± 0.3	1.3 ± 0.4	1.7 ± 0.8	3.6 ± 0.9
120 kHz	0.6 ± 0.3	1.4 ± 0.4	1.6 ± 0.7	3.6 ± 0.9
200 kHz	0.5 ± 0.2	1.3 ± 0.3	1.6 ± 0.6	3.5 ± 0.9

Table 6.2 shows the speed from CW for peak and aggregation in both m/s and bl/s, for all three frequencies. As in Table 6.1 and the test for FM data, aggregation returns a swimming speed with values double the values from peak. From Fig. 6.3 b), the lack of tracks might be a reason for the low speed values from peak on CW data. However, as the results from 2 hours of data in Fig. 5.13, return the same values, it is more likely the algorithm.

6.1.7 EK80

As this thesis is in the preliminary stages of research when it comes to FM and using scientific echo sounders in aquaculture, the computer or settings applied in Section 3.5 for the mission plan in EK80 affected the data collection. The mission plan was set to transmit signals from five echo sounders simultaneously. The echo sounders transmitted one hour of CW signals and one hour of FM. As the hour progressed, the software failed to maintain the ping rate. Due to the large data files acquired from the five FM echo sounders, the folders on the computer quickly became full, and the ping rate was slowed down. According to Kongsberg Maritime, this was a Windows issue [70]. As the issue was

detected early on, a new folder was created for the files, and the software was restarted every morning. However, during the data analysis in LSSS, it was found that the restart had no effect on the ping rate. When CW and FM were split into different files and opened in LSSS individually, the recorded data time deviated from the desired hour. From Section 3.5, the settings in the EK80 mission planner were based on the number of pings and not the time. Therefore, the time was affected when the computer could not maintain the ping rate.

The length of the collected "hour" can be seen in Appendix E. Due to the number of tracks from tracking FM data using aggregation, additional or fewer values should not affect the results as the results are based on the average TS and swimming speed. Further, the TS and swimming speed from CW data were based on two hours of data (ref. Subsection 3.6.3). This was done by subtracting one hour from the start of the FM period and adding one hour at the end of the period, seen in Appendix E. If the selected hour of FM data is longer than an hour, the following period of CW data will be less than an hour, resulting in fewer tracks.

6.2 Discussion of results

6.2.1 Results from measured and modelled TS

Based on previous publications of submerged cages for farmed salmon [23–26], the measured backscattered signals were assumed to decrease as the salmon's swim bladder deflates. This is consistent with the theory from Subsection 2.3.2, where the air in a fish's swim bladder accounts for 90 % of the TS [10]. The strong backscattered signal is due to the high characteristic acoustic impedance between the air and the surrounding seawater [9], and with less air, the signal becomes weaker.

The measured $\overline{TS}$ from the FM data in Fig. 5.2 and from the CW data in Fig. 5.3, shows how the $\overline{TS}$ starts to decrease after being submerged for approximately 6 days. This differs from what was found in [23, 25, 26], where the most significant decrease occurred immediately after the cage was submerged. However, the overall change in $\overline{TS}$ from Figs. 5.2 and 5.3 show a similar plot as in Fig. 1.1, where the values decreases linearly after 4 days of submergence [23]. The R^2 values for the measured $\overline{TS}$ values in Table 5.2 for the FM data and in Table 5.3 for the CW data, are close to 1 for each of the echo sounders during the submerged period. Hence, the daily $\overline{TS}$ values for both signal types are a good fit for the regression lines and are decreasing almost linearly, which is similar to Fig. 1.1 [23]. However, from Figs. 5.2 and 5.3 the $\overline{TS}$ is approximately flat the first 6 days after being submerged, which is seen in Figs. 1.2 and 1.3 [24, 25]. In contrast, in Fig. 1.4, the biggest change occurs the first 10 days of being submerged [26]. This is consistent with the sampled relative air from Fig. 5.6, where the most significant change was between day 0 and day 10.

Common for the experiments in [24–26] is that the measured echo intensity was based on echo integration, which is a measure of the backscattered signals from multiple layers in a volume, ref. Eq. (2.39). Thus, the results from the articles are more comparable to the measured $\overline{S_V}$ data than the $\overline{TS}$. Nevertheless, as the echo intensity in [23–26] is presented as a relative change over time, the

trends can be compared to the measured $\overline{TS}$ from this experiment. Moreover, the cages in [24–26] are submerged to depths between 10 – 24 m, and it can be argued that the results from these experiments are deemed less comparable to the results obtained during this thesis. Further, the cages in [23] were submerged to 3 m depth, and thus, it is conceivable that the decrease from the experiment is more reasonable than the results from [24–26]. The relative change in echo intensity [23–26] does not provide as much information as the measured $\overline{TS}$ values (from FM and CW) found during this experiment. The measured values for $\overline{TS}$ are now quantitative values for 38 cm long salmons and can be used by others to detect a decrease in the air level.

Furthermore, the theoretical calculated TS values presented in Section 1.2 based on Eqs. (2.26) - (2.29) from [28, 29, 47] is compared to the simulated TS and the measured $\overline{TS}$ from FM and CW signals, and is presented in Table 6.3.

Table 6.3: Theoretical calculated TS and simulated TS, and measured $\overline{TS}$ from FM and CW signals. Presented for a full swim bladder, day 0, and when the bladder is assumed empty, day 24. *In [47], Eq.(2.26), is based on a 50 kHz echo sounder, but is here used to compare to the measured and simulated TS from a 70 kHz echo sounder.**Eq. (2.29) [29] is based on measurements on mackerel from a 38 kHz echo sounder.

	70 kHz [dB re. 1 m^2]		120 [dB re. 1 m^2]		200 [dB re. 1 m^2]	
	Day 0	Day 24	Day 0	Day 24	Day 0	Day 24
Measured $\overline{TS}$, FM	-32	-44	-29	-44	-28	-42
Measured $\overline{TS}$, CW	-28	-36	-27	-35	-27	-33
Theoretical calculated TS	-34*	-55**	-30	-55**	-30	-55**
Simulated TS	-33	-44	-37	-47	-37	-47

Table 6.3 addresses the simulated, theoretical calculated, and measured $\overline{TS}$ values from day 0 (assumed full bladder) and day 24 (assumed empty bladder). Eq. (2.26) is based on measurements from a 50 kHz echo sounder but is used in comparison with values from a 70 kHz signal. Further, Eq. (2.29) was established from measurements from a 38 kHz echo sounder on mackerel, a fish without a swim bladder, and is used for comparison with the salmon's empty swim bladder. As seen in Table 6.3, the measured $\overline{TS}$ from the FM data from day 0 is closer to both the theoretical calculation and the simulated TS than the values from CW data.

For an empty bladder, the measured $\overline{TS}$ from FM data acquired from the 70 kHz transducer fits the simulated TS perfectly. The measured $\overline{TS}$ from the CW signals and the 120 and 200 kHz echo sounders transmitting FM signals, however, do not correspond to the low simulated TS values. The theoretical calculated TS for an empty bladder is –55 dB re. 1 m^2 (ref. Eq. (2.29)), and is not comparable to the simulated TS or the measured $\overline{TS}$ from either FM or CW signals from day 24. Eq. (2.29) was established after studying mackerel and thus is not the best estimation for calculating the theoretical TS from an empty salmon swim bladder. As the measured $\overline{TS}$ from CW signals stabilizes from day 22 (ref. Fig. 5.3), and the sampled air levels are approximately 0 from day 10 (ref. Fig. 5.6), it can be assumed the bladder was empty, and the backscattered signal from a salmon will most likely not reach -55 dB re. 1 m^2 as from Eq. (2.29).

From Fig. 5.5 the $\overline{TS}$ from CW signals in a), b), and c) are consequently higher than the $\overline{TS}$ values from FM signals. This applies for the periods *Before*, *Mid*, and *Bubbles* (defined in Table 5.1), while after the cage was resurfaced, the values from the FM signals are higher or at a level equal to the values from CW data. The high $\overline{TS}$ values from the CW data might be explained by the dense shoal and the spatial resolution of the CW signals. A high fish school density may prevent the CW pulses from clearly distinguishing between the targets, creating a stronger backscattered signal.

A recurrence in the measured $\overline{TS}$ from the FM and CW data in Figs. 5.2 and 5.3 is how the 70 kHz echo sounder returned the lowest and the 200 kHz the highest values throughout the submerged period. Additionally, the ratio between the measured values are closer at the beginning of the period than when the bladder was assumed empty. This is mainly seen in Fig. 5.2 for the FM data but is observed in Fig. 5.3 for the CW data as well, where the 200 kHz echo sounder differs from the 70 and 120 kHz. From this, the ratio of $\overline{TS}$ at different frequencies might serve as an indicator of deflated swim bladders. However, the simulated TS from Fig. 5.4 shows the opposite, where the 70 kHz signal returns the highest and the 200 kHz signal the lowest TS values as the swim bladder volume diminishes.

When tracking the FM data from the 200 kHz echo sounder, from Fig. C.1, there are few tracks compared to the number of tracks from the 70 and 120 kHz (ref. Fig. 6.1). Despite this, the .json files returned an equal amount of tracks for all three echo sounders. This suggests something is not correct and should be further investigated. As a result, the credibility of the measurements from tracking FM data using aggregation can be deemed weakened.

The simulated TS values from Fig. 5.4 deviate from the measured $\overline{TS}$ from FM and CW data, and the theoretically calculated values from Eqs. (2.26) - (2.29). The simulated TS values are likely to be less reliable given the insufficient x-ray image of the swim bladder in Fig. 4.2. Since the x-ray image does not show the swim bladder from the dorsal side, the size of the bladder was based on estimations. Hence, the modeled bladder is likely to differ from a real bladder. Additionally, the size was adjusted by the percentage of the assumed full swim bladder while keeping the upper boundary constant. From [71], the bladder is asymmetrically compressed when it diminishes, where one end of the bladder is more compressed than the other. This was not taken into account when adjusting the volume of the bladder. The TS was simulated from a signal normal to the dorsal aspect of the fish, while the measurements were done from the ventral aspect. From [28], the measured TS of salmon from the dorsal and ventral recordings returned different results, where the backscattered values from the ventral aspect were higher than from the dorsal. The same was observed in [69], which measured the TS from gilthead sea breams, where the TS from the ventral aspect gave better signals than from the dorsal. The differences in TS signals from ventral and dorsal measurements are due to the morphometry of the swim bladder [28]. Considering this, the simulations of TS in this thesis are considered less reliable. For better results, the swim bladder in Fig. 4.2 could be modeled 180° to simulate a ventral swim bladder.

As explained in Subsection 2.3.3, the backscattered values are strongly dependent on the tilt angle, i.e., the fish is swimming forward horizontally with head up and tail down as in Fig. 2.2. However, from [7] when fish were less than 500 g and submerged for shorter periods, tilt angles due to insufficient

air did not occur. The fish in this thesis had an average weight of 580 g and can be categorized as a small fish, as in [7]. Only a few fish were observed swimming with a tilt by the end of this experiment. Based on this and the observations from [7], the tilt angles are assumed to be trivial for the measured backscattered signal.

TS is the logarithmic value of σ_{bs} (ref. Eq. (2.21)), which is a value dependent on the size, shape, orientation, and material of the studied target [9]. Occasionally, individual salmon separate from the school and swim with a different orientation than the rest. If this happens while they are swimming through the beam, it will lead to variations in the measured $\overline{TS}$ values, which is illustrated in Fig. 6.5 a) and b).

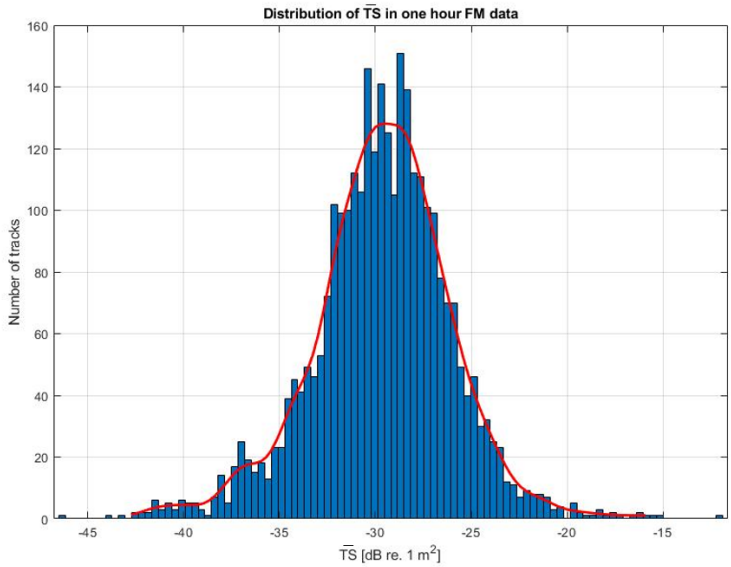

(a) Number of tracks with equal $\overline{TS}$ values, measured from FM signals

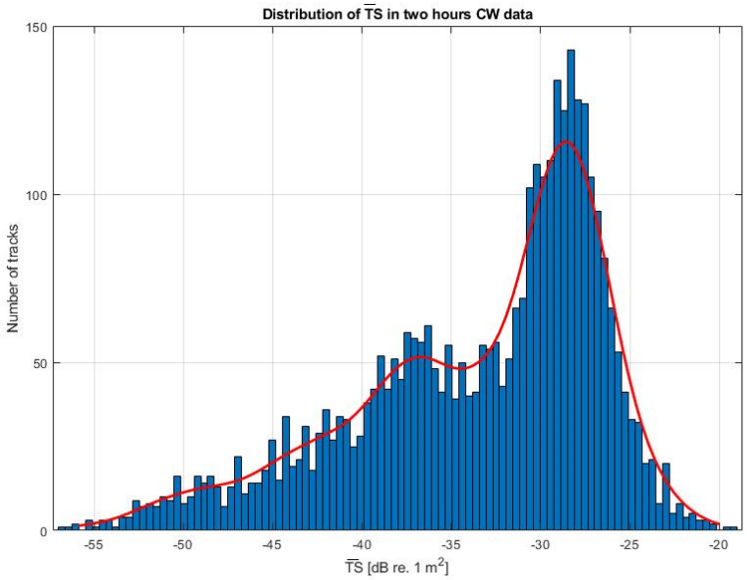

(b) Number of tracks with equal $\overline{TS}$ values, measured from CW signals

Figure 6.5: Number of tracks with equal $\overline{TS}$ values. The blue columns represent the dB re. 1 m^2 values, and how many tracks returned equal values. a) is based on one hour FM data from the 70 kHz frequency band from day 31. Showing the $\overline{TS}$ values from 2993 tracks. b) shows the number of tracks from two hours of CW data from the same day, including 3543 tracks.

Fig. 6.5 shows an overview of the number of tracks returning equal $\overline{TS}$ values within one and two hours of data, presented in a histogram. a) illustrates the tracks from one hour of FM data from day 31, acquired from the 70 kHz frequency, which returned 2993 tracks. b) shows the $\overline{TS}$ data from two hours of CW data from the same day, which obtained 3543 tracks. There are significant variations among the measured $\overline{TS}$ values from both signal types, and it is assumed that the biological variations in the experiment exceed the uncertainties from the echo sounders and the measurement setup.

FM signals can provide information not available from CW signals, such as the measured frequency response from TS in Fig. 5.7. The frequency response from an empty swim bladder on day 24 shows an increase from the 70 kHz frequency band to the 120 kHz and from the 120 kHz to the 200 kHz. This frequency response is found typically among fish without swim bladders, such as Atlantic mackerel, and is due to the fish's backbone [27]. The same results can be seen in the frequency response from S_V, in Fig. 5.11. Comparing the simulated frequency response in Fig. 5.9 to the measured frequency response in Fig. 5.7, it can still be observed some resemblance. Despite this, the increasing dB re. 1 m^2 for increasing frequency is not visible for a 0 % swim bladder in Fig. 5.9, since the simulation does not consider the backbone. By implementing Eq. (2.4), the distance between objects within the fish can be calculated. The minimums for the 120 kHz frequency band in Fig. 5.7 were calculated to be 3 cm apart and can be assumed to be from the top of the fish body to either the top or the bottom of the swim bladder. Day 24, when the bladder is assumed empty, shows the same frequency response, and as the bladder is flat, it is more likely to be from the top of the fish to the top of the swim bladder. The responses are averaged over 100s of fish; thus, some information may be lost due to the averaging. Studying the frequency response from one individual salmon would probably provide more information than the averaged frequency response and should be considered further studied.

6.2.2 Results from measured S_V

As for the measured $\overline{TS}$, the measured $\overline{S_V}$ from FM signals was expected to decrease along with the diminishing air level in the swim bladder [23–26]. S_V is a measure of every backscattered signal within a volume (ref. Eq. (2.40)) and is therefore strongly dependent on the number of fish swimming through the beam. Ultimately, this will even out over time, but the one hour of measured $\overline{S_V}$ from the FM data in Fig. 5.10 might not be long enough for this to happen. As seen from Fig. 5.10, the daily $\overline{S_V}$ values vary significantly throughout the experimental period. The hour of FM data was chosen at approximately the same timestamp each day to make the daily results more comparable. However, when processing the data in LSSS, some days had more fish swimming through the beam than others due to the fish's swimming pattern. With fewer fish within the selected hour, the measured $\overline{S_V}$ decreases, which might be the reason for the day-to-day variations in Fig. 5.10. The low R^2 values from Table 5.4 indicate that the linear regression line is not a good fit for the scattered $\overline{S_V}$ values, and as seen in Fig. 5.10 the measured values do not seem to start decreasing before around day 15.

From Section 3.2, 500 salmon were deemed adequate to achieve normal schooling behavior and, at

the same time, observe individual salmon. In the aquaculture industry, cages can contain thousands of salmon swimming in dense fish shoals, making it difficult to distinguish between individuals and measure TS. Hence, since S_V is measuring all salmon in the sampling volume, this parameter might be better to study the diminishing air in the bladder than TS when applied in a full scaled cage.

In Fig. 5.10 the measured $\overline{S_V}$ values from the three echo sounders are in proximity of each other when the bladder is assumed full, but as the air in the bladder diminishes, the ratio between the three different frequencies increases. A similar pattern can be observed in the measured $\overline{TS}$ from FM (ref. Fig. 5.2) and CW (ref. Fig. 5.3) signals, but is more evident in Fig. 5.10. The increased ratio between the measured $\overline{S_V}$ from the three echo sounders could therefore be implemented as an alert that the air level in the swim bladder is decreasing, e.g., if the ratio exceeds a defined quantity.

The increased ratio between the frequency bands can be seen when studying the measured frequency response of S_V(f) in Fig. 5.11. On day 24, when the bladder is assumed empty, the responses increase for each frequency band; the band from the 70 kHz echo sounder has the lowest dB re. 1 m^{-1} values, and the values increase with increasing frequency. The two frequencies returning the lowest and highest dB re. 1 m^{-1} values can be selected, e.g., 70 and 240 kHz. Then, the ratio between them can be implemented as an alert saying the bladder is diminishing. However, as this is most evidently seen when the bladder is said to be empty, it would not work as early detection of decreasing air levels. From the measured $\overline{S_V}$ values in Fig. 5.10, the ratio between the values from the 200 kHz and the 70 and 120 kHz echo sounder is most prominent from day 16. Hence, it would be valuable to study the frequency response of S_V between day 13 and day 24.

Furthermore, the frequency response from measured S_V differs from the frequency response from measured TS from the FM data in Fig. 5.7. The clearly seen ups and downs in TS values in Fig. 5.7 from the 120 kHz frequency band is not found for the frequency response from S_V in Fig. 5.11. As S_V measures the total backscattering within a volume, valuable information from individual salmon might be lost due to the averaging. Information such as the size of the salmon and the swim bladder, and also the fish's backbone can be seen from the frequency response of TS in Fig. 5.7. However, if every fish in a shoal is of the same age and has equal swimming patterns, a similar frequency response as TS can be obtained from S_V.

6.2.3 Swimming speed from measured CW and FM data

From former experiments, [23–26], the swimming speed was expected to increase as the air in the fish's swim bladder decreased. The increased swimming speed is an indicator of negative buoyancy, which is a result of an insufficient air level in the bladder; the salmon swim faster to compensate for the negative buoyancy [7]. This increase in swimming speed during submergence was observed from both the FM signals (ref. Fig. 5.12) and the CW signals (ref. Fig. 5.13) and additionally from the complementary measurements based on the camera data (ref. Fig. 5.14). The most significant change in swimming speed measured by the echo sounders is observed from day 5, for both signal types.

Compared to previous publications, the swimming speed for the FM and CW data is higher than expected. The swimming speeds from control cages are usually between 0.2 – 0.4 m/s [23–26]. However, from this experiment, the swimming speed before submergence was 0.8 – 0.9 ± 0.3 m/s from the FM data and 0.5 - 0.6 ± 0.2 m/s from the CW data. On day 24, the FM signal returned swimming speeds between 0.9 – 1.0 ± 0.3 m/s, while CW returned 0.6 – 0.7 ± 0.2 m/s. The speed measured from the camera data increased from 0.3 ± 0.1 m/s on day 0 to 0.5 ± 0.2 m/s on day 24.

The overall increase from day 0 to day 24 in Table 5.7 is based on the trend lines in Tables 5.2 and 5.3, from the FM and CW measurements respectively. The increase in swimming speed was approximately equal when measured with CW signals, where the increase from the 70 and 200 kHz echo sunders were 20 %, while for the 120 kHz the increase was 19 %. In contrast, there are some variations in the overall increase from the FM signals. Here, the speed measured by the 200 kHz echo sounder increased only 3 % during the submerged period, while the increase was 15 and 18 % from the 70 and 120 kHz echo sounders.

After being submerged for 4 and 6 days, the fish from [25] swam 1.0 m/s and 1.3 m/s, respectively. The swimming speed increased more during the four days than the entire submerged period for both signal types in this experiment. Nevertheless, in Glaropoulos' study, the cages were submerged at 10 m depth rather than 1 m, which may have contributed to stressing the salmon [25]. However, the cages in [24, 26] were submerged below 10 m depth as in [25], but the swimming speeds increased only to 0.3 m/s in both experiments. The results from [23] was similar to the ones from [24, 26], even when the cages were submerged to 3 m depth. These increases from [23, 24, 26] were not as significant as in [25] and are comparable to the overall change from this experiment for both FM and CW. In the previous experiments [7, 23–25], the swimming speed was measured using a camera and the same technique as described in Section 3.4 and not from acoustical recordings. This method deals with a few fish per measurement and depends on the reaction time from the person using the stopwatch, which can cause uncertainties among the measurements. Due to the high swimming speeds from the acoustical data, the large standard deviations, and the unknown accuracy of the tracking in LSSS, the speed from the camera measurements appears to be the most accurate.

Acoustical recorded data of farmed salmon acquired from EK80 echo sounders have never been processed in LSSS before. In LSSS, positions extracted from FM and CW data depend on the KORONA tracks, where FM was tracked by applying aggregation, and the CW data was tracked using peak. A drawback to LSSS is that it is developed with the most utilized features, so targets' positioning and swimming speed have not been prioritized. It is also likely that FM's high swimming speed is owed to the method used on the FM data, which is designed for CW data. However, the same results were obtained when using aggregation on CW data, as seen in Table 6.2, where aggregation returned higher values than peak. From this, it can be believed that the aggregation tracking method is the reason for the high values, not the FM data alone. According to the results in Figs. 5.12 and 5.13, it indicates that the speed is dependent on the frequency, which is implausible as the fish pass through the beams from three transducers at the same speed. As seen in Figs. 5.12 and 5.13, both signal types have high standard deviations, which reduces the plausibility of the findings.

However, even if the swimming speed is higher than anticipated, the overall change is still of interest. Figs. 5.12 and 5.13 illustrate how day 5 of submersion appears to be a decisive day for both signal types and all three echo sounders. Further, the results from FM keep increasing before it stabilizes at around day 15. There are fewer day-to-day variations from the FM data than from CW, making it easier to detect the changes. Additionally, there is nearly no difference between the trends from the echo sounders when looking at the graphs from CW signals in Fig. 5.13, which is confirmed by the similar trends in Table 5.3. While for FM data, the values from the 120 kHz echo sounder are increasing slightly faster than the other two frequencies, shown both in Fig. 5.12 and in Table 5.2.

Chapter 7

Conclusion

7.1 Conclusions

Different signal types, FM and CW, and frequency bands between 55 - 260 kHz have been studied to determine which parameters are most useful for detecting a diminishing swim bladder; these parameters include TS, S_V, the frequency response from TS and S_V, and the swimming speed. The measured daily $\overline{TS}$ values from both FM and CW signals start to decrease after approximately 6 days. FM data appears to have a slightly faster decline in $\overline{TS}$ than CW data. Moreover, the $\overline{TS}$ measured at 70 kHz, from both FM and CW signals, are decreasing somewhat more rapidly than when measuring using 120 and 200 kHz frequencies. Based on this, FM signals transmitted using a 70 kHz echo sounder are preferred when seeking early detection of low air levels. However, the credibility of the TS measurements from tracking with aggregation is less reasonable and should be further investigated. As a result of this experiment, $\overline{TS}$ is found for individual salmon of 38 cm lengths at different frequencies and can be further used to detect an insufficient air level in the swim bladder.

When studying the daily $\overline{S_V}$ values from the FM data, it is difficult to conclude when the decrease in values begins due to the significant variation from day to day, but it appears to be as of day 15. The $\overline{S_V}$ values from the 200 kHz echo sounder return the highest values and the 70 kHz the lowest. Additionally, the ratio between $\overline{S_V}$ at 70 kHz and $\overline{S_V}$ at 200 kHz increases as the air decreases and was seen in both the daily values and the frequency response. This can be implemented to indicate a low level of air in the swim bladder. Measuring TS, in contrast to S_V, requires few individuals in order to distinguish between them, which is often not the case in commercial aquaculture. Additionally, the uncertainty from the tracking is avoided by using S_V. Hence, even with the late detection of a decreased air level, observing $\overline{S_V}$ might be better to use than $\overline{TS}$ for farmed salmon.

FM data has proven to include valuable information about the salmon from studying both the frequency response from TS(f) and S_V(f). The frequency response from TS can reveal information about a fish's body and swim bladder size based on two minimums within the frequency range. From the frequency response, other frequencies than the nominal frequency can be used when studying the ratio between TS and S_V values at different frequencies.

From the studied parameters, the swimming speed seems to be the first to indicate a decreasing air level, where day 5 appears to be a decisive day for both FM and CW signals. There are variations between the daily values recorded at different frequencies for both signal types, which is not expected since the fish swim through the three transducer beams simultaneously. The unexpected high swimming speed from FM signals and the large standard deviations reduce the plausibility of the findings. This is probably due to the aggregation algorithm used when tracking the FM data. Because of the high density of fish in the middle of the fish shoal, it is not certain how accurate the tracking is. Despite being slightly inaccurate, using a camera and stopwatch to record swimming speed is more reliable than tracking the salmon's position. Considering this, and that both swimming speed and $\overline{TS}$ decreased approximately at the same time, measuring the swimming speed with echo sounders would not be recommended.

FM and CW data from EK80 scientific split beam echo sounders have not previously been used when studying submerged salmon. Due to this, the post-processing program LSSS has not been applied to such data sets before, and it turned out not to properly work when tracking the speed using the aggregation algorithm. Since the tracking algorithms in LSSS are developed for CW data, it is insufficient for FM data and needs to be improved if the same approach is used for future research on data acquired using FM signals. Machine learning or an automatic system is essential to make this work and be used in the aquaculture industry, as it takes much time to analyze the data manually.

Kirchhoff's Ray Mode simulation of the air in the swim bladder is a good approximation for modeling both TS and the frequency response but returned relatively low values compared to the measured values. The results can be considered dubious due to the insufficient x-ray images and assumptions made when creating the swim bladder. Due to the fact that the simulation was done from the dorsal angle of the salmon, whereas the measurements were taken from the ventral angle, the results are not quite comparable. However, similarities were observed between the measured frequency response of TS from the 120 kHz frequency band and the simulated 120 kHz band. Additionally, the decrease in swim bladder was done by a percentage of the full bladder, but in practice, the bladder is diminishing asymmetrically.

7.2 Further work

There are many opportunities for further research based on the outcomes of this master's thesis. The chosen number of fish, 500, is not representable for commercial scaled cages. Hence, it would be necessary to explore the possibility of detecting individual salmon in a much denser fish shoal. More attention needs to be paid to finding the most effective tracking settings on CW and FM signals, while LSSS features should be improved to accommodate FM data. Additionally, if fish farmers are going to use this in submerged cages in the aquaculture industry, the processing needs to be done automatically.

Further, the acquired data set from this thesis contains information from frequencies spanning from 55 – 260 kHz, which can be used for further studies on physostomous and physoclistous fish.

In terms of the simulation, better x-ray images of the swim bladder would provide a more accurate modeled TS. The simulation would be improved if the diminishing volume of the bladder could be done asymmetrically. In addition, it would be interesting to simulate the incident wave with different angles and examine how tilted swimming relates to the TS.

References

[1] T. Steinset, "Oppdrettslaks til heile verda," Available: https://www.ssb.no/jord-skog-jakt-og-fiskeri/artikler-og-publikasjoner/oppdrettslaks-til-heile-verda, May, 18 2020, [Accessed: Oct. 18, 2021].

[2] United Nations, "UN projects world population to reach 8.5 billion by 2030, driven by growth in developing countries," Available :https://news.un.org/en/story/2015/07/505352-un-projects-world-population-reach-85-billion-2030-driven-growth-developing#.VbpBHflViko, Jul. 29, 2015, [Accessed: Oct. 18, 2021].

[3] O. O. Igboeli, J. F. Burka, and M. D. Fast, "Lepeophtheirus salmonis: a persisting challenge for salmon aquaculture," *Animal Frontiers*, vol. 4, no. 1, pp. 22–32, Jan. 2014. [Online]. Available: https://doi.org/10.2527/af.2014-0004

[4] S. Bui, F. Oppedal, M. Sievers, and T. Dempster, "Behaviour in the toolbox to outsmart parasites and improve fish welfare in aquaculture," *Reviews in Aquaculture*, vol. 11, no. 1, pp. 168–186, Dec. 2017. [Online]. Available: https://doi.org/10.1111/raq.12232

[5] Ø. J. Korsøen, T. Dempster, F. Oppedal, and T. S. Kristiansen, "Individual variation in swimming depth and growth in Atlantic salmon (Salmo salar L.) subjected to submergence in sea-cages," *Aquaculture*, vol. 334-337, pp. 142–151, Mar. 2012. [Online]. Available: https://doi.org/10.1016/j.aquaculture.2011.12.031

[6] F. Warren-Myers, T. Vågseth, O. Folkedal, L. H. Stien, J. O. Fosse, T. Dempster, and F. Oppedal, "Full production cycle, commercial scale culture of salmon in submerged sea-cages with air domes reduces lice infestation, but creates production and welfare challenges," *Aquaculture*, vol. 548, no. 1, Feb. 2022. [Online]. Available: https://doi.org/10.1016/j.aquaculture.2021.737570

[7] M. Sievers, Ø. J. Korsøen, F. Warren-Myers, F. Oppedal, G. Macaulay, O. Folkedal, and T. Dempster, "Submerged cage aquaculture of marine fish: A review of the biological challenges and opportunities," *Reviews in Aquaculture*, vol. 14, no. 1, pp. 106–119, Jan. 2022. [Online]. Available: https://doi.org/10.1111/raq.12587

[8] Ø. J. Korsøen, J. E. Fosseidengen, T. S. Kristiansen, F. Oppedal, S. Bui, and T. Dempster, "Atlantic salmon (Salmo salar L.) in a submerged sea-cage adapt rapidly to re-fill their swim bladders in

an underwater air filled dome," *Aquacultural Engineering*, vol. 51, pp. 1–6, Nov. 2012. [Online]. Available: https://doi.org/10.1016/j.aquaeng.2012.04.001

[9] E. J. Simmonds, S, and D. N. MacLennan, *Fisheries Acoustics: Theory and Practice, 2nd Edition*. Oxford, United Kingdom: Blackwell Science Ltd, 2005.

[10] K. G. Foote, "Importance of the swimbladder in acoustic scattering by fish: A comparison of gadoid and mackerel target strengths," *The Journal of the Acoustical Society of America*, vol. 67, no. 6, pp. 2084–2089, June 1980. [Online]. Available: https://doi.org/10.1121/1.384452

[11] P. G. Fernandes, F. Gerlotto, D. Holliday, O. Nakken, and E. Simmonds, "Acoustic applications in fisheries science: The ICES contribution," *ICES Marine Science Symposia*, vol. 215, pp. 483–492, Jan. 2002.

[12] T. Forland, *Personal communication*, IMR, Bergen, Norway, 2021-2022.

[13] E. J. Simmonds, F. Armstrong, and J. C. Philip, "Species identification using wideband backscatter with neural network and discriminant analysis," *ICES Journal of Marine Science*, vol. 53, pp. 189–195, 1996.

[14] J. E. Ehrenberg and T. C. Torkelson, "FM slide (chirp) signals: a technique for significantly improving the signal-to-noise performance in hydroacoustic assessment systems," *Fisheries Research*, vol. 47, no. 2, pp. 193–199, July 2000. [Online]. Available: https://doi.org/10.1016/S0165-7836(00)00169-7

[15] D. B. Reeder, J. M. Jech, and T. K. Stanton, "Broadband acoustic backscatter and high-resolution morphology of fish: Measurement and modeling," *The Journal of the Acoustical Society of America*, vol. 116, no. 2, pp. 747–761, Aug. 2004. [Online]. Available: https://doi.org/10.1121/1.1648318

[16] A. C. Lavery, C. Bassett, G. L. Lawson, and J. M. Jech, "Exploiting signal processing approaches for broadband echosounders," *ICES Journal of Marine Science*, vol. 74, no. 8, pp. 2262–2275, Aug. 2017. [Online]. Available: https://doi.org/10.1093/icesjms/fsx155

[17] K. J. Benoit-Bird and C. M. Waluk, "Exploring the promise of broadband fisheries echosounders for species discrimination with quantitative assessment of data processing effects," *The Journal of the Acoustical Society of America*, vol. 147, no. 1, pp. 411–427, Jan. 2020. [Online]. Available: https://doi.org/10.1121/10.0000594

[18] F. Oppedal, *Personal communication*, IMR, Bergen/Matre, Norway, 2021-2022.

[19] Å. Bjordal and J. E. Juell, "Hydroacoustic monitoring and feeding control in cage rearing of Atlantic salmon (Salmo salar L.)," in *Fish Farming Technology*, H. Reinsertsen, L. A. Dahle, L. Jørgensen, and K. Tvinnereim, Eds. London, United Kingdom: CRC Press, 1993, pp. 203 – 208.

[20] F. Oppedal, T. Dempster, and L. H. Stien, "Environmental drivers of Atlantic salmon behaviour in sea-cages: A review," *Aquaculture*, vol. 311, no. 1, pp. 1–18, Feb. 2011. [Online]. Available: https://doi.org/10.1016/j.aquaculture.2010.11.020

[21] G. Myrebøe, "Havmerde-prosjektet - Sluttrapport prosjekt Ocean Farm 1," Ocean Farming (OF), Norway, Tech. Rep. OF_SR_16122019, 2019. [Online]. Available: https://www.salmar.no/wp-content/uploads/2016/06/OF_SR_16122019.pdf

[22] E. B. Gomez, "New Aquaculture Tool Developed to Estimate Fish Density with Echo-Sounders," Norway/Greece, Nr. 429253, 2021. [Online]. Available: http://performfish.eu/wp-content/uploads/2021/02/PR_Fish-density_echo-sounder_vFINAL.pdf

[23] T. Dempster, Ø. J. Korsøen, O. Folkedal, J.-E. Juell, and F. Oppedal, "Submergence of Atlantic salmon (Salmo salar L.) in commercial scale sea-cages: A potential short-term solution to poor surface conditions," *Aquaculture*, vol. 288, no. 3-4, pp. 254–263, Mar. 2009. [Online]. Available: https://doi.org/10.1016/j.aquaculture.2008.12.003

[24] Ø. J. Korsøen, T. Dempster, P. G. Fjelldal, F. Oppedal, and T. S. Kristiansen, "Long-term culture of Atlantic salmon (Salmo salar L.) in submerged cages during winter affects behaviour, growth and condition," *Aquaculture*, vol. 296, no. 3-4, pp. 373–381, Nov. 2009. [Online]. Available: https://doi.org/10.1016/j.aquaculture.2009.08.036

[25] A. Glaropoulos, L. H. Stien, O. Folkedal, T. Dempster, and F. Oppedal, "Welfare, behaviour and feasibility of farming Atlantic salmon in submerged cages with weekly surface access to refill their swim bladders," *Aquaculture*, vol. 502, pp. 332–337, Mar. 2019. [Online]. Available: https://doi.org/10.1016/j.aquaculture.2018.12.065

[26] M. Sievers, O. Korsøen, T. Dempster, F. P. G, T. Kristiansen, O. Folkedal, and F. Oppedal, "Growth and welfare of submerged Atlantic salmon under continuous lighting," *Aquaculture Environment Interactions*, vol. 10, pp. 501–510, Nov. 2018. [Online]. Available: http://doi.org/10.3354/aei00289

[27] T. L. Nesse, H. Hobæk, and R. J. Korneliussen, "Measurements of acoustic-scattering spectra from the whole and parts of Atlantic mackerel," *ICES Journal of Marine Science*, vol. 66, no. 6, pp. 1169–1175, Apr. 2009. [Online]. Available: https://doi.org/10.1093/icesjms/fsp087

[28] F. R. Knudsen, J. E. Fosseidengen, F. Oppedal, Ø. Karlsen, and E. Ona, "Hydroacoustic monitoring of fish in sea cages: Target strength (TS) measurements on Atlantic salmon (Salmo salar)," *Fisheries Research*, vol. 69, no. 2, p. 205–209, Sep. 2004. [Online]. Available: https://doi.org/10.1016/j.fishres.2004.05.008

[29] O. A. Misund and A. K. Beltestad, "Target-strength estimates of schooling herring and mackerel using the comparison method," *ICES Journal of Marine Science*, vol. 53, no. 2, pp. 281–284, Apr. 1996. [Online]. Available: https://doi.org/10.1006/jmsc.1996.0035

[30] C. S. Clay and J. K. Horne, "Acoustic models of fish: The Atlantic cod (Gadus morhua)," *The Journal of the Acoustical Society of America*, vol. 96, no. 3, pp. 1661–1668, Sep. 1994. [Online]. Available: https://doi.org/10.1121/1.410245

[31] J. K. Horne, P. D. Walline, and J. M. Jech, "Comparing acoustic model predictions to in situ backscatter measurements of fish with dual-chambered swimbladders," *Journal of Fish Biology*, vol. 57, no. 5, pp. 1105 – 1121, Nov. 2000. [Online]. Available: https://doi.org/10.1111/j.1095-8649.2000.tb00474.x

[32] M. J. Henderson, J. K. Horne, and R. H. Towler, "The influence of beam position and swimming direction on fish target strength," *ICES Journal of Marine Science*, vol. 65, no. 2, pp. 226–237, Feb. 2008. [Online]. Available: https://doi.org/10.1093/icesjms/fsm190

[33] "Simrad ES70-7C, Split beam echo sounder transducer, Rev. C," Kongsberg Maritime AS, Horten, Norway, 2006.

[34] D. A. Demer, L. N. Andersen, C. Bassett, L. Berger, D. Chu, J. Condiotty, G. R. C. Jr., B. Hutton, R. Korneliussen, N. L. Bouffant, G. Macaulay, W. L. Michaels, D. Murfin, A. Pobitzer, J. S. Renfree, T. S. Sessions, K. L. Stierhoff, and C. H. Thompson, "2016 USA–Norway EK80 Workshop Report: Evaluation of a wideband echosounder for fisheries and marine ecosystem science," Jan. 2017. [Online]. Available: https://doi.org/10.17895/ices.pub.2318

[35] J. H. McClellan, W. R. Schafer, and M. A. Yoder, *Digital Signal Processing First, Global Edition*. London, United Kingdom: Pearson Education Limited, 2016.

[36] T. N. Forland, H. Hobæk, E. Ona, and R. J. Korneliussen, "Broad bandwidth acoustic backscattering from sandeel—measurements and finite element simulations," *ICES Journal of Marine Science*, vol. 71, no. 7, pp. 1894–1903, Mar. 2014. [Online]. Available: https://doi.org/10.1093/icesjms/fsu010

[37] "Installation Manual: Simrad EK80, Rev. E," Kongsberg Maritime AS, Horten, Norway, 2022.

[38] L. N. Andersen, D. Chu, H. Heimvoll, R. Korneliussen, G. J. Macaulay, and E. Ona, "Quantitative processing of broadband data as implemented in a scientific splitbeam echosounder," Apr. 2021. [Online]. Available: https://doi.org/10.48550/arXiv.2104.07248

[39] L. Kinsler, A. R. Frey, A. B. Coppens, and J. V. Sanders, *Fundamentals of Acustics: Fourth Edition*. New Jersey, USA: John Wiley & Sons, Inc, 2000.

[40] R. E. Francois and G. R. Garrison, "Sound absorption based on ocean measurements. Part II: Boric acid contribution and equation for total absorption," *The Journal of the Acoustical Society of America*, vol. 72, no. 6, pp. 1879–1890, Aug. 1982. [Online]. Available: https://doi.org/10.1121/1.388673

[41] "Simrad EK80 Wide band scientific echo sounder Reference Manual," Kongsberg Maritime, 2022.

[42] C. S. Clay and H. Medwin, *Fundamentals of Acoustical Oceanography (Applications of Modern Acoustics)*, 2nd ed. London, UK: Academic Press, 1997.

[43] P. Lunde, A. O. Pedersen, R. J. Korneliussen, F. Tichy, and H. Nes, "Power-budget and echo-integrator equations for fish abundance estimation," Institute of Marine Research, Bergen, Norway, Tech. Rep. 10, Dec. 2013. [Online]. Available: http://doi.org/10.13140/RG.2.2.33159.80809

[44] P. Lunde and R. J. Korneliussen, "Power-Budget Equations and Calibration Factors for Fish Abundance Estimation Using Scientific Echo Sounder and Sonar Systems," *Journal of Marine Science and Engineering*, vol. 4, no. 3, July 2016. [Online]. Available: https://doi.org/10.3390/jmse4030043

[45] B. D. Pflugrath, R. S. Brown, and T. J. Carlson, "Maximum Neutral Buoyancy Depth of Juvenile Chinook Salmon: Implications for Survival during Hydroturbine Passage," *Transactions of the American Fisheries Society*, vol. 141, no. 2, pp. 520–525, Mar. 2012. [Online]. Available: https://doi.org/10.1080/00028487.2012.670187

[46] ISO, *Guide to the expression of uncertainty in measurement (GUM)* . Geneva, Switzerland: International Organisation for Standardisation, First edition, 1995.

[47] J. Juell and J. Fosseidengen, "Akustisk mengdemåling av oppdrettslaks," *Fisken og Havet*, vol. 21, 1995.

[48] X. Lurton, *An introduction to underwater acoustics. Princples and applications.* Berlin, Germany: Springer and Praxis Publishing, 2010.

[49] R. J. Korneliussen, Y. Heggelund, G. J. Macaulay, D. Patel, E. Johnsen, and I. K. Eliassen, "Acoustic identification of marine species using a feature library," *Methods in Oceanography*, vol. 17, pp. 187–205, Dec. 2016. [Online]. Available: https://doi.org/10.1016/j.mio.2016.09.002

[50] R. Korneliussen, *Personal communication*, IMR, Bergen, Norway, 2021-2022.

[51] N. O. Handegard, "Observing individual fish behavior in fish aggregations: Tracking in dense fish aggregations using a split-beam echosounder," *The Journal of the Acoustical Society of America*, vol. 122, no. 1, pp. 177–187, July 2007. [Online]. Available: https://doi.org/10.1121/1.2739421

[52] J. Devore, K. N. Berk, and M. A. Carlton, *Modern Mathematical Statistics with Applications, Third Edition.* New York, USA: Springer, 2021.

[53] "Brukermanual Orbit 3000/3300/3500 Kamera," Steinsvik AS, Førresfjorden, Norway, 2015.

[54] AKVA Group, "BLÅ LED 400W," Available: https://www.akvagroup.com/sea-based-aquaculture/lights/blue-led-400w, [Accessed Nov. 05, 2021].

[55] K. Berg, "Welfare objectives of Atlantic Salmon (Salmo salar) observed with broadband acoustic in a submerged cage," MSt, University of Bergen, Faculty of Mathematics and Natural Science, Department of Biological Sciences, Bergen, Norway, 2022.

[56] "Simrad ES120-7C, Split beam echo sounder transducer, Rev. D," Kongsberg Maritime AS, Horten, Norway, 2009.

[57] "Simrad ES200-7C, Split beam echo sounder transducer, Rev. E," Kongsberg Maritime AS, Horten, Norway, 2009.

[58] NorseAqua, "The Mid-Norwegian Ring," Available: https://norseaqua.com/products/the-mid-norwegian-ring/, [Accessed: Nov. 05, 2021.

[59] C. Noble, K. Gismervik, M. H. Iversen, J. Kolarveic, L. H. Stien, and J. F. Turnbull, *Welfare Indicators for farmed Atlantic salmon: tools for assessing fish*. Norway: Nofima, 2018.

[60] Marel, "M1100 Bench Scales, PL2062," Available: https://marel.com/en/products/m1100-bench-scales, [Accessed: Nov. 05, 2021.

[61] Thomas Scientific, "Intramedic Lower Density Polyethylene Micro Bore Tubing," Available: https://www.thomassci.com/Laboratory-Supplies/Tubing/_/INTRAMEDIC-LOWER-DENSITY-POLYETHYLENE-MICRO-BORE-TUBING?q=Clay%20Adams, [Accessed: Nov. 05, 2021].

[62] Restek, "NORM-JECT and HENKE-JECT Plastic Syringes," Available: https://www.restek.com/row/products/sample-preparation--air-sampling/sample-preparation-products/syringes/8027/, [Accessed: Nov. 05, 2021].

[63] SAIV A/S, "CTD profiler Model SD204," Available: https://saiv.no/sd204-ctd-profiler, [Accessed: Nov. 05, 2021.

[64] D. T. Zallen, "The "Light" Organism for the Job: Green Algae and Photosynthesis Research," *Journal of the History of Biology*, vol. 26, no. 2, pp. 269–279, Summer 1993. [Online]. Available: http://www.jstor.org/stable/4331264

[65] G. Pedersen, *Personal communication*, IMR, Bergen, Norway, 2021-2022.

[66] S. Gastauer, D. Chu, P. Roland, Y. Ladroit, G. Pedersen, and P. Escobar, "Open Source Acoustic Scattering Models for fisheries acoustics," https://github.com/SvenGastauer/scatmod, 2020, [Accessed: Nov. 23, 2021].

[67] J. Volff, "Genome evolution and biodiversity in teleost fish," *Heredity*, vol. 94, no. 3, pp. 280–294, Dec. 2004. [Online]. Available: https://doi.org/10.1038/sj.hdy.6800635

[68] J. Jech, J. Horne, D. Chu, D. Demer, D. Francis, N. Gorska, B. Jones, A. Lavery, T. Stanton, G. Macaulay, D. Reeder, and K. Sawada, "Comparisons among ten models of

acoustic backscattering used in aquatic ecosystem research," *The Journal of the Acoustical Society of America*, vol. 138, no. 6, pp. 3742–3764, Dec. 2015. [Online]. Available: http://doi.org/10.1121/1.4937607

[69] V. Espinosa, E. Soliveres, A. Cebrecos, V. Puig, S. Sainz-Pardo, and F. de-la Gándara, "Growing monitoring in sea cages: TS measurements issues," Proceedings at the 34th Scandinavian Symposium on Physical Acoustics, Geilo, Norway, 2011.

[70] K. Maritime", "Personal communication," Phone call, Kongsberg Maritime, Matre/Kongsberg, Norway, 2021.

[71] J. K. Horne, K. Sawada, K. Abe, R. B. Kreisberg, D. H. Barbee, and K. Sadayasu, "Swimbladders under pressure: anatomical and acoustic responses by walleye pollock," *ICES Journal of Marine Science*, vol. 66, no. 6, pp. 1162–1168, Apr. 2009. [Online]. Available: https://doi.org/10.1093/icesjms/fsp101

[72] P. Bogetoft and L. Otto, *Benchmarking with DEA, SFA, and R*. New York, USA: Springer New York, 2011.

[titletoc]appendix

Appendix A

Weight, length and air quantity

Here, the results from the samplings described in section 3.3 will be presented in two tables, where Table A.1 includes the average values of every measured value per day (purple dots in Fig. 5.6), while Table A.2 includes the individual measurement per fish (blue dots in Fig. 5.6). The tables include the day of sampling, as seen in Table 3.1, the number of fish sampled, and the length and weight of the fish. Additionally, the measured air quantity and neutral buoyancy are included, along with the calculated relative air quantity. The uncertainty in the tables is from the steps (0.2 ml) on the syringe [62] and is classified as a Type B evaluation of the uncertainty [46].

Table A.1: The daily average of the length, weight, air and neutral buoyancy measurements, and the calculated relative air from Table A.2

Day	Fish	Length ± 0.5 [cm]	Weight ± 0.5 [g]	Air ± 0.1 [ml]	Neutral buoyancy ± 0.1 [ml]	Relative air ± 0.1
0	25	38	578	5.0	28.3	0.2
7	12	39	606	3.7	33.1	0.1
10	11	38	559	2.1	30.7	0.0
14	14	38	574	1.9	34.3	0.1
19	18	38	536	1.1	33.6	0.0
24	16	39	579	0.2	29.2	0.01
27	26	39	566	0.5	27.2	0.0
32	25	38	584	1.6	28.4	0.1

Table A.2: All measurements of length, weight, air, neutral buoyancy, and relative air throughout the experiment. *bubbles came out of the mouth, resulting in a less accurate measure of the neutral buoyancy.

Day	Fish	Length ± 0.5 [cm]	Weight ± 0.5 [g]	Air ± 0.1 [ml]	Neutral buoyancy ± 0.1 [ml]	Relative air ± 0.1
0	1	35.5	500	4.6	22.0	0.2
	2	39.5	660	4.1	20.0	0.2
	3	36.0	500	5.8	25.9	0.2
	4	41.0	695	7.3	36.2	0.2
	5	37.0	570	4.6	25.2	0.2
	6	33.0	405	3.4	18.0	0.2
	7	38.0	585	3.5	27.5	0.1
	8	39.5	620	5.2	32.2	0.2
	9	39.0	640	n.d	n.d	n.d
	10	36.0	530	4.0	27.9	0.1
	11	37.5	545	1.1	28.2	0.04
	12	37.5	525	4.4	25.6	0.2
	13	39.0	645	8.9	35.5	0.3
	14	36.5	530	3.8	34.5	0.1
	15	37.5	560	10.2	34.9	0.3
	16	42.0	785	6.2	43.8	0.1
	17	38.0	565	2.8	24.2	0.1
	18	38.0	610	4.8	27.8	0.2
	19	38.0	605	3.6	28.7	0.1
	20	37.0	650	5.7	24.4	0.2
	21	39.5	645	n.d	n.d	n.d
	22	35.5	480	6.1	20.8	0.3
	23	37.0	555	8.6	35.0	0.3
	24	36.0	520	2.6	28.6	0.1
	25	36.5	515	2.6	24.6	0.1

Day	Fish	Length ± 0.5 [cm]	Weight ± 0.5 [g]	Air ± 0.1 [ml]	Neutral buoyancy ± 0.1 [ml]	Relative air ± 0.1
7	1	37.5	545	2.4	n.d	n.d
	2	39.5	685	0.9	35.4	0.03
	3	39.5	660	4.0	30.0	0.1
	4	39.5	625	10.8	34.9	0.3
	5	41.0	735	9.6	44.4	n.d
	6	36.5	515	2.7	27.3	0.1
	7	40.5	660	0.7	39.0	0.02
	8	37.5	540	1.6	35.1	0.1
	9	39.5	675	8.2	n.d	n.d
	10	37.5	565	0.9	35.2	0.03
	11	39.5	670	0.6	30.0	0.02
	12	34.0	400	2.5	19.8	0.1
10	1	38.5	585	0.2	39.8	0.01
	2	40.0	640	3.8	37.9	0.1
	3	38.5	595	0.4	32.6	0.01
	4	38.5	600	3.0	27.8	0.1
	5	37.5	555	7.9	27.4	n.d
	6	34.5	405	0.1	23.8	0.00
	7	41.0	670	0.2	28.2	0.01
	8	37.0	485	n.d	nd	n.d
	9	39.0	610	2.0	28.3	0.1
	10	37.5	520	1.2	nd	n.d
	11	36.5	480	nd	nd	n.d
14	1	39.5	620	3.1	38.7	0.08
	2	36.0	420	0.5	28.0	0.02
	3	39.5	620	2.0	28.0	0.1
	4	37.0	515	1.8	35.0	0.1
	5	39.0	615	0.0	32.1	0.00
	6	37.0	520	0.9	32.4	0.03
	7	36.0	500	0.7	34.2	0.02
	8	41.5	710	3.6	40.0	0.1

Day	Fish	Length ± 0.5 [cm]	Weight ± 0.5 [g]	Air ± 0.1 [ml]	Neutral buoyancy ± 0.1 [ml]	Relative air ± 0.1
	9	42.0	740	5.3	40.0	0.1
	10	39.0	580	1.0	36.2	0.03
	11	36.0	485	0.5	27.6	0.02
	12	41.5	720	3.4	42.6	0.1
	13	36.0	480	2.2	28.4	0.1
	14	37.0	505	1.4	36.4	0.04
19	1	39.0	580	4.0	33.2	0.1
	2	39.0	660	0.0	37.2	0.00
	3	41.5	690	2.8	42.0	0.1
	4	39.0	600	3.6	38.8	0.1
	5	36.5	460	0.2	30.0*	0.01
	6	36.0	460	0.1	35.8	0.00
	7	38.0	540	1.4	37.8	0.04
	8	34.5	405	0.4	28.0*	0.01
	9	39.0	595	2.0	38.2	0.1
	10	38.5	580	0.0	47.0*	0.00
	11	34.0	405	0.5	29.6	0.02
	12	38.0	550	0.0	35.6	0.00
	13	39.0	575	1.7	38.0*	0.04
	14	38.5	535	0.0	36.2	0.00
	15	35.0	410	0.0	30.0*	0.00
	16	37.5	505	2.8	30.0*	0.1
	17	40.0	600	n.d.	n.d.	n.d.
	18	37.0	490	0.0	3.4	0.00
24	1	40.0	645	1.0	33.2	0.03
	2	37.5	515	0.0	23.2	0.00
	3	40.0	625	0.4	21.0	0.02
	4	39.0	580	0.0	28.0*	0.00
	5	42.0	720	0.0	36.2	0.00
	6	40.0	620	0.0	30.0*	0.00

Day	Fish	Length ± 0.5 [cm]	Weight ± 0.5 [g]	Air ± 0.1 [ml]	Neutral buoyancy ± 0.1 [ml]	Relative air ± 0.1
	7	39.5	610	0.2	28.2	0.01
	8	37.0	495	0.0	25.8	0.00
	9	41.5	640	0.1	31.6	0.00
	10	39.5	625	0.2	n.d. *	n.d.
	11	36.5	460	0.0	n.d.*	n.d.
	12	38.0	515	0.2	29.0*	0.01
	13	42.0	665	0.4	39.2	0.01
	14	37.5	530	0.0	28.8	0.00
	15	35.0	480	0.1	26.8	0.00
	16	38.0	535	0.0	28.0	0.00
27	1	36.0	470	0.2	23.6	0.01
	2	39.0	565	0.3	25.0	0.01
	3	38.5	560	0.6	28.0*	0.02
	4	37.5	515	0.5	25.0*	0.02
	5	39.5	540	0.4	30.2	0.01
	6	37.0	480	0.4	22.0	0.02
	7	41.0	655	0.3	29.2	0.01
	8	38.5	530	0.3	29.0*	0.01
	9	37.5	495	0.5	20.0*	0.03
	10	37.0	465	0.4	27.2	0.01
	11	40.0	625	0.3	30.4	0.01
	12	39.5	570	3.6	23.6*	0.2
	13	38.0	530	0.5	27.6	0.02
	14	41.0	690	0.4	33.6	0.01
	15	40.5	625	0.4	30.0	0.01
	16	41.0	650	0.4	29.8	0.01
	17	41.0	645	0.2	30.2	0.01
	18	36.0	445	0.6	21.0*	0.03
	19	40.0	570	0.3	28.0*	0.01
	20	38.5	530	0.3	23.4*	0.01
	21	40.0	605	0.6	28.0*	0.02

Day	Fish	Length ± 0.5 [cm]	Weight ± 0.5 [g]	Air ± 0.1 [ml]	Neutral buoyancy ± 0.1 [ml]	Relative air ± 0.1
27	21	40.0	605	0.6	28.0*	0.02
	22	39.0	535	0.5	26.0*	0.02
	23	43.0	805	0.4	30.0*	0.01
	24	37.5	510	0.3	26.0*	0.01
	25	41.0	620	0.9	29.2*	0.03
	26	36.5	480	0.4	30.0*	0.01
32	1	41.0	640	3.4	30.6	0.11
	2	3.0	565	2.5	32.8	0.1
	3	42.5	720	0.0	33.6	0.00
	4	38.0	525	2.0	26.6	0.1
	5	36.0	460	2.4	23.6	0.10
	6	45.0	810	0.8	41.0	0.02
	7	39.5	580	1.0	26.2	0.04
	8	40.5	640	0.0	29.8	0.00
	9	40.0	585	0.0	31.8	0.00
	10	39.0	590	1.6	26.2	0.1
	11	42.5	735	0.7	34.8	0.02
	12	41.5	645	5.3	28.6	0.19
	13	37.0	480	3.5	24.4	0.14
	14	42.0	710	0.0	32.2	0.00
	15	40.5	640	0.5	29.8	0.02
	16	36.0	415	0.2	19.8	0.01
	17	41.0	600	2.0	30.0	0.1
	18	38.5	520	0.4	25.4	0.02
	19	40.5	620	0.0	29.6	0.00
	20	40.0	590	0.5	28.6	0.02
	21	39.5	560	7.4	26.6	0.3
	22	36.0	455	5.7	22.2	0.3
	23	38.0	540	0.2	27.6	0.01
	24	38.5	505	0.1	24.2	0.00
	25	37.0	476	0.5	23.6	0.02

Appendix B

LSSS: Splitting, Tracking, and Exporting

In this appendix, the settings in LSSS from sections 2.4 and 3.6 will be presented. This includes the settings used when splitting the recordings from different channels into separate files, which settings were used tracking FM and CW data, and an overview of the exporting.

B.1 Splitting

The experiment was conducted in conjunction with another student [55], and the experimental setup was the same for both master's theses, where the student had two additional pens equipped with a 200 kHz transducer each. The mission planner in EK80 was configured to run all five transducers simultaneously. Therefore, the output files contain data not relevant to this thesis. A setup was created in KORONA to split the data files and the different signal types, FM and CW, from each other. Which channel to keep can be decided when when choosing "channel removal" in KORONA Relay. For cage 16, channels 1, 3, and 5 indicate CW pulses, and channels 2, 4, and 6 indicate FM pulses. Fig. B.1 shows the setting module applied for splitting.

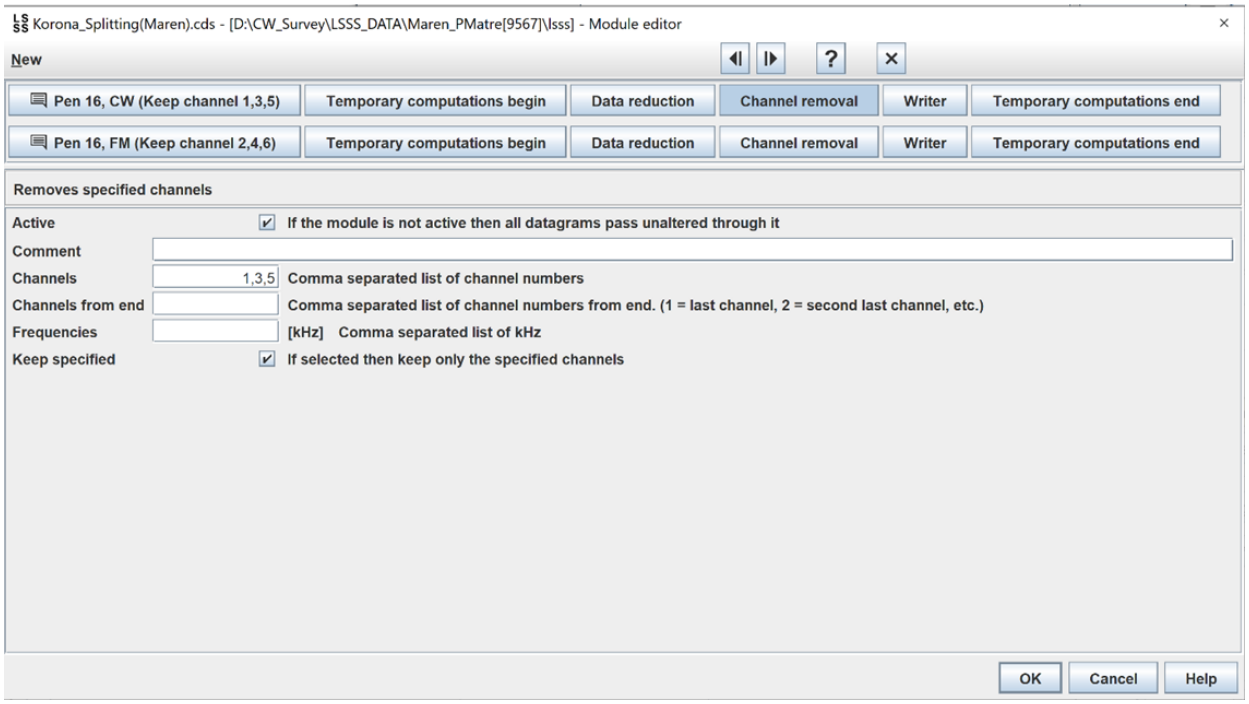

Figure B.1: Settings applied for splitting the two pulse types from each other and which channels to keep

Fig. B.1 shows a screenshot from LSSS KORONA Relay. There are two lines in the upper part of the figure, each representing a pulse type. The first module adds a comment to state the pulse type and the channels used in that line. *Temporary computations begin* is then added to make the line begin. Without this module, the settings that come after will not initiate. Further, in *data reduction*, unnecessary depths can be removed. Since the bottom of the cage was at 14 m and the transducers at 25 m, it is possible to exclude 11 m and reduce the amount of data. LSSS shows the data set upside down; the minimum depth must be written as the maximum depth and vice versa.

The following module is *channel removal*. The module allows the user to decide which channels to keep and which ones to discard. Channels 1, 3, and 5 are kept for CW pulses, and 2, 4, and 6 are kept for FM. To ensure that the specified channels are kept, check the box next to "Keep specified." Otherwise, all channels are maintained except the ones defined. Lastly, the files are written to a folder, and the line is closed.

B.2 Tracking

After splitting the data set into FM and CW files, the fish could be tracked. CW and FM have been tracked with different methods, which will be presented in subsections B.2.2 and B.2.1.

B.2.1 Tracking FM data

For the FM signals, aggregation was the chosen tracking algorithm. The setup used for tracking can be seen in Fig. B.2.

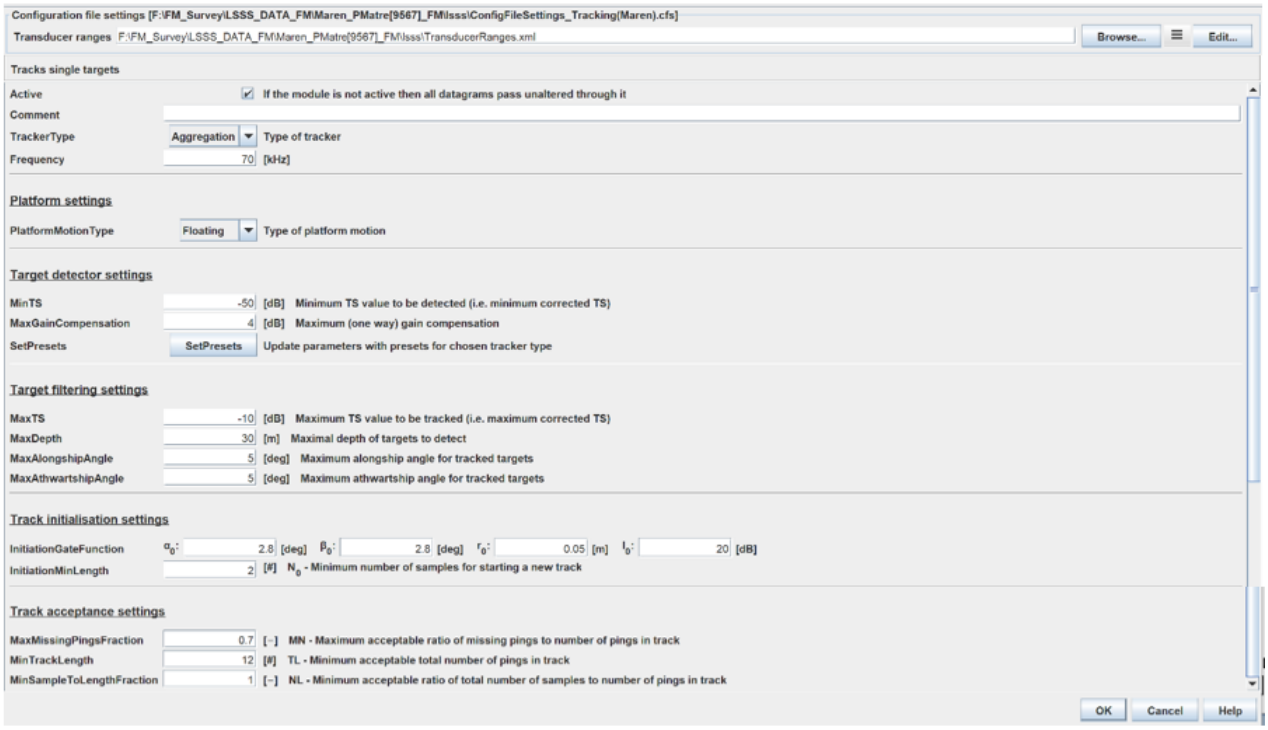

Figure B.2: Settings from KORONA Relay used when tracking FM data with the aggregation algorithm.

In Fig. B.2, the setup used when tracking the data set from the FM signals is presented, which is equal for all three frequencies. As seen in the figure, aggregation is the tracker type used. MinTS was changed throughout the data set as the air level decreased, see Table B.1 for the applied TS thresholds.

Table B.1: dB re. 1 m^2 thresholds used for different periods during the experimental period, when tracking FM data using aggregation as tracking algorithm.

Days, from-to	Threshold [dB re. 1 m^2]
-4 to 1	-45
2 to 13	-50
14 to 27	-55
28 to 31	-45

KORONA Playbox was run every other day to see how the tracks changed with different thresholds, and the observations were the basis for choosing the minimum TS values seen in Table B.1. *KORONA Playbox* is a feature in LSSS where different settings can be applied to a few files before the processing is applied to the data set. The thresholds were chosen based on observations and might not be the best possible. It was challenging to determine which threshold was best since the thresholds were changed only by a few dB re. 1 m^2 during each observation. Both the values in "Target filtering settings" and "track initialization settings," which are based on [51], were kept constant throughout the tracking. Moreover, the "track acceptance settings" were set based on observations in the KORONA playbox, but as with the "Target detector settings," it was challenging to observe the changes. The MaxMissingPingsFraction is set to 0.7, which means the track will not be accepted if 70% of the pings

in the tracks are missing. Additionally, the track needs to include 12 pings to be accepted. In addition to the tracking module, the algorithm included a "TS detection" module, as seen in Fig. B.3.

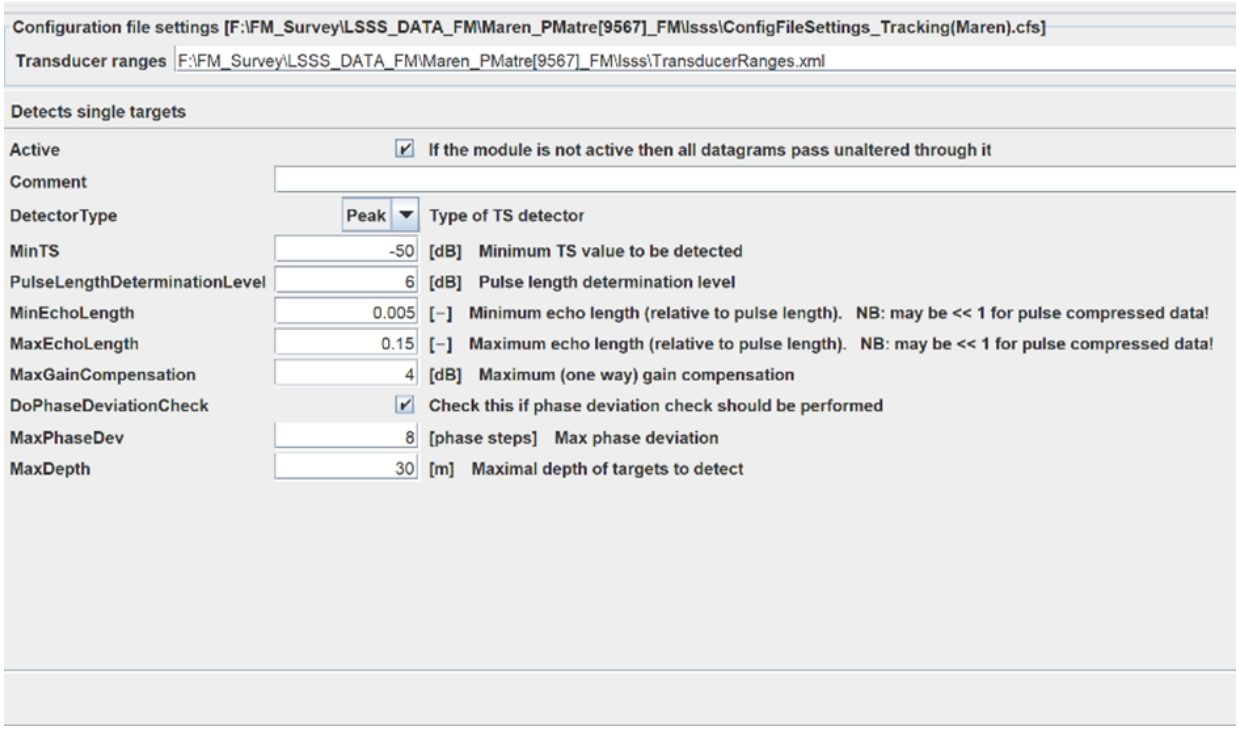

Figure B.3: Settings used to for TS detection of FM data

The figure shows peak as detector type, even when aggregation has been used for tracking. The only detector type in TS detection is peak or SED, which is the reason for choosing peak.

B.2.2 Tracking CW data

The setting used in KORONA Relay to track the CW files is shown in Fig. B.4, where peak was used as the tracking algorithm.

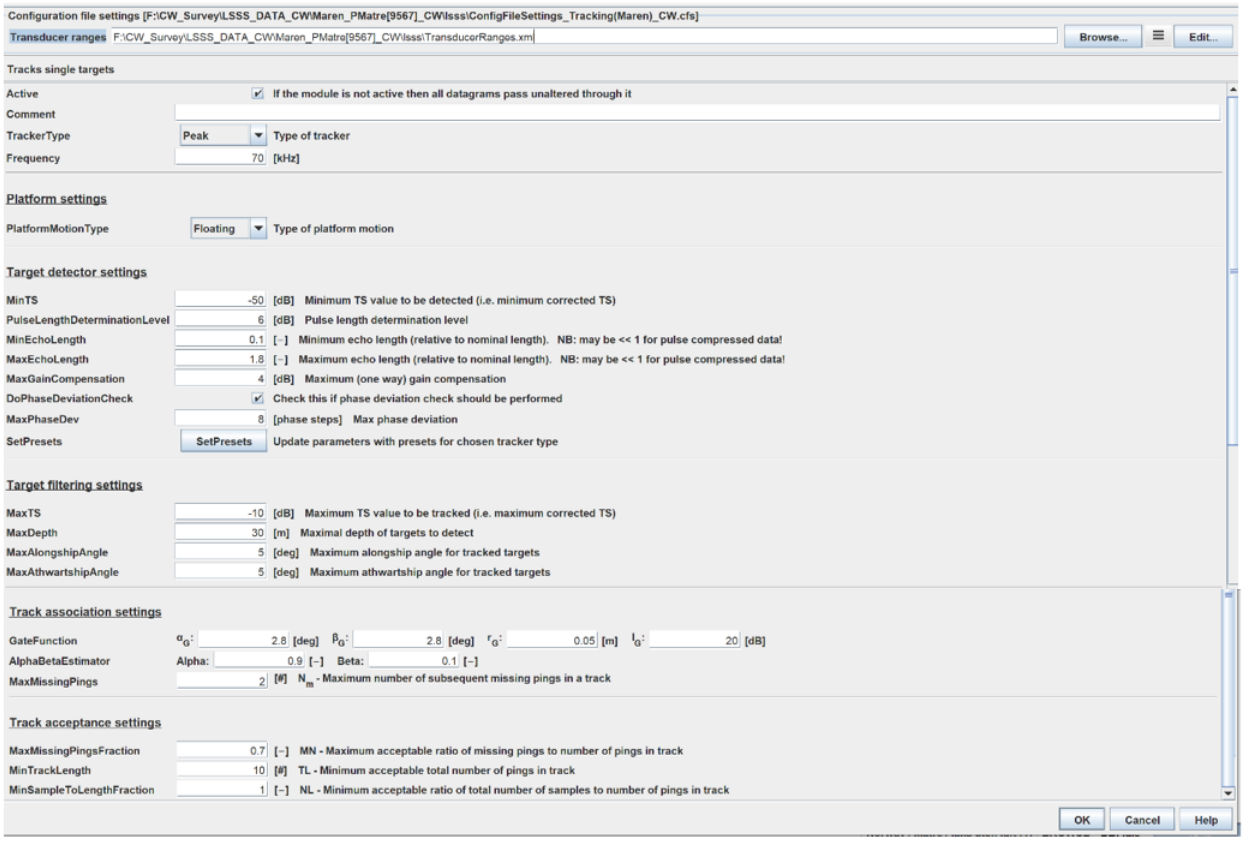

Figure B.4: Settings from KORONA Relay used when tracking CW data with the peak algorithm.

The settings in Fig. B.4 were applied for all three frequencies. Every setting was kept constant throughout the processing, except MinTS which was changed as the air level decreased. The threshold was tested in KORONA Playbox every third – fourth day to check the quality of the tracks for a given threshold before being applied for the actual tracking, and the values can be seen in Table B.2. Further, as opposed to aggregation (seen in Fig. B.2), the minimum and maximum echo length can be changed when choosing peak.

Table B.2: Selected dB re. 1 m^2 threshold for different periods in the experiment when tracking CW data using peak

Days, from-to	Threshold [dB re. 1 m^2]
-4 to 0	-45
1 to 12	-50
14 to 20	-55
21 to 27	-60
28 to 31	-45

The same method for FM tracking was applied to obtain the thresholds for CW tracking. Comparing Fig. B.2 and B.4, the only difference is the target detector settings. Further, the TS detection settings used for CW tracking are presented in Fig. B.5.

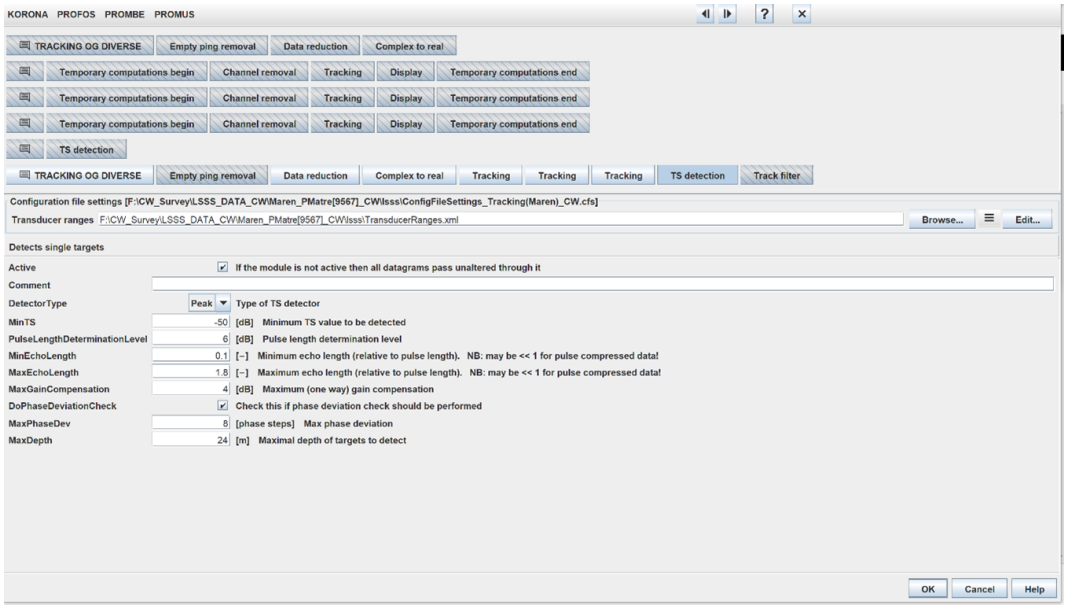

Figure B.5: Settings used to for TS detection of CW data

B.3 Export

Exporting was different for FM and CW data, TS, S_V, and swimming speed. The tracks were used when studying TS from FM and CW data and the swimming speed for both FM and CW. BBTS(f) tracks were used when extracting TS from FM data, and all three frequencies were returned in the same .json file. For the TS from CW data and the swimming speed for both FM and CW, the function "Tracks" was used. "Tracks" returns a text file including an ID per fish, but only for one of the frequency bands, thus, three files were extracted, one per frequency. The resulting tracks include multiple pings with the same ID within the same track. Due to this, it is possible to distinguish between the different tracks in the file.

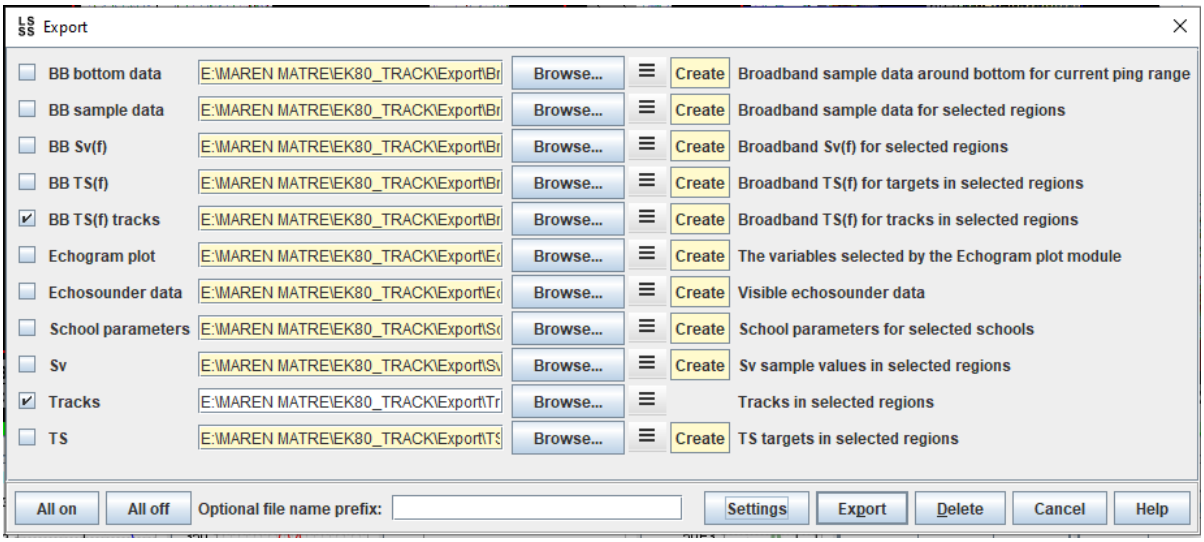

Figure B.6: Showing the different parameters that can be exported from using the "Export" feature in LSSS. The BBTS(f) tracks and Tracks are selected.

Fig. B.6 shows which parameters can be exported from LSSS using the "Export" feature. Only the BB TS(f) tracks and Tracks were used in this thesis. Moreover, exporting can be done without the "Export" function, e.g., with a separate Python script.

Appendix C

LSSS: Testing peak and aggregation as tracking methods on FM data from the 200 kHz echo sounder

The tests as described in section 6.1.5 were repeated for the same area and boxes using 200 kHz instead of the 120 kHz. Fig. C.1 shows the tracks from using aggregation in a) and peak in b). Fig. C.1 shows an approximately equal number of tracks for the two tracking algorithms.

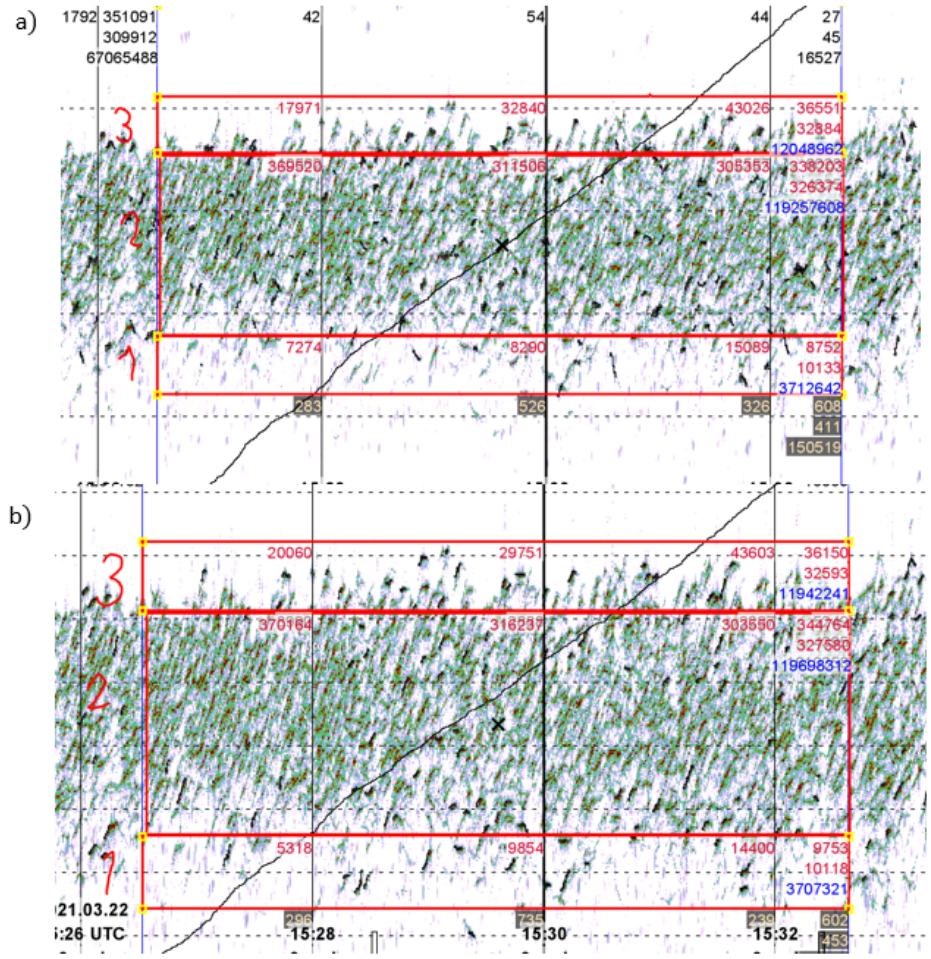

Figure C.1: The red boxes represents 6 minutes of tracks and is equal in a) and b), and is based on the data from 200 kHz transducer from using aggregation in a) and peak in b). The boxes are divided into layers 1, 2, and 3 to study the swimming speed from different amount of tracks

Fig. C.1 a) shows the tracks from the 200 kHz FM echo sounder after applying the aggregation algorithm, where the black lines represent one track/fish. While Fig. C.1 b) shows tracks from 200 kHz FM data after using the peak algorithm. In addition to the swimming speed, the MATLAB script from appendix F returns the number of individual tracks. The results show 118 tracks from applying aggregation and 100 tracks using peak as the tracking method. Further, the swimming speeds for both algorithms are shown in Table C.1.

Table C.1: Swimming speed from the 200 kHz transducer, when using both aggregation and peak for tracking. Results are shown both in m/s and bl/s

	Aggregation [m/s]	Peak [m/s]	Aggregation [bl/s]	Peak [bl/s]
Layer 1 + 2 + 3	0.9 ± 0.3	0.4 ±0.1	2.5 ± 0.9	1.0 ± 0.2
Layer 1	0.8 ± 0.2	0.4 ± 0.1	2.0 ± 0.6	1.0 ± 0.2
Layer 2	1.0 ± 0.3	0.4 ±0.1	2.6 ± 0.9	1.0 ± 0.2
Layer 3	0.7 ± 0.3	0.4 ± 0.04	1.9 ± 0.8	1.0 ± 0.1
Layer 1 + 2	1.0 ± 0.3	0.4 ± 0.1	2.6 ± 0.9	1.0 ± 0.2

Even if the number of tracks was approximately equal, it is still a gap between the speed of the two algorithms. The speeds for both aggregation and peak in Table C.1 are approximately the same as for the 120 kHz transducer despite the number of tracks from aggregation in Fig. 6.1. When zooming in on Fig. C.1 a), the tracks are not following individual fish as accurately as in b). There are more cases of tracking two fish at once and the background noise when comparing aggregation in Fig. C.1 a) to peak in b). As a result of this test, it appears that the high values of swimming speed are not due to the number of tracks from aggregation used on the 120 kHz transducer in Fig. 6.1, but aggregation as a tracking method.

Appendix D

Validation of the Kirchhoff's Ray Mode method

To determine if the KRM method [30] from chapter 4 is an approving approximation to simulate TS from a swim bladder, a validation of the model is required and is given by [66]. This is done in the software R for a fluid-filled and a gas-filled sphere surrounded by water. The KRM simulation is conducted using Eqs. (4.6) - (4.10) and the theory from [30], while the analytical simulation is based on a built-in analytical benchmark from [72], based on Data Envelopment Analyses (DEA) and Stochastic Frontier Analyses (SFA) [72].

The validation is considered for frequencies between 10 to 400 kHz. Additionally, the function depends on the radius of the sphere, a, and the input values shown in Table D.1. In this instance, the radius is set to 0.02 m, and the sphere can be seen in Fig. D.1,

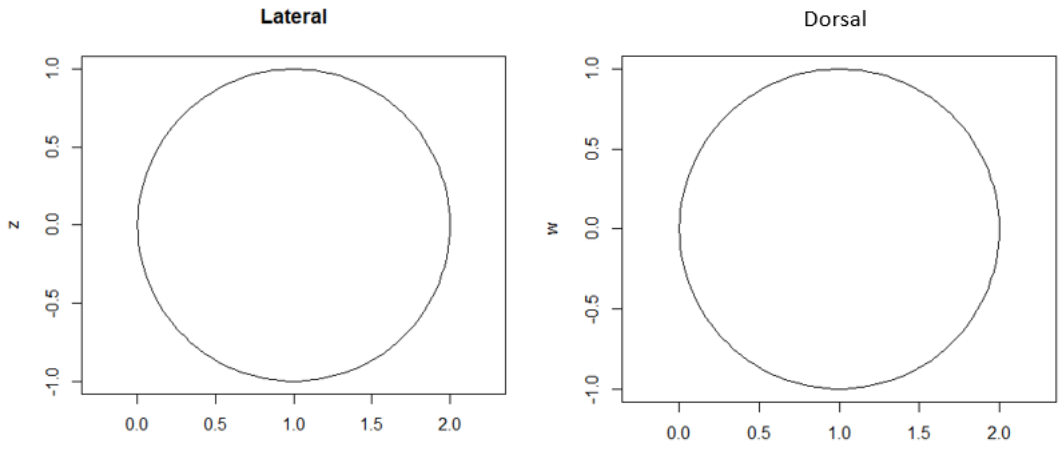

Figure D.1: The modeled sphere seen from the lateral and the dorsal aspect, with a radius of 0.02 m.

Fig. D.1 shows a generated sphere from the lateral and dorsal aspect, where the coordinates are found by [66],

$$x = sin\left(\psi \cdot \frac{\pi}{180}\right) + 1, \tag{D.1}$$

$$w = 2cos\left(\psi \cdot \frac{\pi}{180}\right), \tag{D.2}$$

$$z_U = cos\left(\psi \cdot \frac{\pi}{180}\right), \tag{D.3}$$

$$z_L = -cos\left(\psi \cdot \frac{\pi}{180}\right), \tag{D.4}$$

where ψ is an angle between $-90° - 90°$ with a resolution of 60 steps [66]. The coordinates are the same as defined in Table 4.1.

Table D.1: Values for speed of sound and density used in the simulation

	Speed of sound, c [m/s]	Density, ρ $[kg/m^3]$
Surroundings, water	1477.4	1026.8
Sphere, fluid	1480.3	1028.9
Sphere, gas	345.0	1.24

Table D.1 includes the necessary input values for simulating the TS. Firstly, the KRM method was compared to a sphere filled with fluids. The simulation was run using the values from Table D.1 and the results can be seen in Fig. D.2

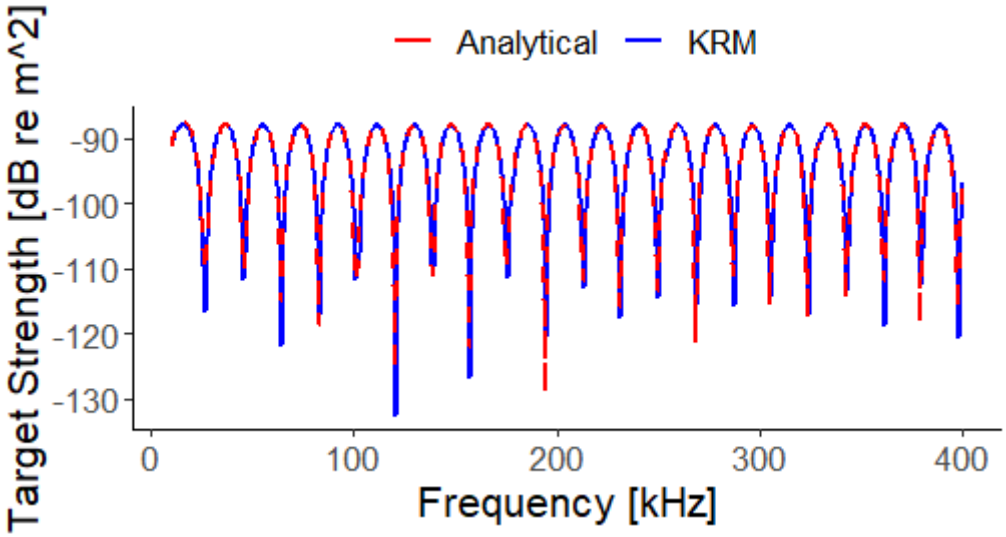

Figure D.2: Simulating the TS from a fluid-filled sphere using both an analytical method and the KRM model. Where the red represents the analytical [72] and the blue is the KRM [42]

Fig. D.2 are the results from running the KRM simulation, blue, and comparing it with the analytical model, red. This shows that the KRM simulation provides a close approximation to the analytical model for a sphere filled with fluids. In addition to a fluid-filled sphere, the validation was done for a sphere filled with gas. For this simulation, the values in the bottom row, c in air and ρ of air, in Table D.1 were used. The results from running the simulation are shown in Fig. D.3.

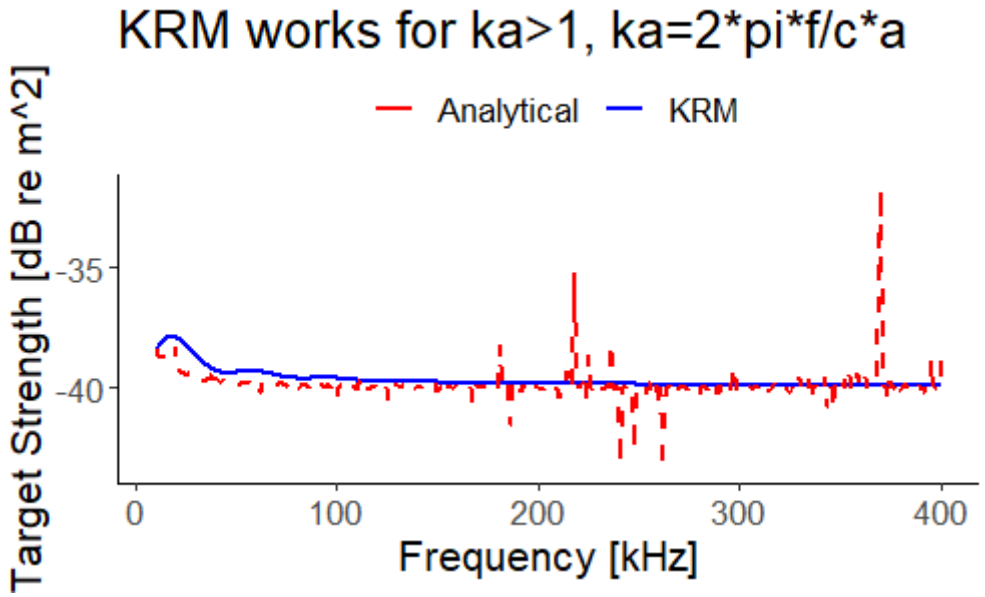

Figure D.3: Simulating the TS from a gas-filled sphere using both an analytical method [72] and the KRM model [42]. Where the red represents the analytical and the blue is the KRM.

Fig. D.3 shows the analytical TS as a function of frequency (red) and the simulated TS as a function of frequency (blue). The results indicate that KRM is a better approximation for higher frequencies than for frequencies below 100 kHz. The results seen in Figs. D.2 and D.3 indicate that the KRM approach provides a plausible approximation of the TS from gas-filled swim bladders.

Appendix E

Hours of collected data

This appendix includes the selected hours of FM and CW data, explained in 3.6. First, 12 hours of CW data was extracted every day, which was a quick process as the data files were relatively small. However, the FM files include much more information than the CW files, resulting in a prolonged process when extracting the files. Due to this, it was decided to analyze only one hour of FM data, and the timestamps can be seen in Table E.1. The table shows that the FM "hour" is seldom precisely one hour.

In order to compare CW with FM, it was decided to analyze two hours of CW data; one hour before and one hour after the FM hour. To avoid retrieving the data all over again, a small line was included in the MATLAB script used to process the CW data, see appendix F. The line is based on the columns "startTime(FM)" and "endTime(FM)" and subtracts one hour to obtain an hour before the FM hour and adds an hour in order to obtain the hour after. The data is extracted based on the length of the whole FM period and not by the hour, resulting in varying lengths in the data setss.

Table E.1: The timestamps used for extracting the FM data. One hour from FM is added and subtracted to obtain two hours of CW data.

Day	CW - 1 hour	endTime(CW)/startTime(FM)	endTime(FM)/startTime(CW)	CW + 1 hour
-4	15:37:24	16.37.24	17:36:13	18:36:13
-3	14:23:18	15:23:18	16:26:18	17:26:18
-2	13:19:41	14:19:41	14:44:08	15:44:08
-1	13:45:23	14:45:23	15:59:28	16:59:28
0	16:15:38	17:15:38	19:01:00	20:01:00
1	14:56:57	15:56:57	17:32:04	18:32:04
2	13:56:11	14:56:11	16:21:02	17:21:02
3	13:55:08	14:55:08	15:59:35	16:59:35
4	14:10:56	15:10:56	16:56:14	17:56:14
5	14:50:20	15:50:20	17:00:55	18:00:55
6	13:05:06	14:05:06	15:40:21	16:40:21
7	14:57:13	15:57:13	16:56:10	17:56:10
8	14:02:45	15:02:45	16:27:16	17:27:16
9	13:05:22	14:05:22	15:49:42	16:49:42
10	16:05:49	17:05:49	19:07:43	20:07:43
11	14:23:14	15:23:14	15:56:29	16:56:29
12	12:58:37	13:58:37	15:21:17	16:21:17
13	13:56:22	14:56:22	16:01:08	17:01:08
14	13:00:28	14:00:28	15:04:57	16:04:57
15	13:02:17	14:02:17	15:00:33	16:00:33
16	13:13:51	14:13:51	15:58:30	16:58:30
17	14:36:55	15:36:55	17:24:06	18:24:06
18	14:58:24	15:58:24	17:02:33	18:02:33

Date	CW - 1 hour	endTime(CW)/startTime(FM)	endTime(FM)/startTime(CW)	CW + 1 hour
19	13:15:55	14:15:55	15:34:49	16:34:49
20	12:55:29	13:55:29	15:01:20	16:01:20
21	13:10:55	14:10:55	15:24:27	16:24:27
22	12:57:45	13:57:45	15:07:44	16:07:44
23	12:59:39	13:59:39	15:48:03	16:48:03
24	13:02:30	14:02:30	15:07:34	16:07:34
25	13:22:15	14:22:15	15:55:40	16:55:40
26	13:02:42	14:02:42	15:01:06	16:01:06
27	12:57:00	13:57:00	15:01:27	16:01:27
28	13:03:21	14:03:21	15:38:52	16:38:52
29	13:11:52	14:11:52	15:37:38	16:37:38
30	12:56:33	13:56:33	15:01:01	16:01:01
31	11:00:35	12:00:35	12:43:19	13:43:19

Appendix F

Codes

F.1 *TS_FM.m*

```
%=========================================================================
%     MATLAB R2021b script for calculating the average TS
%                              from FM data
%=========================================================================
% Script to read .json files extracted from LSSS
%
% AUTHOR: Maren Forstr nen Rong
% INSTITUTE OF PHYSICS AND TECHNOLOGY
% UNIVERSITY OG BERGEN
% 2021-2022
%=====================================
close all
clear all

path =  ''; %Reading from folder
files = dir(fullfile([path, '*.json']));   %Finds files with * name in folder

%Reads one file/day at the time
for k=1:length(files)
jsonData = jsondecode(fileread([files(k).name]));
deg = 2; %bounday, excludes values outside 2 degrees

%creating structs for the desired TS and standard deviations
Target_strength(length(files)) = struct('Date', [], 'TS_60', [], 'TS_70', ...
[], 'TS_80', [], 'TS_70_all', [], 'TS_100', [], 'TS_110', [], 'TS_120', ...
[], 'TS_130', [], 'TS_140', [], 'TS_150', [], 'TS_120_all',[], 'TS_170', ...
[], 'TS_180', [], 'TS_190', [], 'TS_200', [], 'TS_210', [], 'TS_220', [], ...
'TS_230', [], 'TS_240', [], 'TS_250', [], 'TS_200_all', []);


%Goes through every track in the file
for l = 1:length(jsonData.tracks)
s = 1;
```

```
34
35 %Goes through the three channels (70, 120, 200 kHz) seperately and
36 %extracts maksimum and minimum frequencies
37 for q = 1:length(jsonData.tracks(l).channels)
38 minFr=jsonData.tracks(l).channels(q).minFrequency;
39 maxFr=jsonData.tracks(l).channels(q).maxFrequency;
40 nominal =jsonData.tracks(l).channels(q).nominalFrequency;
41 df = (jsonData.info.parameters.FrequencyResolution);
42 fr = minFr:df:maxFr;
43 f1=minFr+5e3; %selected lower freq
44 f2=maxFr-5e3;%seleced higher freq
45 indf=((f1≤fr)&(fr≤f2)); %indexes of wanted frequency range
46 n = 1500;       %CW has a 3 kHz bandwidth. Included here to match
47
48 %Goes through every TS value in each channel
49 for m = 1:length(jsonData.tracks(l).channels(q).tsc(:,1))
50 ang_atv(:,:) = jsonData.tracks(l).channels(q).athwartshipAngle(m);
51 ang_alo(:,:) = jsonData.tracks(l).channels(q).alongshipAngle(m);
52 theta(:,:) = (sqrt((ang_atv(:,:).^2) + (ang_alo(:,:).^2)));
53
54 %If the TS value is within the 2 degree boundary, the
55 %desired TS from the selected frequency is extracted
56 if -deg≤ang_alo(:,:) && ang_alo≤deg(:,:) && ang_atv≤deg(:,:) && -deg≤ang_atv(:,:)
57 if theta(:,:)≤deg
58
59
60 if nominal == 70000
61 fr1 = minFr:df:maxFr;
62 f1_1=minFr+5e3; %selected lower freq
63 f2_1=maxFr-5e3;%seleced higher freq
64 indf_1=((f1_1≤fr1)&(fr1≤f2_1)); %indexes of wanted frequency range
65 x_60 = fr≥60000-n & fr≤60000+n;
66 x_70 = fr≥70000-n & fr≤70000+n;
67 x_80 = fr≥80000-n & fr≤80000+n;
68
69 tsc_70_all = jsonData.tracks(l).channels(q).tsc;
70 tsc_60 = jsonData.tracks(l).channels(q).tsc(:,x_60);
71 tsc_70 = jsonData.tracks(l).channels(q).tsc(:,x_70);
72 tsc_80 = jsonData.tracks(l).channels(q).tsc(:,x_80);
73
74 avg_70_all(:,:) = 10*log10(mean(10.^(tsc_70_all./10)));
75 avg_70_all(avg_70_all==0) = [];
76 avg_60(:,:) = 10*log10(mean(10.^(tsc_60./10)));
77 avg_60(avg_60==0) = [];
78 avg_70(:,:) = 10*log10(mean(10.^(tsc_70./10)));
79 avg_70(avg_70==0) = [];
80 avg_80(:,:) = 10*log10(mean(10.^(tsc_80./10)));
81 avg_80(avg_80==0) = [];
82 avg_70_all(:,:) = 10*log10(mean(10.^(tsc_70_all./10)));
83 avg_70_all(avg_70_all==0) = [];
84
85 %For the frequency response
86 avg_70_all_2(l,:) = avg_70_all;
87 avg_70_all_2( ¬any(avg_70_all_2,2), : ) = [];
```

```
88
89  avg_60_2(l,:) = 10*log10(mean(10.^(avg_60./10)));
90  avg_60_2(avg_60_2==0) =[];
91  avg_70_2(l,:) = 10*log10(mean(10.^(avg_70./10)));
92  avg_70_2(avg_70_2==0) =[];
93  avg_80_2(l,:) = 10*log10(mean(10.^(avg_80./10)));
94  avg_80_2(avg_80_2==0) =[];
95
96  end
97
98  if nominal == 120000
99  fr2 = minFr:df:maxFr;
100 f1_2=minFr+5e3; %selected lower freq
101 f2_2=maxFr-5e3;%seleced higher freq
102 indf_2=((f1_2≤fr2)&(fr2≤f2_2)); %indexes of wanted frequency range
103 x_100 = fr≥ 100000-n & fr≤ 100000+n;
104 x_110 = fr≥ 110000-n & fr≤ 110000+n;
105 x_120 = fr≥ 120000-n & fr≤ 120000+n;
106 x_130 = fr≥ 130000-n & fr≤ 130000+n;
107 x_140 = fr≥ 140000-n & fr≤ 140000+n;
108 x_150 = fr≥ 150000-n & fr≤ 150000+n;
109
110 tsc_100 = jsonData.tracks(l).channels(q).tsc(:,x_100);
111 tsc_110 = jsonData.tracks(l).channels(q).tsc(:,x_110);
112 tsc_120 = jsonData.tracks(l).channels(q).tsc(:,x_120);
113 tsc_130 = jsonData.tracks(l).channels(q).tsc(:,x_130);
114 tsc_140 = jsonData.tracks(l).channels(q).tsc(:,x_140);
115 tsc_150 = jsonData.tracks(l).channels(q).tsc(:,x_150);
116 tsc_120_all = jsonData.tracks(l).channels(q).tsc;
117
118 avg_100(:,:) = 10*log10(mean(10.^(tsc_100./10)));
119 avg_100(avg_100==0) = [];
120 avg_110(:,:) = 10*log10(mean(10.^(tsc_110./10)));
121 avg_110(avg_110==0) = [];
122 avg_120(:,:) = 10*log10(mean(10.^(tsc_120./10)));
123 avg_120(avg_120==0) = [];
124 avg_130(:,:) = 10*log10(mean(10.^(tsc_130./10)));
125 avg_130(avg_130==0) = [];
126 avg_140(:,:) = 10*log10(mean(10.^(tsc_140./10)));
127 avg_140(avg_140==0) = [];
128 avg_150(:,:) = 10*log10(mean(10.^(tsc_150./10)));
129 avg_150(avg_150==0) = [];
130 avg_120_all = 10*log10(mean(10.^(tsc_120_all./10)));
131 avg_120_all(avg_120_all==0) = [];
132
133 %For the frequency response
134 avg_120_all_2(l,:) = avg_120_all;
135 avg_120_all_2( ¬any(avg_120_all_2,2), : ) = [];
136
137 avg_100_2(l,:) = 10*log10(mean(10.^(avg_100./10)));
138 avg_100_2(avg_100_2==0) = [];
139 avg_110_2(l,:) = 10*log10(mean(10.^(avg_110./10)));
140 avg_110_2(avg_110_2==0) = [];
141 avg_120_2(l,:) = 10*log10(mean(10.^(avg_120./10)));
```

```
142 avg_120_2(avg_120_2==0) = [];
143 avg_130_2(l,:) = 10*log10(mean(10.^(avg_130./10)));
144 avg_130_2(avg_130_2==0) = [];
145 avg_140_2(l,:) = 10*log10(mean(10.^(avg_140./10)));
146 avg_140_2(avg_140_2==0) = [];
147 avg_150_2(l,:) = 10*log10(mean(10.^(avg_150./10)));
148 avg_150_2(avg_150_2==0) = [];
149
150 end
151
152 if nominal == 200000
153 fr3 = minFr:df:maxFr;
154 f1_3=minFr+5e3;
155 f2_3=maxFr-5e3;
156 indf_3=((f1_3≤fr3)&(fr3≤f2_3));
157 x_170 = fr≥170000-n & fr≤170000+n;
158 x_180 = fr≥180000-n & fr≤180000+n;
159 x_190 = fr≥190000-n & fr≤190000+n;
160 x_200 = fr≥200000-n & fr≤200000+n;
161 x_210 = fr≥210000-n & fr≤210000+n;
162 x_220 = fr≥220000-n & fr≤220000+n;
163 x_230 = fr≥230000-n & fr≤230000+n;
164 x_240 = fr≥240000-n & fr≤240000+n;
165 x_250 = fr≥250000-n & fr≤250000+n;
166
167 tsc_170 = jsonData.tracks(l).channels(q).tsc(:,x_170);
168 tsc_180 = jsonData.tracks(l).channels(q).tsc(:,x_180);
169 tsc_190 = jsonData.tracks(l).channels(q).tsc(:,x_190);
170 tsc_200 = jsonData.tracks(l).channels(q).tsc(:,x_200);
171 tsc_210 = jsonData.tracks(l).channels(q).tsc(:,x_210);
172 tsc_220 = jsonData.tracks(l).channels(q).tsc(:,x_220);
173 tsc_230 = jsonData.tracks(l).channels(q).tsc(:,x_230);
174 tsc_240 = jsonData.tracks(l).channels(q).tsc(:,x_240);
175 tsc_250 = jsonData.tracks(l).channels(q).tsc(:,x_250);
176 tsc_200_all = jsonData.tracks(l).channels(q).tsc;
177
178 avg_170(:,:) = 10*log10(mean(10.^(tsc_170./10)));
179 avg_170(avg_170==0) = [];
180 avg_180(:,:) = 10*log10(mean(10.^(tsc_180./10)));
181 avg_180(avg_180==0) = [];
182 avg_190(:,:) = 10*log10(mean(10.^(tsc_190./10)));
183 avg_190(avg_190==0) = [];
184 avg_200(:,:) = 10*log10(mean(10.^(tsc_200./10)));
185 avg_200(avg_200==0) = [];
186 avg_210(:,:) = 10*log10(mean(10.^(tsc_210./10)));
187 avg_210(avg_210==0) = [];
188 avg_220(:,:) = 10*log10(mean(10.^(tsc_220./10)));
189 avg_220(avg_220==0) = [];
190 avg_230(:,:) = 10*log10(mean(10.^(tsc_230./10)));
191 avg_230(avg_230==0) = [];
192 avg_240(:,:) = 10*log10(mean(10.^(tsc_240./10)));
193 avg_240(avg_240==0) = [];
194 avg_250(:,:) = 10*log10(mean(10.^(tsc_250./10)));
195 avg_250(avg_250==0) = [];
```

```
196 avg_200_all = 10*log10(mean(10.^(tsc_200_all./10)));
197 avg_200_all(avg_200_all==0) = [];
198
199 %For the frequency response
200 avg_200_all_2(l,:) = avg_200_all;
201 avg_200_all_2( ¬any(avg_200_all_2,2), : ) = [];
202
203 avg_170_2(l,:) = 10*log10(mean(10.^(avg_170./10)));
204 avg_170_2(avg_170_2==0) = [];
205 avg_180_2(l,:) = 10*log10(mean(10.^(avg_180./10)));
206 avg_180_2(avg_180_2==0) = [];
207 avg_190_2(l,:) = 10*log10(mean(10.^(avg_190./10)));
208 avg_190_2(avg_190_2==0) = [];
209 avg_200_2(l,:) = 10*log10(mean(10.^(avg_200./10)));
210 avg_200_2(avg_200_2==0) = [];
211 avg_210_2(l,:) = 10*log10(mean(10.^(avg_210./10)));
212 avg_210_2(avg_210_2==0) = [];
213 avg_220_2(l,:) = 10*log10(mean(10.^(avg_220./10)));
214 avg_220_2(avg_220_2==0) = [];
215 avg_230_2(l,:) = 10*log10(mean(10.^(avg_230./10)));
216 avg_230_2(avg_230_2==0) = [];
217 avg_240_2(l,:) = 10*log10(mean(10.^(avg_240./10)));
218 avg_240_2(avg_240_2==0) = [];
219 avg_250_2(l,:) = 10*log10(mean(10.^(avg_250./10)));
220 avg_250_2(avg_250_2==0) = [];
221
222 end
223
224 end
225
226 end
227
228 end
229 end
230
231
232 end
233
234 %calculating the average TS of each frequency to obtain one TS value
235 %per day
236 if k ≠ 28
237 %For TS from 70 kHz
238 avg_60_TS = 10*log10(mean(10.^(avg_60_2./10)));
239 avg_70_TS = 10*log10(mean(10.^(avg_70_2./10)));
240 avg_80_TS = 10*log10(mean(10.^(avg_80_2./10)));
241 avg_70_TS_all_TS = 10*log10(mean(10.^(avg_70_all_2(:,:)./10)));
242 Target_strength(k).TS_60 = avg_60_TS;
243 Target_strength(k).TS_70 = avg_70_TS;
244 Target_strength(k).TS_80 = avg_80_TS;
245 Target_strength(k).TS_70_all = avg_70_TS_all_TS;
246
247 end
248
249
```

```
250 %For TS from 120 kHz
251 avg_100_TS = 10*log10(mean(10.^(avg_100_2./10)));
252 avg_110_TS = 10*log10(mean(10.^(avg_110_2./10)));
253 avg_120_TS = 10*log10(mean(10.^(avg_120_2./10)));
254 avg_130_TS = 10*log10(mean(10.^(avg_130_2./10)));
255 avg_140_TS = 10*log10(mean(10.^(avg_140_2./10)));
256 avg_150_TS = 10*log10(mean(10.^(avg_150_2./10)));
257 avg_120_TS_all_TS = 10*log10(mean(10.^(avg_120_all_2(:,:)./10)));
258
259 Target_strength(k).TS_100 = avg_100_TS;
260 Target_strength(k).TS_110 = avg_110_TS;
261 Target_strength(k).TS_120 = avg_120_TS;
262 Target_strength(k).TS_130 = avg_130_TS;
263 Target_strength(k).TS_140 = avg_140_TS;
264 Target_strength(k).TS_150 = avg_150_TS;
265 Target_strength(k).TS_120_all = avg_120_TS_all_TS;
266
267
268 %For TS from 200 kHz
269 avg_170_TS = 10*log10(mean(10.^(avg_170_2./10)));
270 avg_180_TS = 10*log10(mean(10.^(avg_180_2./10)));
271 avg_190_TS = 10*log10(mean(10.^(avg_190_2./10)));
272 avg_200_TS = 10*log10(mean(10.^(avg_200_2./10)));
273 avg_210_TS = 10*log10(mean(10.^(avg_210_2./10)));
274 avg_220_TS = 10*log10(mean(10.^(avg_220_2./10)));
275 avg_230_TS = 10*log10(mean(10.^(avg_230_2./10)));
276 avg_240_TS = 10*log10(mean(10.^(avg_240_2./10)));
277 avg_250_TS = 10*log10(mean(10.^(avg_250_2./10)));
278 avg_200_TS_all_TS = 10*log10(mean(10.^(avg_200_all_2(:,:)./10)));
279
280 Target_strength(k).TS_170 = avg_170_TS;
281 Target_strength(k).TS_180 = avg_180_TS;
282 Target_strength(k).TS_190 = avg_190_TS;
283 Target_strength(k).TS_200 = avg_200_TS;
284 Target_strength(k).TS_210 = avg_210_TS;
285 Target_strength(k).TS_220 = avg_220_TS;
286 Target_strength(k).TS_230 = avg_230_TS;
287 Target_strength(k).TS_240 = avg_240_TS;
288 Target_strength(k).TS_250 = avg_250_TS;
289 Target_strength(k).TS_200_all = avg_200_TS_all_TS;
290 Target_strength(k).Date = (jsonData.channelInfo(1).parameters.startTime);
291
292 end
```

F.2 *TS_vel_CW.m*

From this script both the swimming speed and $\overline{TS}$ from CW data were found. The swimming speed is seen in Fig. 5.13 and $\overline{TS}$ in Fig. 5.3.

```
%=========================================================================
%     MATLAB R2021b script for calculating the swimming speed and average TS
%                                from CW data and
%=========================================================================
% Script to read .text files extracted from LSSS
%Name of file: TS_vel_CW.m
%
% AUTHOR: Maren F. Rong
% INSTITUTE OF PHYSICS AND TECHNOLOGY
% UNIVERSITY OG BERGEN
% 2021-2022
%
%CO-AUTHOR: Tonje Nesse Forland
%THE INSTITUTE OF MARINE RESEARCH
%2021 - 2022
%=====================================

clear all
close all

path = 'C:'; %Reading from folder
files = dir(fullfile(path, '*.txt'));   %Finds files with * name in folder

%average fish length throughout the experiment [m]
avg_length = 0.38;

%Reading one file at the time
for i = 1:length(files)
data(:,i) = importdata(fullfile([path '\' files(i).name]));
d = data(i).data(:,2);
time = data(i).data(:,3);
Time = num2str(time,'%08.f'); %adding zeros to the time in order to have 8 digits
T=zeros(length(Time),1);

%find time in order to select wanted time-range:
for c=1:length(Time)
tmp = [num2str(d(c)),'T',(Time(c,:))];
T(c)=datenum(tmp,'yyyymmddTHHMMSS');
end

D=datenum(num2str(d(1)),'yyyymmdd'); %creating date
%Reads timestamps for FM data from xlsx file
[~,~,raw] = xlsread('Tp.xlsx');

%Defining a struct
fish(50000) = struct('distx', [], 'disty',[], 'distz', [], 'distT', ...
[], 'Tot_dist', [], 't', [], 'Tot_time', [], 'tsc', [], 'avg_tsc', []);
```

```
48 avg_speed(length(files)) = struct('Date', [], 'mps', [], 'std_mps', ...
49 [], 'flps', [], 'std_flps', [], 'avg_TS', []);
50 m = 1; %counting the number of tracks/fish in the file
51 n = 1; %counting the number of pings within a track
52
53 %-1 hour returns 1 hour Cw before FM, - 3 returns 1 hour CW after FM
54 %File 28 = 11 april, only data at night
55 %-1143, starts at 021614, -9, stops at 06.45
56 if i == 28
57 t_start=datenum(raw(i,10),'yyyymmddTHHMMSS')-datenum(0000,0,0,11,43,0);
58 t_stop=datenum(raw(i,11),'yyyymmddTHHMMSS')-datenum(0000,0,0,9,0,0);
59 %File 36 = 19 april, end of experiment.
60 elseif i == 36
61 t_start=datenum(raw(i,10),'yyyymmddTHHMMSS')-datenum(0000,0,0,3,0,0);
62 t_stop=datenum(raw(i,11),'yyyymmddTHHMMSS');
63 else
64 t_start=datenum(raw(i,10),'yyyymmddTHHMMSS')-datenum(0000,0,0,1,0,0);
65 t_stop=datenum(raw(i,11),'yyyymmddTHHMMSS')+datenum(0000,0,0,1,0,0);
66 end
67
68 %find indexes to keep - giving data for the selected period
69 t_test=datenum(raw(i,10),'yyyymmdd');
70
71 if t_test==D
72 ind_tid = T>t_start & T<t_stop; %read t_start and stop values from excel sheet
73 %Extracts the values within the time boundaries
74 id = data(i).data(ind_tid,1);
75 d = data(i).data(ind_tid,2);
76 time = data(i).data(ind_tid,3);
77 tsc = data(i).data(ind_tid,7);
78 x = data(i).data(ind_tid,8);
79 y = data(i).data(ind_tid,9);
80 z = data(i).data(ind_tid,10);
81 end
82
83 %Loop to extract tracks for each fish
84 for l = 1:length(id)-1
85 dist(l,:) = id(l)-id(l+1);
86
87 %Goes through the length of the ID's. If the difference between two ID's
88 %are equal to 0, the ID belongs to the same track/fish. The distanc
89 % between x, y, and z is found
90 if dist(l,:) == 0
91 fish(m).tsc(n) = tsc(l);
92 fish(m).distx(n) = x(l+1) - x(l);
93 fish(m).disty(n) = y(l+1) - y(l);
94 fish(m).distz(n) = z(l+1) - z(l);
95 fish(m).distT(n) = sqrt((fish(m).distx(n))^2 ...
96 + (fish(m).disty(n))^2 + (fish(m).distz(n))^2);
97 %time between pings in sec:
98 fish(m).t(n) = (time(1+l) - time(l))*0.01;
99 %avg TS value for each fish:
100 fish(m).avg_tsc = 10*log10(mean(10.^(fish(m).tsc./10)));
101 avg_tsc(m,:) = fish(m).avg_tsc;
```

```
102 n = n + 1;
103 else
104 m = m + 1;
105 n = 1;
106 end
107 end
108
109 %Removing the access spaces from the fish struct
110 fish=fish(1:m);
111
112 bbb = 1; %counts time/distance outside boundaries
113 aaa = 1; %counts number of tracks within the boundaries
114
115 for b=1:length(fish)
116 fish(b).Tot_time = sum(fish(b).t);
117 fish(b).Tot_dist = sum(fish(b).distT);
118
119 %notes row number of time and speed outside boundary
120 if (fish(b).Tot_time > 10 || fish(b).Tot_dist > 4)
121 ind_F(bbb,:)=b;
122 bbb=bbb+1;
123 %calculates the swimming speed for the fish within the boundary
124 else
125 Speed_mPs(aaa) = fish(b).Tot_dist/fish(b).Tot_time;
126 Speed_flPs(aaa) = (Speed_mPs(aaa)/avg_length); %Fish length per second
127 aaa=aaa+1;
128 end
129
130 end
131 %average TS for the whole file:
132 avg_TS = 10*log10(mean(10.^(avg_tsc./10)));
133 %average swimming speed in m/s for the whole file:
134 avg_mps = mean(Speed_mPs(¬isnan(Speed_mPs)));
135 std_mps = std(Speed_mPs(¬isnan(Speed_mPs)));
136 %average fish length per sec, for the whole file
137 avg_fl = mean(Speed_flPs(¬isnan(Speed_flPs)));
138 std_flps = std(Speed_flPs(¬isnan(Speed_flPs)));
139
140 avg_speed(i).Date = d(i);
141 avg_speed(i).mps = avg_mps;
142 avg_speed(i).std_mps = std_mps;
143 avg_speed(i).flps = avg_fl;
144 avg_speed(i).std_flps = std_flps;
145 avg_speed(i).avg_TS = avg_TS;
146
147 clear data %to prevent using previous data in next run
148 end
149
150 speed_TS_200 = (avg_speed);      %table with values from the struct speed
151 save('speed_TS_200');
```

F.3 *Velocity_FM.m*

This script was applied when calculating the average swimming speed per day, seen in Fig. 5.12.

```
%=========================================================================
%   MATLAB R2021b script for calculating the swimming speed from FM data
%=========================================================================
% Script to read .text files extracted from LSSS
%Name of file: Velocity_FM.m
%
% AUTHOR: Maren Forstr nen Rong
% INSTITUTE OF PHYSICS AND TECHNOLOGY
% UNIVERSITY OG BERGEN
% 2021-2022
%
%=====================================

clear all
close all

path = 'C:'; %Reading from folder
files = dir(fullfile(path, '*.txt'));

avg_length = 0.38; %average fish length throughout the experiment [m]


%Goes through each file and extracts the necesarry values to calculate the
% swimming speed.
for i = 1:length(files)
data(:,i) = importdata(fullfile([path '\' files(i).name]));
id = data(i).data(:,1);   %Every ID in the file
d = data(i).data(:,2);
time = data(i).data(:,3);
x = data(i).data(:,8);
y = data(i).data(:,9);
z = data(i).data(:,10);

%creating structs for saving the desired parameters
fish(50000) = struct('distx', [], 'disty',[], 'distz', [], 'distT', [], ...
    'avg_tsc', [], 'Tot_dist', [], 't', [], 'Tot_time', [], 'Date', [], ...
    'Speed', [], 'Fish_length', []);
avg_speed(length(files)) = struct('Date', [], 'mps', [], 'std_mps', ...
    [], 'flps', [], 'std_flps', []);
m = 1; %Counts the number of trakcs/fish in the file
n = 1; %Counts the length of the track (number of pings in the track)

%Goes through the length of the ID's. If the difference between two ID's
%are equal to 0, the ID belongs to the same track/fish. The distance
%between x, y, and z is found.
for l = 1:length(id)-1
dist(l,:) = id(l)-id(l+1);
if dist(l,:) == 0
```

```
49      fish(m).distx(n) = x(l+1) - x(l);
50      fish(m).disty(n) = y(l+1) - y(l);
51      fish(m).distz(n) = z(l+1) - z(l);
52      fish(m).distT(n) = sqrt((fish(m).distx(n))^2 + ...
53          (fish(m).disty(n))^2 + (fish(m).distz(n))^2);
54      fish(m).t(n) = (time(1+1) - time(l))*0.01;        %time between pings in sec
55      n = n + 1;
56  else
57      m = m + 1;
58      n = 1;
59  end
60  end
61
62  %Shortens the length of the struct
63  fish = fish(1:m);
64
65  aaa = 1; %counts the fish within the boundaries
66  bbb = 1; %counting the time and distance outside the defined conditions
67  for b=1:length(fish)
68  fish(b).Tot_time = sum(fish(b).t);
69  fish(b).Tot_dist = sum(fish(b).distT);
70
71  %The indexes of fish outside the boundaries
72  % set for the time and distance
73  if (fish(b).Tot_time > 10 || fish(b).Tot_dist > 4)
74      ind_F(bbb,:) = b; %Finds index for the fish that exceeds the conditions
75      bbb = bbb + 1;
76  else         %If within the boundaries: calculates the swimming speed
77      Speed_mPs(aaa) = fish(b).Tot_dist/fish(b).Tot_time;
78      Speed_flPs(aaa) = (Speed_mPs(aaa)/avg_length);
79      aaa = aaa + 1;
80  end
81  end
82
83  %calculating the average values over every fish in the file to obtain
84  %one value per day.
85  avg_mps = mean(Speed_mPs(¬isnan(Speed_mPs)));
86  std_mps = std(Speed_mPs(¬isnan(Speed_mPs)));
87  avg_fl = mean(Speed_flPs(¬isnan(Speed_flPs)));
88  std_flps = std(Speed_flPs(¬isnan(Speed_flPs)));
89
90
91  %Creating a struct for the desired values
92  avg_speed(i).Date = d(i);
93  avg_speed(i).mps = avg_mps;
94  avg_speed(i).std_mps = std_mps;
95  avg_speed(i).flps = avg_fl;
96  avg_speed(i).std_flps = std_flps;
97
98  end
99  speed_200_FM = (avg_speed);
100 %save('speed_200_FM')
```

F.4 *KRMr_Salmon.R*

Script from [66] applied in the R software to simulate the TS from a swim bladder, as explained in Chapter 4.

```
library(KRMr)
library(dplyr)
#####################################################################
# Run KRMr on salmon body and swimbladder
# Author: Geir Pedersen (IMR), Bergen, Norway
#####################################################################

fb <- read.csv('C:')
sb <- read.csv('C:/')


layout(matrix(c(1,2,3,3), 2, 2, byrow = TRUE))l
par(mar=c(1,1,1,1))
shplot(x_fb = fb$x_fb, w_fb = fb$w_fb,
       x_sb = sb$x_sb, w_sb = sb$w_sb,
       z_fbU = fb$z_fbU, z_fbL = fb$z_fbL,
       z_sbU = sb$z_sbU, z_sbL = sb$z_sbL)

# Define parameters for the sphere (fluid) and water
# Feel free to use something else e.g. for water if you have measurements
#freqs = c(70,120,200)*1000
#freqs = 56.8:88.2 * 1000 #Hz frequencies to be considered in Hz, 70
#freqs = 93.5:156.5 * 1000 #Hz frequencies to be considered in Hz, 120
freqs = 165:255 * 1000 #Hz frequencies to be considered in Hz, 200
#freqs = 1:30*1000 #Hz frequencies to be considered in Hz
cw = 1489       # m/s sound speed surrounding water
cfb = 1480.3      #m/s sound speed inside the fish body
csb = 345.0       #m/s soundspeed inside the swimbladder
rhow = 1026.8      #kg/m3 density surrounding water
rhofb = 1028.9    #kg/m3 density fish body
rhosb = 1.24      #kg/m3 density gas in swimbladder

kfs = krm.sim(frequency = freqs,
 c.w =cw,
 rho.w = rhow,
 # Angle of incidence, 90=normal to the fish, max 20'ish degrees of 90:
 theta=90,
 c.fb = cfb,
 rho.fb = rhofb,
 c.sb = csb,
 rho.sb = rhosb,
 # This can be used to scale length e.g. L=0.38 the fish length will be 38 cm:
  L=0.38,
 # Width, height parameters:
 x_fb = fb$x_fb,
 x_sb = sb$x_sb,
 w_fb = fb$w_fb,
```

```
  w_sb = sb$w_sb,
  z_fbU = fb$z_fbU,
  z_sbU = sb$z_sbU,
  z_fbL = fb$z_fbL,
  z_sbL = sb$z_sbL)

colors <- c("KRM" = "blue")
ggplot2::ggplot()+
   ggplot2::geom_point(data=kfs, ggplot2::aes(x=frequency/1000,y=TS, group=L,
   col='KRM'),lwd=1)+
   ggplot2::scale_color_manual(values = colors, name='')+
   ggplot2::xlab('Frequency [kHz]')+
   ggplot2::ylab('Target Strength [dB re m^2]')+
   ggplot2::theme_classic()+
   ggplot2::theme(text=ggplot2::element_text(size=16),
                  legend.position='top')
```